

Université de Strasbourg  
École Doctorale des Sciences Chimiques

Thèse pour l'obtention du diplôme de  
DOCTEUR DE L'UNIVERSITÉ DE STRASBOURG

Discipline : Chimie biologique et thérapeutique

Soutenue publiquement par

**Jiahui FAN**

le 17/12/2018

**Evaluation of the safety and drug delivery efficacy of  
carbon dots in *in vitro* and *in vivo* models**

UMR 7199 - Conception et Application de Molécules Bioactives  
Directeurs de thèse: Prof. Françoise PONS & Dr. Luc LEBEAU

**Members of the jury:**

Dr. **Hervé HILLAIREAU**, Rapporteur externe, Université Paris-Sud

Dr. **Olivier JOUBERT**, Rapporteur externe, Université de Lorraine

Dr. **Luc LEBEAU**, Directeur de thèse, Université de Strasbourg

Prof. **Françoise PONS**, Co-directeur de thèse, Université de Strasbourg



# **Étude de la toxicité des “carbon dots” et de leur efficacité de délivrance de drogues dans des modèles *in vitro* et *in vivo***

## **Introduction**

Les carbon dots constituent le dernier membre de la famille des nanoparticules carbonées à avoir été découvert. Ils ont été isolés pour la première fois en 2004, lors d'expériences de purification de nanotubes de carbone par électrophorèse. Outre leur taille nanométrique, les carbon dots sont des objets quasi-sphériques et hydrophiles, ce qui leur vaut d'être, en général, présentés comme des nanoparticules très faiblement toxiques, voire biocompatibles. Ils sont assez facilement accessibles par voie de synthèse et peuvent être commodément modifiés par réaction des groupements fonctionnels présents à leur surface (amines, carboxyles, hydroxyles...). Enfin, ils présentent des propriétés de fluorescence intrinsèque, sont relativement résistants au photoblanchiment, et peuvent être excités par irradiation multi-photonique. Ainsi, à l'instar des autres membres de la famille des nanoparticules carbonées (graphène, nanodiamants, fullerènes, nanotubes), les carbon dots présentent des propriétés remarquables qui suscitent d'intenses recherches pour des applications dans des domaines aussi différents que ceux de l'électronique, de la catalyse, du stockage de l'énergie, de l'imagerie, ou encore de la médecine. Dans ce dernier domaine, les carbon dots pourraient trouver des applications comme vecteurs de délivrance de drogues, à l'instar d'autres nanoparticules développées avec succès dans ce domaine.

Si les nanotechnologies permettent d'envisager des évolutions technologiques formidables dans de nombreux domaines, y compris le domaine de la santé, l'irruption des nanoparticules dans un nombre croissant de produits manufacturés grand public (produits de soin et d'hygiène, habillement, cosmétiques, équipements sportifs, produits ménagers et de jardinage, équipements automobiles, peintures, alimentation animale et humaine...) pose des questions en termes de santé publique. Les risques redoutés à la lumière des données actuelles ne sont pas sans rappeler ceux associés à l'exposition à l'amiante ou à la pollution aux particules fines responsables notamment d'une toxicité respiratoire et/ou cardiovasculaire. Aussi, y a-t-il une demande importante de la part des citoyens, au travers des diverses agences de sécurité sanitaire, nationales et internationales, d'informations claires et fiables quant aux risques encourus en cas d'exposition aux nanoparticules manufacturées.

Dans ce contexte, les travaux développés au cours de cette thèse visaient deux objectifs distincts. Dans un premier temps, il s'agissait d'étudier la toxicité des carbon dots, et en particulier, d'identifier, si possible, les propriétés intrinsèques responsables de la toxicité éventuelle de ces particules, afin d'établir des relations "structure-toxicité". Pour cela, nous avons étudié le profil toxicologique d'une large collection de particules aux caractéristiques de taille, charge, et chimie de surface variées. Le deuxième objectif visé était d'évaluer le potentiel d'utilisation des carbon dots dans le domaine de la délivrance de drogues. En particulier, je me suis intéressé au potentiel que présentent les carbon dots chargés positivement en tant que vecteurs synthétiques de transfert de gène. En effet, les nanoparticules chargées positivement peuvent interagir, *via* des interactions électrostatiques, avec l'acide nucléique qui est chargé négativement. Ceci laisse espérer la formation de particules discrètes par complexation des carbon dots positifs avec un ADN double brin. Ces complexes sont susceptibles d'être internalisées dans les cellules et de modifier leur profil d'expression génique. Ceci a effectivement été démontré *in vitro* dès 2012, puis *in vivo* en 2015, notamment dans notre laboratoire. L'ensemble de mon travail a été conduit dans des modèles expérimentaux *in vitro* (cellules en culture) et *in vivo* (souris).

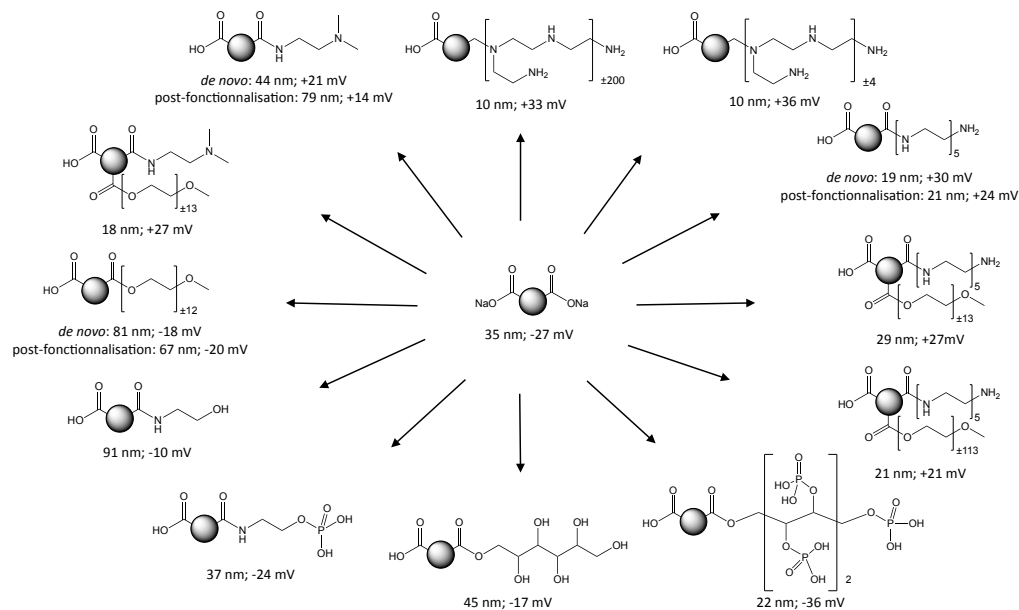
## **Résultats et discussion**

### **- Particules utilisées dans ce travail**

Les particules utilisées de ce travail ont toutes été fabriquées au laboratoire. Elles ont été préparées selon différents procédés (réactions solvothermales à pression atmosphérique et sous haute pression, pyrolyse au four à micro-onde domestique, irradiation sous micro-ondes en conditions solvothermales, pyrolyse à haute température à sec), à partir de précurseurs variés (acide citrique ou citrates variés, glucose, poly(éthylène glycol)...) et en présence de divers additifs (oligoamines, acides minéraux...) afin de générer la diversité structurale recherchée. Une diversité additionnelle a été apportée, dans certains cas, par des étapes de fonctionnalisation ultérieure de la surface des nanoparticules. Parmi le grand nombre de particules



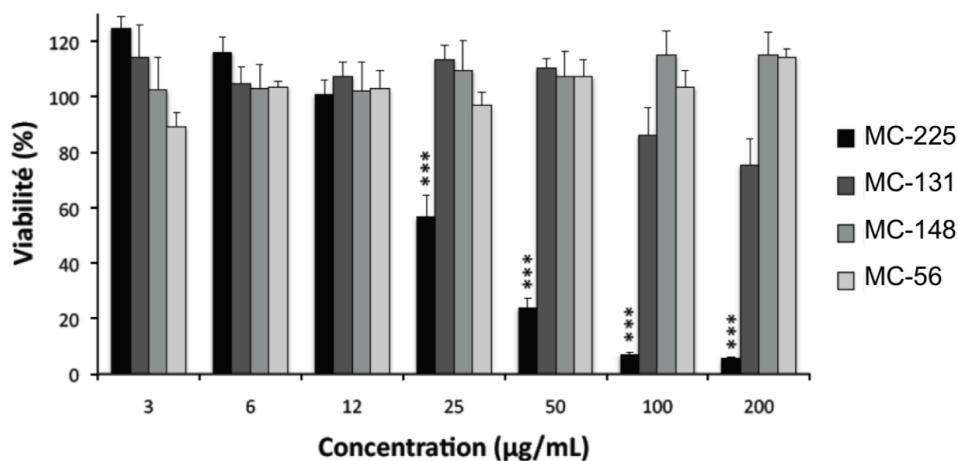
disponibles, une sélection représentative (30 à 40 carbon dots) a été réalisée en prenant en compte les caractéristiques de taille, charge et chimie de surface des objets (figure 1).



**Figure 1.** Représentation schématique de la diversité des NPs étudiées dans le cadre de nos travaux.

#### - Étude de la toxicité des carbon dots

Afin d'étudier la toxicité des carbon dots en fonction de leurs caractéristiques physico-chimiques, notre premier objectif a été de mener une étude de cytotoxicité comparative sur la collection complète de nanoparticules carbonées dans la lignée cellulaire THP-1 (test au MTT) suite à une incubation de 24 h en présence de concentrations croissantes de particules. Comme l'illustre la figure 2 réalisée à partir d'un échantillon représentatif de nanoparticules, les carbon dots ont montré une cytotoxicité variable. Par une approche de groupage, nous avons pu classer l'ensemble des particules évaluées en 3 niveaux de toxicité : 1- toxicité élevée (IC50 calculable et comprise entre 18 et 100  $\mu\text{g/mL}$ ), 2-toxicité modérée (IC80 calculable et comprise entre 33 et 123  $\mu\text{g/mL}$ ) et 3-absence de toxicité (perte maximale de viabilité inférieure à 20%). Pour les carbon dots présentant une toxicité élevée, nous avons montré que celle-ci est importante dès 1 h d'incubation et presque maximale à 4 h. De plus, elle s'accompagne d'une sécrétion dose- et temps-dépendante de cytokines, marqueurs d'une réponse inflammatoire. Cette réponse inflammatoire était absente dans le cas des particules de toxicité modérée ou non cytotoxiques.

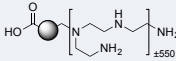
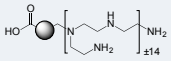
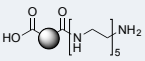
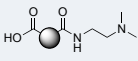
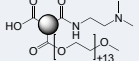
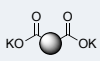


**Figure 2.** Viabilité des cellules THP-1 exposées pendant 24 h à des carbon dots fortement cytotoxiques (MC-225), modérément cytotoxiques (MC-131) et non cytotoxiques (MC-148 et MC-56).

L'analyse de la relation entre cytotoxicité et caractéristiques physicochimiques des carbon dots a montré que les nanoparticules très ou modérément cytotoxiques sont chargées positivement (par exemple MC-225 et MC-131), alors que les nanoparticules non cytotoxiques sont chargées négativement (MC-56). Toutefois, certains carbon dots chargés positivement se sont avérés non cytotoxiques. Il s'agit de carbon dots dont la fabrication fait intervenir du poly(éthylène glycol), un polymère connu pour ses propriétés d'exclusion stérique et qui, par conséquent, tend à masquer les charges à la surface des nanoparticules (par exemple MC-148), ou de carbon dots formant de gros agrégats en milieu salin. Ces données suggèrent un rôle de la charge, mais aussi de la chimie de surface dans la toxicité des nanoparticules.

Dans un deuxième temps, six carbon dots, représentatifs de l'échantillonnage initial en particules et des différents groupes de toxicité identifiés, ont fait l'objet d'une étude comparative descriptive et mécanistique approfondie sur différentes lignées cellulaires (THP-1, Calu-3 et A549). Il est ressorti de ce travail que le niveau de cytotoxicité des nanoparticules et leur capacité à induire une réponse inflammatoire varient selon le type cellulaire, les cellules A549 et Calu-3 s'avérant significativement moins sensibles que les cellules THP-1, ceci quel que soit le type de carbon dot (fortement ou modérément toxique). Une étude d'internalisation cellulaire des particules par cytométrie en flux et microscopie de fluorescence (grâce aux propriétés

de fluorescence intrinsèque des carbon dots) a montré que seules les particules cytotoxiques sont internalisées, et que les mécanismes de cette internalisation dépendent du type cellulaire. Ainsi, si dans la lignée THP-1, l'internalisation des carbon dots fait intervenir des processus actifs et implique plusieurs voies d'endocytose, dans les cellules A549, aucun mécanisme clair d'endocytose n'a pu être identifié. Pour compléter cette étude comparative, nous avons montré que les carbon dots cytotoxiques, contrairement aux carbon dots peu ou non toxiques, induisent un stress oxydant et perturbent le fonctionnement de la mitochondrie, deux effets qui expliquent leur toxicité. Les données de cette étude comparative *in vitro* résumées dans le tableau 1 suggèrent que la charge nette positive des particules n'est pas suffisante pour prédire leur toxicité, mais que la densité de groupements aminés protonables (titrables) pourrait, quant-à-elle, être un élément déterminant.

	MC-34	MC-225	MC-136	MC-131	MC-148	MC-56
Reactants	Citric acid bPEI 25K	Citric acid bPEI 600	Citric acid PEHA	Citric acid DMEDA	Citric acid DMEDA mPEG 550	Citrate NH <sub>4</sub> <sup>+</sup> KH <sub>2</sub> PO <sub>4</sub>
Surface chemistry						
Size (nm) (Saline solution, DLS)	13 ± 3	10 ± 2	19 ± 4	44 ± 10	18 ± 4	25 ± 5
Charge (mV) (Saline solution, DLS)	+43 ± 9	+25 ± 3	+30 ± 2	+21 ± 2	+27 ± 2	-40 ± 1
Cytotoxicity (MTT assay)	High	High	Moderate	Moderate	None	None
Oxidative stress (Reduced GSH)	Yes	Yes	None	None	None	None
Inflammation (IL-8)	Yes	Yes	None	None	None	None
Inflammasome (IL-1 beta)	Yes	Yes	None	None	None	None
Mitochondrial perturbation (JC-10)	Yes	Yes	None	Test interaction		None
Cell uptake (FACS, Imaging)	Yes	Yes	Yes	Yes	None	None

**Tableau 1** : Données issues de l'étude de cytotoxicité comparative approfondie menée sur 6 carbon dots représentatifs de l'échantillonnage initial en nanoparticules.

Dans une dernière partie de ce travail d'évaluation de la toxicité des carbon dots en fonction de leurs caractéristiques physico-chimiques, la sélection de particules a fait l'objet d'une étude de toxicité respiratoire *in vivo* chez la souris, après administration pulmonaire. Les résultats obtenus chez la souris ont confirmé les données mises en évidence *in vitro*, à savoir que seuls les carbon dots s'étant avérés cytotoxiques pour les cellules en culture ont induit une réponse inflammatoire pulmonaire caractérisée par une infiltrat de neutrophiles et de macrophages et la production de cytokines dans le poumon. Nous avons également montré que l'inflammation induite par ces particules est dose-dépendante.

#### - Carbon dots, vecteurs de transfert de gène

Dans la deuxième partie de mon travail, nous nous sommes attachés à étudier le potentiel de différents carbon dots chargés positivement en tant qu'agents de transfection. Nous avons ainsi essayé de dégager des relations "structure-activité" et de concevoir de nouvelles nanoparticules avec des aptitudes au transfert de gène optimisées. Plusieurs dizaines de carbon dots ont été évalués dans un crible utilisant un gène rapporteur. Ce gène code pour la luciférase, une protéine qui émet de la (bio)luminescence en présence de son substrat. Ainsi, la mesure de la bioluminescence émise permet de quantifier directement l'efficacité de transfection du vecteur utilisé et, ainsi, de comparer les vecteurs entre-eux. Ces évaluations ont été conduites sur la lignée de cellules épithéliales pulmonaires A549. Pour chacune des nanoparticules étudiées, une optimisation de la formulation (rapport en poids vecteur/ADN, quantité d'ADN utilisée) a été réalisée et la cytotoxicité des complexes carbon dots-ADN a été systématiquement déterminée. Le résultat majeur qui ressort de notre étude est que le mode de fabrication des carbon dots est un facteur critique pour l'efficacité des nanoparticules en transfection. Toutes choses étant égales par ailleurs (nature de la source de carbone et des additifs, et stœchiométrie des réactifs), le mode d'activation utilisé lors de la pyrolyse de la matière organique pour former les carbon dots s'est révélé excessivement important pour l'activité de transfection. De façon tout à fait intéressante et intrigante, la charge positive intrinsèque des carbon dots ne semble pas directement liée à l'efficacité de transfection de ces vecteurs. Certes, seules les particules

chargées positivement ( $\square \square > +15 \text{ mV}$ ) sont capables de permettre l'internalisation cellulaire du gène rapporteur, mais abondance de charges positives ne rime pas forcément avec efficacité de transfection plus élevée.

Les carbon dots préparés à partir d'oligoamines de haut poids moléculaire (bPEI25k et bPEI600) se sont révélés les plus performant en transfection. Cependant, l'élimination du bPEI25k en excès lors de la phase de purification des carbon dots par dialyse n'est pas totale et le résidu (10 à 30 %) induit une forte toxicité et masque en partie le potentiel de transfection des carbon dots. Pour les carbon dots préparés à partir du bPEI600, l'élimination de bPEI600 résiduel ne pose pas de problème particulier. Par ailleurs, contrairement au bPEI25k qui est un agent de transfection efficace, le bPEI600 à l'état de polymère est incapable de promouvoir l'internalisation cellulaire d'un ADN et présente une très faible cytotoxicité. Pour ces deux raisons, nous avons concentré nos travaux sur les nanoparticules à base de bPEI600, en optimisant les paramètres du procédé de fabrication (stœchiométrie des réactifs, mode d'activation/chauffage, température, durée...). Ceci a permis de produire des nanoparticules très performantes en transfection et peu cytotoxiques (figure 3).

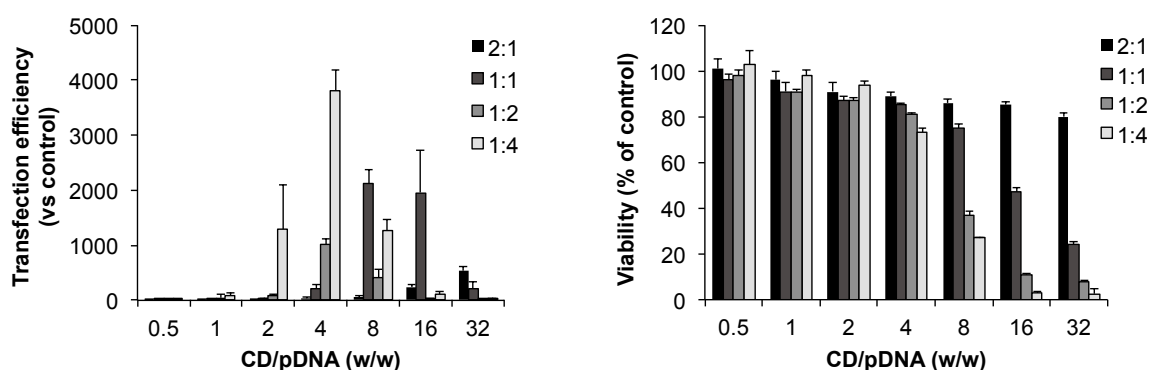


**Figure 3.** Efficacité de transfection et cytotoxicité de carbon dots préparés à partir d'acide citrique et de bPEI600 dans des rapports en poids variables (2:1 à 1:4).

## Conclusions

À partir d'une collection de carbon dots disponible au laboratoire et qui a été complétée tout au long de ce travail de thèse, nous avons développé une étude visant à identifier les déterminants de la toxicité des nanoparticules. Si la taille des nanoparticules joue un rôle important (forte surface spécifique et réactivité), elle ne constitue pas, à elle seule, un élément

prédictif de la toxicité des nanoparticules. La charge et, surtout, la chimie de surface conditionnent dans un large mesure les interactions entre les nanoparticules et le milieu biologique et, donc, leur toxicité intrinsèque.

Dans la deuxième partie de mon travail de thèse visant à évaluer l'activité de carbon dots cationiques dans des expériences de transfert de gène, nous avons pu montrer la supériorité des nanoparticules préparées à partir d'acide citrique et de bPEI600 sur toutes les autres que j'ai pu tester. Ces évaluations nous ont permis, étape par étape, d'améliorer l'efficacité de ces agents de transfection jusqu'à surpasser celle du bPEI25k, sans toxicité notable.

# Table of Contents

<b>Abbreviation table</b> .....	<b>iii</b>
<b>Acknowledgements</b> .....	<b>v</b>
<b>Abstract</b> .....	<b>vii</b>
<b>Part 1 Introduction</b> .....	<b>1</b>
<b>1.1. Nanoparticles</b> .....	<b>3</b>
1.1.1. Lipid-based NPs .....	3
1.1.2. Polymeric NPs .....	6
1.1.3. Inorganic NPs .....	10
1.1.4. Carbon-based NPs .....	12
<b>1.2. NPs for biomedical applications</b> .....	<b>15</b>
1.2.1. Bioimaging .....	16
1.2.2. Biosensing .....	16
1.2.3. Drug delivery .....	17
1.2.4. Gene therapy.....	19
<b>1.3. Cellular internalization and fate of NPs</b> .....	<b>20</b>
1.3.1. Internalization pathways.....	20
1.3.2. Intracellular fate of NPs.....	24
<b>1.4. Nanotoxicology and underlying mechanisms</b> .....	<b>28</b>
1.4.1. NP cytotoxicity and underlying mechanisms .....	29
1.4.2. NPs and the immune system.....	31
1.4.3. Physicochemical characteristics that govern NP toxicity .....	32
1.4.4. Cell susceptibility to NP toxicity .....	35
<b>1.5. Carbon dots</b> .....	<b>36</b>
1.5.1. Structure.....	36
1.5.2. Photoluminescent properties.....	37
1.5.3. Synthesis .....	38
1.5.4. Biomedical applications .....	42
1.5.5. Toxicology.....	46
<b>Part 2 Objectives, materials, and methods</b> .....	<b>49</b>
<b>2.1. Objectives of the thesis</b> .....	<b>51</b>
<b>2.2. Materials</b> .....	<b>52</b>
2.2.1. Preparation of the CDs .....	52
2.2.2. Characterization of CDs .....	54
<b>2.3. In vitro evaluation of CDs</b> .....	<b>54</b>

2.3.1. Cell culture .....	54
2.3.2 Viability assay after cell exposure to CDs .....	55
2.3.3. Assessment of CD internalisation .....	56
2.3.4. Measurement of mitochondrial membrane potential in response to CDs: JC-10 assay .....	57
2.3.5. Measurement of oxidative stress in response to CDs: determination of reduced glutathione .....	58
2.3.6. Cytokine assays .....	58
2.3.7. Evaluation of CD transfection efficiency .....	59
<b>2.4. In vivo evaluation of CDs.....</b>	<b>60</b>
2.4.1. Animals.....	60
2.4.2. Animal exposure to CDs .....	60
2.4.3. Bronchoalveolar lavage fluid collection.....	60
2.4.4. Evaluation of lung inflammation evoked by CDs .....	61
<b>2.5. Statistical analysis of the results.....</b>	<b>61</b>
<b>Part 3 Results and discussion .....</b>	<b>63</b>
<b>3.1 Safety evaluation of CDs in in vitro and in vivo models .....</b>	<b>65</b>
3.1.1 Presentation of the CD library .....	65
3.1.2. Analysis of factors contributing to CD cytotoxicity using the whole library ...	71
3.1.3. In-depth toxicity study on a focused CD library .....	79
3.1.4. Conclusions .....	99
<b>3.2. Evaluation of CDs as gene carriers.....</b>	<b>101</b>
3.2.1. Description of the CD Library.....	101
3.2.2. Factors affecting the transfection efficiency of CDs .....	105
3.2.3. Conclusion.....	115
<b>3.3. General conclusions.....</b>	<b>116</b>
<b>Outlook .....</b>	<b>117</b>
<b>Bibliography.....</b>	<b>119</b>



## Abbreviation table

ALT	Alanine aminotransferase
AST	Aspartate aminotransferase
BAL	Bronchoalveolar lavage fluid
CA	Citric acid
CDs	Carbon dots
CLSM	Confocal laser scanning microscopy
CM	Cell membrane
CME	Clathrin-mediated endocytosis
CNDs	Carbon nanodots
CNTs	Carbon nanotubes
CQDs	Carbon quantum dots
CT	Computed tomography
DDS	Drug delivery system
DOX	Doxorubicin
EPR	Enhanced permeability and retention
FACS	Flow cytometry
FRET	Förster Resonance Energy Transfer
GQDs	Graphene quantum dots
GSH	Glutathione
HA	Hyaluronic acid
HPG	Hyperbranched polyglycerol
LDL	Low-density lipoprotein
miRNA	Micro RNA
MRI	Magnetic resonance imaging
MSNs	Mesoporous silica nanoparticles
NAD	Nicotinamide
NPs	Nanoparticles
PDT	Photodynamic therapy
PEG	Poly(ethylene glycol)
PEI	polyethylenimine
PK	Pharmacokinetics
PL	Photoluminescence
QDs	Quantum dots
ROS	Reactive oxygen species
siRNA	Small interfering RNA
SLNP	Solid-lipid nanoparticle



## Acknowledgements

I would like to express my deepest appreciation to my advisors, Professor Françoise PONS and Dr. Luc LEBEAU, who continuously shared their wisdom, knowledge and experience with me. During the last three years, Professor Françoise PONS always encouraged and supported me in every single step I took towards conducting good research. I am lucky to have Dr. Luc LEBEAU as my mentor and I will always be motivated by his attitude and substance of a scientist.

My sincere thanks also go to my collaborators and fellow lab members: Dr. Carole RONZANI, Dr. Anne CASSET, Dr. Maud WEISS, Mickaël CLAUDEL, Boris GAILLARD, Thomas SONNTAG. They are great colleagues and friends, always helpful and supportive.

Thanks to those outside of the lab who have spurred me on to achieve what is written on these pages. To my parents, for their constant encouragements even when they did not understand the science, for their financial help and for many supportive phone calls. I have to say thank you to my wife Mimi and my son Yinxi: together we had good times, and there is nothing more meaningful to me than your unconditional love and support in these years.

Last, I am grateful to the China Scholarship Council for providing scholarship for my studies in France. Also, thanks to the beautiful France, where I completed my studies and formed my family. I will always miss this beautiful period in France.



## Abstract

Carbon dots (CDs) are the latest member of the family of carbon nanoparticles (NPs) to be discovered. They were isolated for the first time in 2004, during electrophoresis purification of carbon nanotubes. In addition to their nanometric size, these objects are almost spherical and hydrophilic, and are generally presented as biocompatible and very weakly toxic NPs. They are fairly easily accessible by synthesis and can be conveniently modified by reaction of the functional groups present on their surface (amines, carboxylic acids, alcohols, *etc.*). Finally, they exhibit intrinsic fluorescence properties, are relatively resistant to photobleaching, and can be excited by multi-photon irradiation. Thus, like the other members of the family of carbon NPs (graphene, nanodiamonds, fullerenes, nanotubes), CDs have remarkable properties which are the subject of intense research for applications in fields as different as those of electronics, catalysis, energy storage, imaging, and medicine. In the latter area, CDs can find applications as drug delivery systems, like other NPs successfully developed in this field. The work developed during this thesis had two distinct objectives. The first one was to identify the intrinsic physicochemical properties responsible for the toxicity of NPs. For this, the toxicological profile of a large collection of CDs produced in the laboratory and exhibiting various size, charge, and surface chemistry was characterized using *in vitro* lung models and mice. We then found that although the size of the NPs plays an important role (high specific surface area and reactivity), it is not, by itself, a predictive element of the toxicity of the NPs. The charge and the surface chemistry largely effect the interactions between the NPs and the biological medium systems and, therefore, their intrinsic toxicity. The second objective of this thesis was to assess the potential of CDs in the field of drug delivery. In particular, I have been interested in the potential of positively charged CDs as synthetic gene carriers. In this part of my PhD work, we were able to show the superiority of NPs prepared from citric acid and bPEI600 over all other cationic CDs produced in the laboratory. A systematic evaluation has allowed us, step by step, to improve the efficiency of these transfection agents, to exceed that of bPEI25k, a gold standard for *in vitro* transfection, without significant toxicity.

Overall, this work opens up new horizons in NPs research that may provide 1-a better understanding of the toxicological mechanisms of NPs, especially their determinants, and 2-identification of the relationship between the CDs synthesis methods and the efficiency of these NPs as DNA transfection reagents.



# **Part 1**

## **Introduction**





## 1.1. Nanoparticles

Nanoparticles are generally considered as any particulate solid or colloidal material of size ranging from 1 to 100 nm in one or more dimensions ([Schmid, 2005](#)). NPs exhibit a wide diversity in terms of size, chemical composition (lipid, polymer, carbon, metal, *etc.*), shape (sphere, cube, rod, plate, *etc.*), and surface properties (charge, chemistry, *etc.*) ([Sun et al., 2014](#)). Compared to their corresponding bulk material, NPs exhibit unique optical, magnetic, catalytic, thermodynamic and electrochemical properties ([Brites et al., 2012](#)). Their physicochemical features can be tuned by modifying their chemical composition and surface properties, introducing various functional groups at their surface to suit particular applications ([Dam et al., 2014](#); [Subbiah et al., 2010](#)). It is thus possible to provide NPs with potential for a wide range of applications in various fields, such as electronics, energy collection and storage, communications, imaging and medicine ([Wolfbeis, 2015](#)). In the following paragraphs, I will briefly introduce the NPs that are widely studied in the biomedical field.

### 1.1.1. Lipid-based NPs

Lipids are organic compounds containing hydrocarbons that can be extracted from plants and animals by low polarity solvents. Common lipids include oils, waxes, cholesterol, sterols, monoglycerides, diglycerides, triglycerides, phospholipids and fat-soluble vitamins. Lipid-based nanoparticles have been widely used in bioimaging and drug carrier applications ([Li and Szoka, 2007](#); [Mulder et al., 2006](#)). Here, I briefly introduce liposomes and solid-lipid NPs.

#### 1.1.1.1. Liposomes

Liposomes were first discovered by Alec D. Bangham in the late 1960s at the Babraham Institute (Cambridge University) ([Bangham and Horne, 1964](#); [Kraft et al., 2014](#)). Liposomes are representative NPs that have been successfully transformed into clinical applications. They are spherical vesicles of a diameter of 50 to 500 nm that consist of one or more phospholipid bilayers. They are spontaneously formed when lipids are emulsified in an aqueous medium, the aqueous medium being captured within the core of the liposome after the formation process is completed. Thus, liposomes are widely used to encapsulate drugs. The liposome-forming lipids include phosphatidylcholine-rich phospholipids, which are either natural or synthetic. The bilayer membrane composition determines the liposome permeability, surface charge and hydrodynamic behavior. The morphology of liposomes is similar to that of cell membranes, and because they are capable of encapsulating or binding

various substances, liposomes are considered as ideal drug carrier systems. Sercombe *et al.* recently reviewed the literature related to liposomes as drug delivery systems (DDS) (Sercombe *et al.*, 2015). In figure 1, a schematic representation of four main types of liposomes used as DDS is shown, including conventional (A), pegylated (B), ligand-targeted (C) and theranostic (D) liposomes. Poly(ethylene glycol) (PEG) coated (*i.e.* pegylated) liposomes, often referred as stealth liposomes, exhibit improved stability and enhanced circulation time in the blood. The establishment of a steric barrier around the particle improves the efficacy of the encapsulant by reducing the *in vivo* conditioning by serum components and the rapid identification and uptake by the reticuloendothelial system (RES). This not only reduces drug elimination by prolonging blood circulation and accumulation in pathological sites, but also reduces side effects (Ishida *et al.*, 2001). Ligand-targeted liposomes can localize drugs to specific cell types or organs in the body, selectively expressing or overexpressing specific receptors at disease sites (Forssen and Willis, 1998). There are many ligands that can be used, such as antibodies, peptides/proteins and carbohydrates (figure 1, C). Multifunctional liposome formulations have the potential to be integrated tools for therapeutic and diagnostic use. Controlled drug release, delivery of therapeutic combinations, and imaging capabilities can be obtained by employing targeting strategies that involve one or more targeting ligands (figure 1, D) (Cole and Holland, 2015).

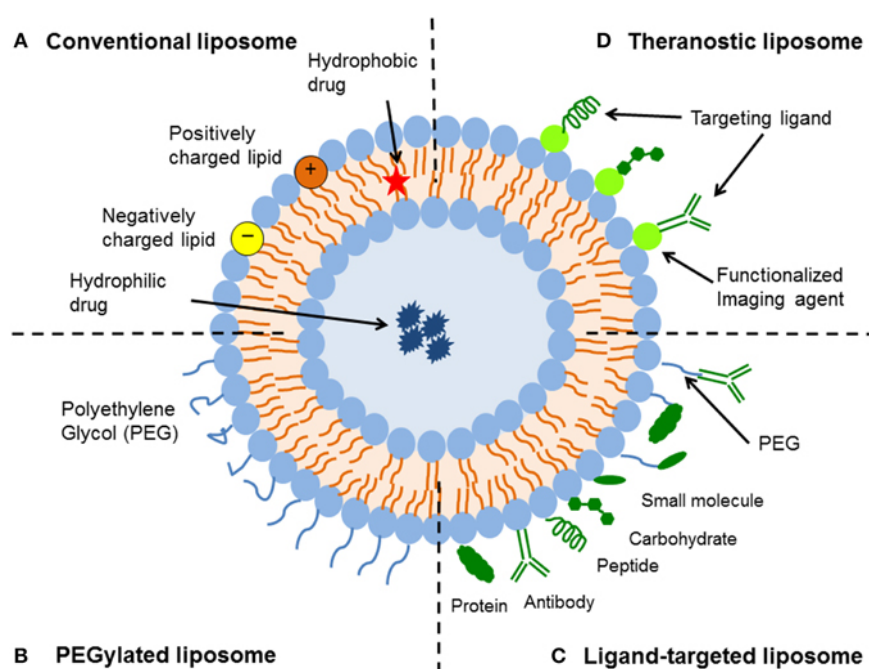


**Figure 1.** Four types of liposome-based DDS. (A) Conventional liposome: composed of a lipid bilayer and encapsulating an aqueous core; (B) PEGylated liposome: a hydrophilic polymer coating (PEG) is introduced at the surface of the liposome to improve steric stabilization. (C) Ligand-targeted liposome: Antibodies, peptides or carbohydrates are attached to the surface, eventually through a PEG spacer, for specific targeting. (D) Theranostic liposome: incorporating targeting elements, imaging components and therapeutic components (Sercombe *et al.*, 2015).

In the past few decades, liposomes have been extensively studied as DDS and significant progress have been made in this research field (Sercombe *et al.*, 2015). However, though liposomes have moved into clinical applications some challenges remain, especially the establishment of methods for large scale production and full characterization of ligand-functionalized liposome preparations, as well as of preclinical models of *in vivo* tumors for assessing their performances as DDS (Belfiore *et al.*, 2018).

### 1.1.1.2. Solid-lipid nanoparticles (SLNPs)

Discovered in the early 1990s, SLNPs stand for a class of colloidal particles composed of lipids that are solid at both room and body temperature (Müller *et al.*, 2000). The use of solid lipids, instead of liquid oils, allows a controlled drug release because the flowability of drugs in solid lipid matrices is much lower than in liquid oils. Therefore, SLNPs are used as an alternative carrier system for emulsions and polymer NPs (Mehnert and Mäder, 2012). SLNPs whose size ranges from 50 to 100 nm are biodegradable, and thus are considered as biocompatible. They have a stable structure and therefore provide a better protection against chemical degradation of encapsulated drugs (figure 2)(Yingchoncharoen *et al.*, 2016). In addition, their side effects are greatly reduced compared to other lipid/micelle nanostructures (Chen *et al.*, 2016; Wissing *et al.*, 2004). However, how to reduce the burst release of drugs from SLNPs is currently a huge challenge (Geszke-Moritz and Moritz, 2016). Furthermore, the health risks associated with exposure to SLNPs in humans remain to be explored.

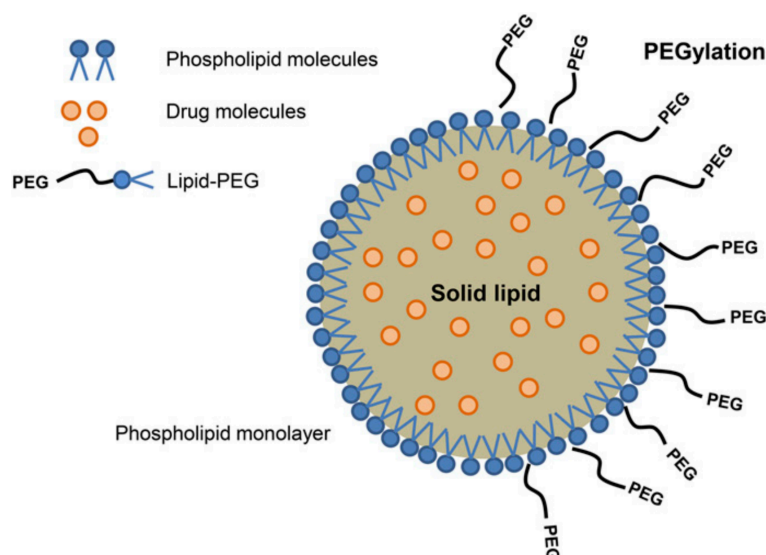


**Figure 2.** Scheme of SLNs. Solid lipids are used as matrix materials in which hydrophobic drugs can be stored. The lipid matrix is then stabilized by a biocompatible surfactant, in which case the surfactant is a phospholipid and/or a lipid-PEG (Yingchoncharoen *et al.*, 2016).

## 1.1.2. Polymeric NPs

Polymeric NPs are nanocapsules or nanospheres prepared from natural (chitosan, alginate...) or synthetic (polylactic acid, poly(lactic-co-glycolic) acid...) polymers, which are usually biodegradable ([Hans and Lowman, 2002](#); [Soppimath et al., 2001](#)). These NPs offer a great flexibility in terms of chemical composition, size, biodegradability, morphology, and surface functionalization. Because of these advantages, applications of polymeric NPs are expected in several fields including sensing, imaging and drug delivery ([Chan et al., 2010](#); [Gagliardi et al., 2012](#)). As drug carriers, they offer the possibility to control the release of their cargo through the tunable kinetics of the biodegradation of the polymer backbone and, in some cases, by exploiting appropriate stimuli to activate this degradation. These stimuli include passive ones, such as changes in pH that cause NP swelling, and active ones such as light-activation for cleavage of photolabile bonds in the polymer backbone ([Abdal-hay et al., 2015](#); [Bae et al., 2007](#)). Here, I will introduce some selected polymeric NPs: polyethylenimine (PEI), polymeric micelles, and dendrimers.

### 1.1.2.1 Polyethylenimine

Polyethylenimine (PEI) and derivatives have received attention as DNA and RNA delivery carriers. They exist as branched as well as linear polymers. The synthetic route to linear and branched PEI is shown in figure 3 ([Neu et al., 2005](#)). PEI molecular weight ranging from 5 to 25 kDa was shown to be suitable for nucleic acid delivery applications ([Fischer et al., 2003](#)). The most prominent feature of PEI is its high cationic charge density, allowing to control polymer dissociation, aggregation, interaction with biomolecules, and activation of the complement system.

PEI has become a very interesting candidate for enhancing DNA uptake and expression under *in vitro* and *in vivo* conditions. And their transfection efficiency is similar to viral vectors ([Neu et al., 2005](#)). The complex of DNA and PEI protects DNA from nucleases. PEI is capable of condensing plasmid DNA and RNA into stable complexes by electrostatic interaction. The complexation and condensation behavior depends on several polymer properties, such as molecular weight, number and charge density, and the composition of the complex, *i.e.*, the weight ratio of polymer to nucleic acid. In fact, lower charge density and lower molecular weight affect the ability of the polymer to condense DNA ([Wolfert and Seymour, 1996](#)). PEI and DNA form complexes due to electrostatic interactions, but quantifying free PEI is a challenge. Recent studies using fluorescence correlation spectroscopy have shown that when prepared at N/P ratios (molar ratio of PEI nitrogen atoms to DNA phosphate) of 6 and

10, approximately 86% of PEI was found to be in the free form ([Clamme et al., 2003](#)). These free PEI molecules have an effect on cytotoxicity. A study indicated that removal of excess PEI can reduce cytotoxicity, however, this also leads to reduced transfection efficiency ([Boeckle et al., 2004](#)). Thus, PEI is an excellent gene vector but much work needs to be done before it goes to the clinic. For example, more research is needed on the systemic stability of the PEI/DNA complexes and their interaction with the body. In addition, more detailed studies are needed to characterize acute and long-term toxicity of this carrier ([Neu et al., 2005](#)).

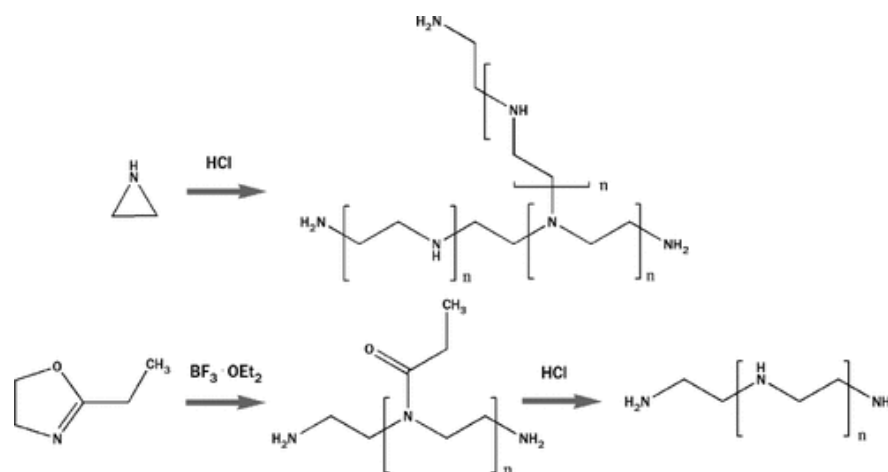


**Figure 3.** The synthetic route of linear and branched PEI is summarized by Michael *et al.* The acid catalyzed polymerization of aziridine results in branched PEI, while the ring opening polymerization of 2-ethyl-2-oxazoline produces an N-substituted polymer which can be converted to linear PEI by hydrolysis ([Neu et al., 2005](#)).

### 1.1.2.2. Polymeric micelles

Polymeric micelles are vesicular structures composed of amphiphilic polymers that spontaneously self-assemble in water to form usually spherical nanostructures of 10 to 200 nm in size. In aqueous media, the hydrophilic moieties of the polymer are in contact with water, forming a corona and sequestering the hydrophobic, *i.e.* solvophobic, polymer regions in the core of the micelle ([Tuzar and Kratochvil, 1976](#)). Polymeric micelles can thus sequester hydrophobic drugs within their core, and their versatility makes them useful in the field of drug delivery so they are widely explored as DDS ([Kataoka et al., 2001](#)). The structure of polymeric micelles is shown in figure 4 ([Riggio et al., 2011](#)). The polymeric micelles, as a drug delivery vehicle, can simultaneously encode two or more therapeutic agents and are capable of releasing the drug in a regulated manner. The hydrophobic core dissolves and physically embeds the drug (lipophilic drug) in the internal region with high load capacity. Hydrophilic shells

not only improve their stability in the blood, but also provide functional groups suitable for further micelle modification. The encapsulated drug can be released by a variety of routes, such as erosion of a biodegradable polymer, diffusion of the drug through the polymer matrix, or swelling of the polymer followed by drug diffusion. In addition, changes in external conditions such as pH and temperature can also induce micelle release of the drug (Riggio *et al.*, 2011). Thus, with the tremendous advances in nanoscience, these colloidal systems have been designed to selectively accumulate in solid tumors, to have improved loading capacity, to possess targeting ability through surface modification with tumor-homing ligands or aptamers, and thus exhibit better therapeutic efficacy. Although many polymeric micelle-based DDS are involved in clinical trials (Cabral and Kataoka, 2014), their process scalability remains a serious challenge, and more sound methods are still needed to fully translate basic research into clinical practice. In addition, the limited understanding of the preclinical and clinical aspects of these materials has caused serious failures to realize their full potential in clinical practice. To address these issues, a thorough understanding of biodistribution, pharmacokinetics, pharmacodynamics, immunogenic reactions, and *in vivo* degradation profiles is essential (Deshmukh *et al.*, 2017).

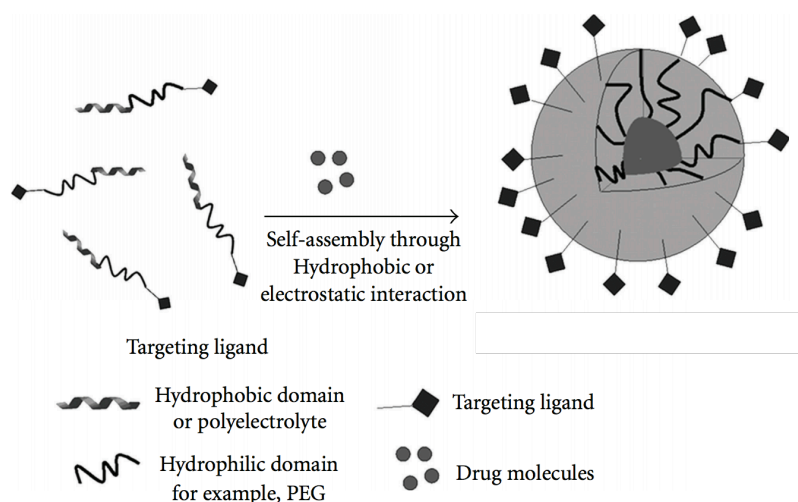


**Figure 4.** The core-shell structure of polymer micelles and their drug encapsulation scheme. Polymeric micelles are formed by self-assembly of block copolymers composed of two or more polymer chains having different hydrophobicities. These copolymers are spontaneously assembled to form a core-shell structure in an aqueous medium (Riggio *et al.*, 2011).

### 1.1.2.3. Dendrimers

Dendrimers are a family of synthetic polymers with three-dimensional, highly branched and well-defined structures. Voegtle and colleagues reported the production-of the first dendrimer-like compound, polypropylene imine (PPI) in 1978 (Buhleier *et al.*, 1978). In the mid-1980s, Tomalia and colleagues synthesized advanced dendrimers with well-



defined structures (Tomalia *et al.*, 1985). A review by Liu *et al.* summarizes the structural features of dendrimers (figure 5) (Liu *et al.*, 2012a). Typical dendrimers display a central core with two or more reactive groups. Their inner layers consist of repeated branched units covalently linked to the core. In addition, terminal functional groups are present on the outer surface of the dendrimer molecule. In general, dendrimers are synthesized in a decentralized or convergent manner by stepwise iterative coupling methods.

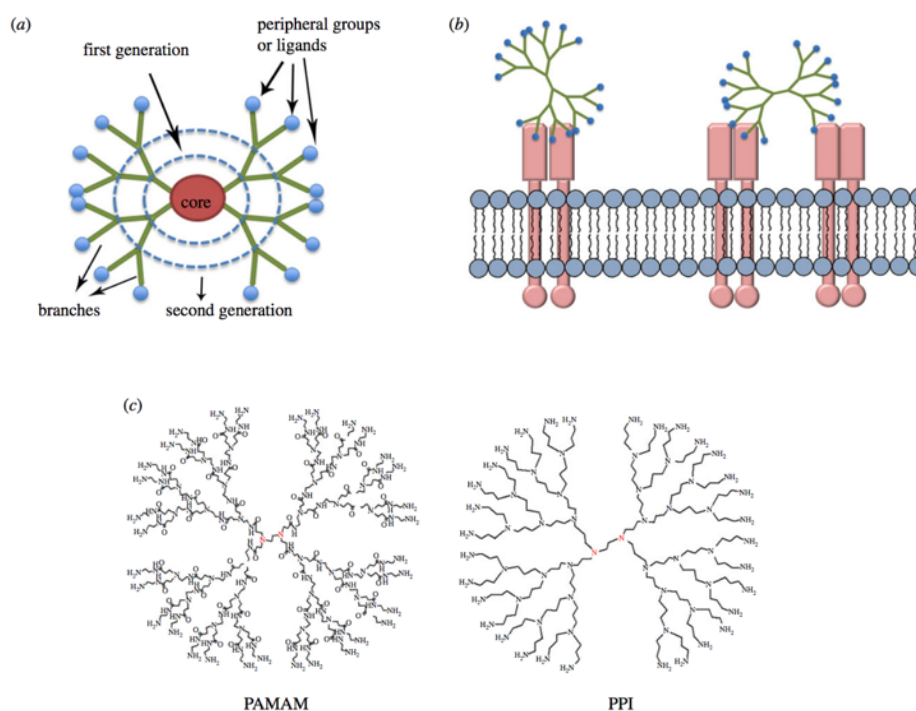


**Figure 5.** (a) Schematic diagram of the dendrimer structure: the core, internal branches and peripheral groups. The branches grow radially with each generation, then, the size and function of the dendrimers can be adjusted simultaneously. (b) Biologically active dendrimer can interact with specific receptors on the cell membrane. (c) Structure of two commonly used dendrimer materials (Liu *et al.*, 2012a).

Dendrimers are considered as promising drug carriers. The drug can be physically entrapped into the inner lumen of the dendrimer or chemically conjugated to the terminal functional groups thanks to the rich internal cavity and surface functionality. In the past few decades, a large number of biodegradable dendrimers with various structures and properties have been successfully designed for different purposes (Abbasi *et al.*, 2014). Compared with non-degradable dendrimers, biodegradable dendrimers display all the advantages of dendrimers, further demonstrating the advantages of being degraded into small fragments that can be metabolized or excreted from the body (Lee *et al.*, 2005).

However, despite significant progress in the synthesis and application of biodegradable dendrimers, there are still some issues that need to be addressed ([Cheng et al., 2011](#)). In the first place, most of the reported biodegradable dendrimers are polyester dendrimers, many of which can undergo unwanted hydrolysis leading to acidic by-products that can cause local inflammation. Secondly, drug encapsulation by dendrimers is often characterized by low capacity and unavoidable burst release. Furthermore, conjugation strategies may be inaccurate and inconsistent conjugates result in inefficiencies. Finally, the synthesis of most biodegradable dendrimers remains tedious and expensive. Therefore, the synthesis and application of novel biodegradable dendrimers need to be further explored ([Cheng et al., 2011](#)).

### **1.1.3. Inorganic NPs**

The advantages of inorganic nanoparticles stem from their stability and high resistance to enzymatic degradation. Among inorganic NPs, metallic NPs also enable multifunctional therapeutics and diagnosis based on their intrinsic electronic, optical and magnetic properties. Though these NPs can be excreted *via* the renal or fecal route due to their small size (< 20 nm), an important issue is that they can evoke toxicity due to the release of toxic metal ions, such as Cd<sup>2+</sup>, Fe<sup>3+</sup> or Ag<sup>+</sup> ([Park et al., 2007](#); [Pujalté et al., 2011](#)).

#### **1.1.3.1. Mesoporous silica nanoparticles (MSNs)**

MSNs are one of the earliest NPs used in the biomedical field, firstly introduced by Mobil corporation scientists in 1992 ([Kresge et al., 1992](#)). The size of MSNs can be controlled in the range of 50 to 300 nm, which is suitable for endocytosis by living cells. MSNs have a uniform pore size and a long-range ordered mesoporous structure, which allow precise control of drug loading and release kinetics. They show a high potential for molecule loading and dissolution enhancement due to the large pore volume and surface area. The external surface of the MSNs can be conjugated to a targeting ligand for efficient cell-specific drug delivery ([Wang et al., 2015b](#)). In addition, MSNs are considered to be biocompatible and degrade after administration, which facilitates the release of the cargo ([He et al., 2010b](#)). MSNs are mainly excreted in feces and urine ([Fu et al., 2013](#)). Some MSN-derived products for targeted molecular imaging have been approved by the FDA for Phase I human clinical trials ([Benezra et al., 2011](#)). However, basic information about their blood circulation characteristics, *in vivo* clearance time, possible immunogenicity and tissue accumulation remains to be investigated in more details.



### 1.1.3.2. Magnetic NPs (MNPs)

Common examples of MNPs include several types of iron oxide nanoparticles such as  $\text{Fe}_3\text{O}_4$ ,  $[\alpha]\text{-Fe}_2\text{O}_3$  and  $[\gamma]\text{-Fe}_2\text{O}_3$ . Among them, superparamagnetic iron oxide ( $\text{Fe}_3\text{O}_4$ ) NPs have been widely used in bioseparation, biosensing, magnetic field-assisted drug and gene delivery, and magnetic therapy for cancer ([Berry and Curtis, 2003](#)). MNPs also can be designed for highly specific targeted delivery by surface coating with high affinity biomolecules ([Majewski and Thierry, 2007](#)). These NPs are suitable for the detection and manipulation of biological materials such as proteins, viruses, genes, or whole cells, based on their narrow size distribution (between 5 and 50 nm) ([Berry and Curtis, 2003](#); [Pankhurst et al., 2009](#)). However, the toxicity of MNPs needs to be considered. Excess iron can be extremely toxic. After their endocytosis-mediated internalization into cells, MNPs accumulate in lysosomes and are degraded into iron ions by a series of hydrolases at acidic pH of lysosomes ([Gupta et al., 2007](#)). Iron released from MNPs is metabolized in the RES and subsequently used to form red blood cells or excreted through the kidneys ([Anzai et al., 2003](#)). High levels of free iron ions released from MNPs can cause homeostasis imbalances and lead to abnormal cellular responses, including DNA damage, oxidative stress, epigenetic events, and inflammatory processes ([Häfeli et al., 2009](#)). The toxicity of MNPs can be reduced by surface functionalization. For example, magnetite NPs coated with a triblock copolymer comprising poly(ethylene glycol) (PEG) are biocompatible and suitable for *in vivo* applications ([Häfeli et al., 2009](#)).

### 1.1.3.3. Silver NPs

Silver has high thermal conductivity and electrical conductivity, and nanoscale silver is considered to be more effective than its macroscopic form ([Firdhouse and Lalitha, 2015](#)). Silver NPs (AgNPs) have gained wide attention due to their physicochemical and biological properties. They are thus considered to be particularly suitable for wound healing applications due to their antibacterial activity ([Konop et al., 2016](#)). In any case, some toxicological studies have shown that AgNPs are toxic to the environment and the human body. Therefore, when using AgNPs, their size, dosage and exposure pathway should be considered ([Antony et al., 2015](#)).

### 1.1.3.4. Gold NPs

Gold NPs are potential vehicles for drug and gene delivery, providing a useful complement to more “traditional” DDS ([Ghosh et al., 2008](#)). They have low intrinsic toxicity, high surface area, and adjustable stability, which provide them with a broader

application prospect. The surface of gold NPs can be easily modified and then combined with drugs and genes by various methods. Gold NPs can thus act as a carrier to achieve controlled release and targeted drug delivery. In addition, by changing the shape and size of gold NPs, unique fluorescence, photothermal and photochromic properties can be obtained. Therefore, gold NPs can have applications in photothermal therapy and bioimaging ([Liang et al., 2015](#)). However, the key issue that needs to be addressed is the optimized engineering properties of the particle surface, such as bioavailability and non-immunogenicity.

#### **1.1.3.5. Quantum dots (QDs)**

Quantum dots (QDs) are a class of semiconductor nanocrystals, with size of 2-10 nm. QDs generally have a core/shell conjugated structure, the core being composed of Group II-VI (e.g., CdSe, CdTe, CdS, PbSe, ZnS, and ZnSe) and III-V (e.g., GaAs, GaN, InP, and InAs) atoms ([Chan et al., 2002](#)). The fluorescence bands of QDs depend on their composition, size and shell thickness. In addition, the advantages of QDs include tunable optical properties, high quantum yield, and photostability. Today, QDs have been applied in solar cells, photovoltaic devices, light-emitting diode photodetector and computer manufacturing, and in biomedical imaging ([Matea et al., 2017](#)). In any case, QDs are expected to release free metal ions when exposed to conditions that promote degradation, such as under physiological conditions and many of the metals used to form the core of QDs are toxic at low concentration, as is the case for cadmium, tellurium, lead and arsenic. Therefore, toxicity is a key factor that restricts QD applications, especially in the biomedical field ([Lewinski et al., 2008](#)).

#### **1.1.4. Carbon-based NPs**

Carbon is abundant in nature and it has  $sp^3$ ,  $sp^2$  and  $sp$  hybrid orbitals. Carbon materials are superior to many other materials in terms of hardness, optical properties, heat resistance, radiation characteristics, chemical resistance, electrical insulation, electrical conductivity, and surface and interfacial properties. More and more new carbon-based NPs continue to be discovered and synthesized. These materials have very different morphologies and unique chemical properties, but they still have much in common, especially in terms of basic structural units (figure 6) ([Yan et al., 2016](#)).

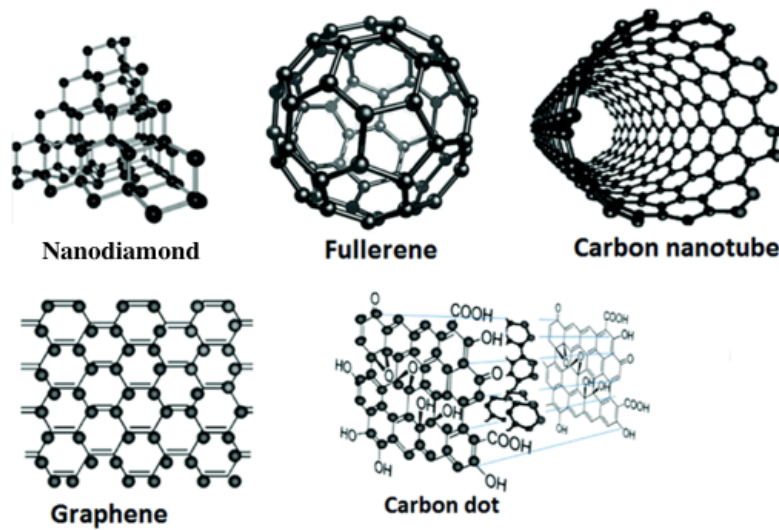


**Figure 6.** Schematic diagram of carbon-based nanomaterials ([Yan et al., 2016](#)).

#### 1.1.4.1. Graphene

Graphene is one of the carbon allotropes. The plane monolayers of carbon atoms are arranged in two-dimensional honeycomb hexagonal lattices with a carbon-carbon bond length of 0.142 nm ([Allen et al., 2009](#)). Graphene has many specificities, such as high surface area, adjustable bandgap, excellent thermal conductivity, significant high carrier mobility at room temperature, chemical stability and very high Young’s modulus due to its single atomic thickness. Graphene is often referred to as “supermaterial” in the field of material science. It is widely considered as a promising material for high-conductivity thin film applications in the construction of high-performance field emitters, photodetectors, solar cells, sensors, super capacitors, *etc.* ([Chen et al., 2018](#)).

#### 1.1.4.2. Nanodiamonds

Diamond is a carbon metastable allotrope, where carbon atoms are arranged in the face-centered cubic crystal structure ([Shao et al., 2004](#)). Nanodiamonds have a complex structure consisting of a diamond core and an amorphous carbon shell. The average particle size of nanodiamonds was determined to be 4-5 nm from X-ray diffraction and small-angle X-ray scattering, which makes it possible to exist in a colloidal suspension of individual particles ([Aleksenskii et al., 1999](#)). Nanodiamonds have several properties including high specific surface area, wide potential window, low background current, high electrochemical stability and high resistance. Low cytotoxicity is one of the major advantages of nanodiamond particles, which promotes their widespread use in polymer

composites, electronics, energy, environmental and biological fields ([Zhang et al., 2018](#)). However, many difficulties have not been overcome, especially to reduce costs and better control surface chemistry. More work needs to be done to better understand its surface chemistry and its structure, which can lead to improve the performance and manufacturing processes of nanodiamonds ([Zhang et al., 2018](#)).

#### **1.1.4.3. Fullerenes**

Fullerenes are allotropes of carbon that were first discovered in 1985 by Richard Smalley, Robert Curl, James Heath, Sean O'Brien and Harold Kroto of Rice University ([Kroto et al., 1985](#)). Fullerenes exhibit diversity in their shape, such as hollow spheres, ellipsoids, tubes and many other shapes. Spherical fullerenes are similar to a soccer ball, and are also known as Buckminsterfullerenes or buckyballs, whereas cylindrical fullerenes are known as buckytubes ([Liu et al., 1998](#); [Williams et al., 1992](#)). The important properties of fullerenes are their nanoscale size, electron transfer and antioxidant capacity, photoactivity, hydrophobicity, and high reactivity, allowing structural modifications ([Markovic and Trajkovic, 2008](#)). These properties make fullerenes good candidates for therapeutic and diagnostic applications. The first biological applications of fullerenes were reported in 1993, when researchers discovered their light-induced cytotoxicity and DNA cleavage activity in both acute and chronically infected cells, and their antiviral properties towards HIV-1 ([Schinazi et al., 1993](#)). Fullerenes have also been studied as targeted therapeutics in osteoporosis and cancer, anti-inflammatory, antiviral, or antibacterial agents, or vehicles for drug and gene delivery. Their potential in diagnostics and medical imaging has also been evaluated ([Dellinger et al., 2013](#)).

#### **1.1.4.4. Carbon nanotubes**

Carbon nanotubes (CNTs) are distinguished from long tubular hollow structure. CNTs can be formed by rolling up single-layered graphene sheets (single-walled carbon nanotubes, SWCNTs), or by rolling up many layers to form concentric cylinders (multi-walled carbon nanotubes, MWCNTs). CNTs have nanometer-scale diameters. Their length-to-diameter ratio is significantly higher than most materials, and can be up to 132,000,000:1 ([Wang et al., 2009b](#)). Raw CNTs are completely insoluble in all solvents, which has caused some health problems ([Bianco et al., 2005](#)). The development of efficient methods for chemical modification of CNTs has facilitated the preparation of soluble CNTs, which can be used in a variety of biological applications where drug delivery looks particularly promising. Functionalized CNTs (F-CNTs) can be linked to a variety of active molecules including peptides, proteins, nucleic acids and other

therapeutic agents. F-CNTs can carry biologically active moieties that can then be delivered to cells, in the cytoplasm or the nucleus. The chemical properties of CNTs make it possible to introduce multiple functions on the same tube, so targeting molecules, contrast agents, drugs or gene can be used simultaneously. Since raw CNTs are highly toxic, mainly due to their insolubility, it is very important to verify the solubility of CNTs in physiological media. Anyway, though it is too early to establish CNTs for clinical use, these NPs are undoubtedly interesting and worthy of further study.

#### **1.1.4.5. Carbon dots (CDs)**

Carbon dots (CDs), first reported in 2004, are a new class of carbon-based fluorescent nanomaterials, and they are widely recognized for their potential use in biomedical applications ([Zhu et al., 2013](#)). They have a typical size of less than 10 nm in all three dimensions and can be easily functionalized. Compared with semiconductor quantum dots, they exhibit high resistance to photobleaching, and have better biocompatibility and lower toxicity. Their light emission wavelength is determined by their size, crystallinity and surface chemistry ([Wang et al., 2009a](#)). Their ability to be rapidly removed from the body after injection through intravenous, intramuscular, or subcutaneous route makes them attractive as nanocarriers for a variety of biomedical applications ([Huang et al., 2013](#); [Yang et al., 2009d](#)). Specificities and applications of CDs will be extensively described in section 1.5.

## **1.2. NPs for biomedical applications**

NPs have entered the biomedical field for decades, and innovative applications are continuously implemented ([Whitesides, 2003](#)). Indeed, NPs play a key role in nanomedicine because they can efficiently transport imaging probes, therapeutic agents or gene to target sites, such as specific organs, tissues, or even underlying cells. The most promising applications use nanoscale particles to simultaneously deliver a therapeutic agent and carry out imaging. There are thus unique opportunities to use multifunctional NPs for combined therapeutic and diagnostic purposes, paving the way to the new field of theranostics ([Janib et al., 2010](#)). In addition, NPs may display active surface functional groups allowing their use as nanoprobe for molecular sensing.

### 1.2.1. Bioimaging

Bioimaging is an important tool in healthcare for the diagnosis of human diseases. It ranges from full bioanatomical imaging (e.g., magnetic resonance imaging, MRI) to molecular imaging (e.g., optical fluorescence). Most currently available imaging probes and contrast agents are chemical or radioactive agents ([Debbage and Jaschke, 2008](#)). Fluorescent probes have the following disadvantages ([Sharma et al., 2006](#)): 1) the imaging observation time has to be short due to the lack of resistance to photobleaching; 2) the probes are not applicable for simultaneous multicolor imaging applications as the emission of most organic fluorophores may overlap with each other because of their broad emission spectrum; 3) emission/excitation is easily affected by external factors such as changes in pH; 4) their emission can overlap with the autofluorescence from the tissue, autofluorescence originating from trace fluorophores in tissues such as nicotinamide (NADH), flavin, collagen, or elastin. Lanthanide with paramagnetic properties is a candidate for MRI contrast agents. Currently, the most widely used MRI contrast agents in clinic are  $Gd^{3+}$  complexes. The main problem associated with their use is unsafety. Hamm *et al.* reported that Gd-DTPA has long residence time *in vivo* and is deposited in bone and liver ([Hamm et al., 1995](#)).

NPs can effectively function as multimodal imaging contrast agents. Multiple imaging modalities may be introduced into the same NP, providing additional and complementary information for accurate disease diagnosis ([Na et al., 2009](#)). The unique nanoscale features of NPs may thus provide electronic, magnetic, and optical functions so they are developed for optical imaging, magnetic resonance imaging (MRI), X-ray computed tomography (CT scan), and radioisotope imaging ([Wolfbeis, 2015](#)).

### 1.2.2. Biosensing

Biosensing is the main driver of medical diagnosis. Classical biosensors are formed by biometric units that specifically identify targets and transducers that convert biological interactions into physical signals to determine the amount of target ([Chao et al., 2016](#)). *In vitro* biosensors provide access to human physiological disease data through the analysis of biopsy cells, blood, urine, sweat, sputum, bronchoalveolar lavage fluid (BAL) and other body fluids, playing a key role in the diagnosis and discrimination of human disease. In the case of NP-based biosensors, the target analytes may be captured with high sensitivity due to a large surface to volume ratio. Compared to classical analytical methods such as enzyme-linked immunosorbent assay (ELISA) and chromatography, NPs-based biosensors offer several advantages, including strong specificity for their targets, high sensitivity, simple operation, transportability and

ability to perform real-time detection ([Luo et al., 2006](#)). In addition, the information can be collected by robust spectrum spectroscopy techniques such as absorption, fluorescence, and Raman spectroscopies, and plasmonics ([Lazarides et al., 2000](#)).

The principle of a fluorescent biosensor is to detect the analyte by monitoring changes in fluorescence intensity, wavelengths, or lifetime. Fluorescence-based biosensor is an important technique for monitoring the physiological activity of the cells to diagnose the disease at the cellular level. By using “probes encapsulated by biologically localized embedding” (PEBBLEs), Kopelman’s team successfully prepared fluorescence nanosensors for  $H^+$ ,  $Ca^{2+}$ ,  $Na^+$ ,  $Mg^{2+}$ ,  $Zn^{2+}$ ,  $Cl^-$ ,  $NO^{2-}$ ,  $O_2$ ,  $NO$  and glucose (figure 7) ([Chen et al., 2016](#)). Analyte determination is performed by monitoring the fluorescence intensity of the appropriately encapsulated dye. Chang’s group described a ratiometric  $Cu^+$ -specific fluorescent biosensor “Coppersensor-1” for molecular imaging in living system ([Domaille et al., 2010](#)). This sensor possesses high selectivity for  $Cu^+$  over competing metal ions at cellular concentrations, and a *ca.* 20-fold fluorescence ratio change is observed upon  $Cu^+$  binding.

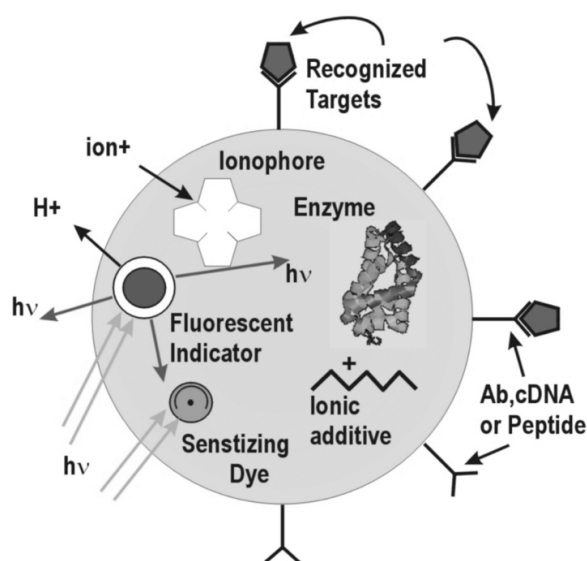


**Figure 7.** Schematic of a PEBBLEs as nanosensor. PEBBLEs are nanoscale devices consisting of sensor molecules trapped in a chemically inert matrix, typically ranging in size from 20 to 200 nm. The PEBBLEs matrix protect the fluorescent sensing molecules from protein interference for reliable *in vivo* calibration of the dye ([Chen et al., 2016](#)).

### 1.2.3. Drug delivery

One of the main causes of cancer mortality is that we are unable to deliver therapeutic drugs only to tumor sites without provoking serious adverse effects on healthy tissues and organs. In addition to surgery, current cancer treatment relies



heavily on radiation and chemotherapeutic agents, which also kill “normal” cells and cause toxicity to patients ([Society, 2013](#)). However, NPs may serve as powerful tools for achieving enhanced therapeutic and diagnostic effectiveness through significant improvement of drug pharmacokinetics and pharmacodynamics. As mentioned earlier, NPs have many unique properties and may be excellent carriers for drugs or macromolecular agents, the resulting “nanomedicines” offering several advantages when compared with “conventional” DDS ([Peer et al., 2007](#)). The association of a drug with a DDS aims at drug protection from degradation by the various biological mechanisms in charge of host defense. It aims as well at the protection of the host from untimely action of the drug or action in unintended tissues. The size, shape, and surface properties of the DDS can be exquisitely tuned by introducing selected functional groups in the DDS components. This may allow NPs to prevent some unfavorable consequences when in biological environment, including enzymatic degradation, chemical degradation under acidic conditions (e.g. in the gastro-intestinal tract), or mechanical clearance (e.g. mucociliary clearance in the respiratory tract), *etc.* ([Prasad, 2012](#)). The tunable size, shape and surface properties of NPs make them not only potentially addressable to specific organs/tissues, but also may provide specificity at the cellular and subcellular levels within the organism ([McCarthy and Weissleder, 2008](#)). Another major advantage of NP-based DDS is that the nanocarrier matrix can be designed for controlled cargo release at the target region to achieve optimal and sustained drug action ([Agasti et al., 2009](#); [Slowing et al., 2008](#)).

One unique aspect of nanomedicine is multimodality, *i.e.* it can serially perform several diagnostic and/or therapeutic functions ([Ma et al., 2011](#)). Nanomedicine aims to use drugs in safe, appropriate and economical manners in patients, optimizing drug efficacy while minimizing side effects, and improving patient health conditions at a lower overall cost. An important factor affecting nanochemotherapy is pharmacokinetics (PK), which describes the effects of the biological environment on the drug, and pharmacodynamics, which deals with the details of the role of the drug in targeting tissue and cells. In addition to meeting the above requirements, NPs-based DDS can overcome biological barriers and selectively target cancerous tissues through the enhanced permeability and retention (EPR) effect. EPR effect refers to the phenomenon that some specific size macromolecules (such as NPs and some macromolecular drugs) are more likely to penetrate into tumor tissues and remain for the long term (compared to normal tissues) ([Matsumura and Maeda, 1986](#)). NPs-based DDS allows for the response to heterogeneous and complex microenvironments within the tumor for the immediate release of therapeutic agents over the optimal dosage range. To date, several NPs-based DDS are in preclinical development or clinical trials for cancer treatment ([Cho et al., 2008](#); [Ulbrich et al., 2016](#)).



## 1.2.4. Gene therapy

Many diseases are caused by defects or dysfunctions of endogenous genes in the body. For example, specific genetic mechanisms control our immune system, which is an important defense against alien substances and pathogens. Mutations in genes may also alter cell proliferation, angiogenesis, metastasis and tumor immunogenicity leading to human cancer ([Gupta et al., 2012](#)). Whereas conventional medicine attempts to control and/or treat symptoms, gene therapy aims at treating genetic or acquired diseases such as cancer at a fundamental level, which is the genetic level ([Li and Huang, 2000](#); [Niidome and Huang, 2002](#)). Gene therapy was initially restricted to the treatment of monogenic genetic diseases by replacing a mutated gene that causes the disease with a healthy copy of the gene ([Hyde et al., 1993](#)). Nowadays, another way for gene therapy is RNA interference, which aims at knocking down expression of a deleterious gene by neutralizing its [mRNA](#), and can be used to treat acquired diseases ([DiGiusto et al., 2010](#)). Small RNAs, including small interfering RNAs (siRNA) and microRNAs (miRNA), are indeed becoming effective therapeutics for the treatment of many diseases.

Several early preclinical studies have shown that viral vectors are very effective in gene transfer processes ([Strayer, 1999](#)). However, in view of the mutagenicity and immunogenicity risks posed by viral vectors, scientists rapidly started to design synthetic carriers for nucleic acid intracellular delivery ([Lungwitz et al., 2005](#)). Ideal gene delivery and transfection systems should have high transfection efficiency, low toxicity to cells and single cell specificity, as well as the ability to simultaneously treat heterogeneous systems with many different cells. So far, due to many factors, gene therapy has not achieved the desired results. How to improve the efficiency of gene transfection in gene therapy, enabling the target gene to be efficiently delivered to the target site of the organism while ensuring safety still remains an issue ([Namiki et al., 2009](#)).

Some NPs-based gene carriers show great potential for gene therapy by improving the pharmacokinetics of nucleic acid, allowing crossing complex biological barriers to promote delivery to target tumors, and providing versatility in carrying multiple diagnostic/therapeutic payloads ([Yin et al., 2014](#)). NPs are of great interest because they can be made from a variety of materials, tailored to be versatile, and designed to provide high gene delivery efficiency ([Dahlman et al., 2014](#); [Wang et al., 2016](#)). Genes can be associated to NPs by electrostatic interactions or conjugated to their surface. The NPs currently used for gene delivery are mainly lipid-based, polymeric and inorganic NPs. Cationic lipids form lipid complexes with nucleic acids that protect the latter from enzymatic degradation in the blood circulation and interact with cell membranes to promote cellular internalization. Their advantages as gene

delivery vehicles include relatively high gene transfer efficiency, biocompatibility and biodegradability ([Akbarzadeh et al., 2013](#)). Polymeric NPs can respond to external stimuli such as temperature, pH or electromagnetic radiation, which can further promote controlled gene delivery and release ([Liechty et al., 2010](#)). Inorganic NPs, including CNTs, magnetic NPs, calcium phosphate NPs, gold NPs, silica NPs and quantum dots, are another important class of nanoscale structures for gene delivery ([Ding et al., 2014](#); [Olton et al., 2011](#); [Probst et al., 2013](#); [Ramos-Perez et al., 2013](#)).

### **1.3. Cellular internalization and fate of NPs**

NPs are increasingly used in various fields, such as consumer goods, electronics and medical. A better understanding of the interactions between NPs and cells contributes to the discovery or design of NPs, and to the prediction of their safety *in vitro* and *in vivo*. To this end, it is necessary to increase our understanding of how NPs are taken up by and transported within cells, and to what extent they are metabolized or secreted. Here, we will mainly discuss the internalization pathways involved in the cellular uptake of NPs, as well as the NPs' intracellular fate.

#### **1.3.1. Internalization pathways**

The NPs enter cells primarily by endocytosis. In the early stages of this process, NPs interact with the cell membrane. This interaction can be mediated by immobilized ligands on the NPs that bind to selective membrane receptors, or can result from non-selective binding of the NPs to the membrane through hydrophobic or electrostatic interactions. Then, the cell membrane forms a membrane retraction which engulfs NPs and produces an endocytic vesicle containing the NPs. Depending on the size and the surface properties of the NPs, the cells will automatically select a viable route to internalize the particles. Endocytosis can be divided into various types depending on the proteins, lipids, and other molecules involved in the process. It includes phagocytosis, clathrin-mediated endocytosis, caveolin-mediated endocytosis, clathrin/alternine-independent endocytosis, and macropinocytosis ([Bareford and Swaan, 2007](#); [Iversen et al., 2011](#); [Kettler et al., 2014](#)).

##### **1.3.1.1. Phagocytosis**

Phagocytosis is mainly accomplished by phagocytic cells, including macrophages, monocytes, neutrophils, and dendritic cells, that are responsible for host defense and uptake of dead cells and cell debris ([Conner and Schmid, 2003](#)). Opsonines such as

immuno- globulins (*i.e.* antibodies), complement proteins or other blood proteins (e.g. laminin and fibronectin) are first adsorbed onto the surface of NPs (opsonization) and then undergo specific ligand-receptor interactions resulting in NP phagocytosis (figure 8). A review article by Hillaireau and Couvreur has summarized the chemical characteristics of NPs that influence their phagocytosis, including size, shape, and surface properties ([Hillaireau and Couvreur, 2009](#)). The type of receptor that interacts with the opsonized NP also affects the mechanism of phagocytosis and subsequent toxicity of the phagocytized material. Fc receptor-dependent phagocytosis results in the production of proinflammatory mediators, whereas complement receptor-dependent phagocytosis does not ([Underhill and Ozinsky, 2002](#)). Therefore, related receptors not only affect the delivery of NPs, but also their safety. Besides, the surface properties of NPs can affect phagocytosis. For example, hydrophilic PEG has a steric shielding effect so PEGylated NPs can repel opsonic effects by preventing or minimizing protein adsorption to their surface ([Hu \*et al.\*, 2007](#)).

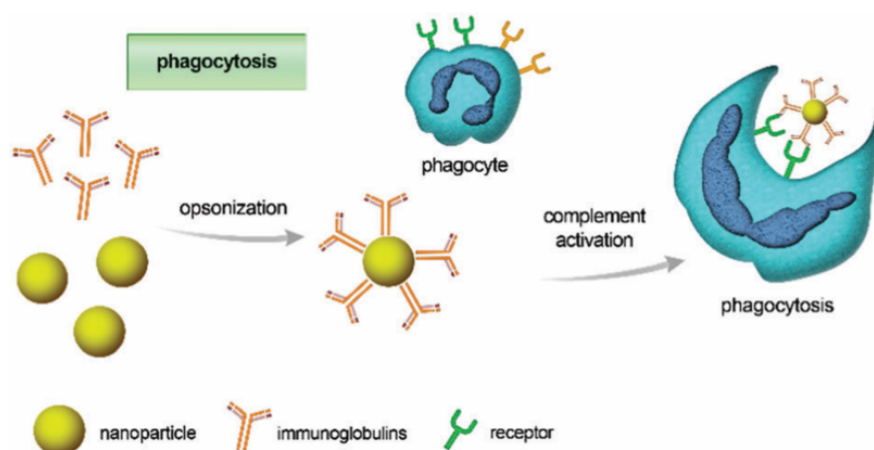


**Figure 8.** A schematic of the opsonization process triggered by the adsorption of immunoglobulins or other complement proteins (opsonins) onto the surface of NPs. The conditioned NPs are then identified by receptors on the phagocytic cells and internalized ([Behzadi \*et al.\*, 2017](#)).

### 1.3.1.2. Clathrin-mediated endocytosis (CME)

Clathrin-mediated endocytosis that refers to the ingestion of material from the cell surface into cells using clathrin-coated vesicles, is the main mechanism by which cells obtain nutrients and plasma membrane components. CME is a complex pathway involving intercellular signaling, membrane recycling and nutrient uptake ([Kirchhausen, 2000](#)). The formation of vesicles packing the cargo begins with the participation of a wide range of clathrin proteins and adaptor protein that can trigger membrane curvature, which finally forms a spherical clathrin coating pit ([Schmid and McMahon, 2007](#); [Tebar \*et al.\*, 1999](#)). The release of vesicles from the plasma

membrane occurs through the activity of a GTPase-inducing protein, a protein that assembles into a loop in the newly formed invaginated neck. When the coated vesicles are released, the grid protein pits are broken down ([McMahon and Boucrot, 2011](#)). After internalization by CME, uncoated vesicles are directed to the early endosomes or recycled to the plasma membrane surface. Vesicles can also target more mature endosomes and subsequently compartments such as lysosomes and multivesicles. Most receptor-mediated uptake of NPs by cells occurs through CME. It has been found that 100 nm-sized cationic NPs derived from D,L-poly(lactide) (PLA) are only internalized by CME ([Harush-Frenkel \*et al.\*, 2007](#)). Poly(L-lysine), a cationic polymer functionalized on the surface of poly(lactide-co-glycolide) (PLGA) NPs, has been found to significantly enhance cellular uptake by CME ([Vasir and Labhasetwar, 2008](#)). Another study reported that mesoporous silica NPs labeled with fluorescein isothiocyanate (~110 nm) were efficiently internalized by CME into human mesenchymal stem cells (hMSCs) and adipocytes (3T3-L1) ([Huang \*et al.\*, 2005](#)).

### 1.3.1.3 Caveolae-dependent endocytosis

Caveolae-dependent endocytosis plays an important role in many physiological processes, such as signaling and adjustment of the lipid and membrane protein composition of the plasma membrane. It is also associated with a variety of diseases, including cancer, diabetes, and viral infections ([Pelkmans and Helenius, 2002](#)). Caveolae consist of the cholesterol-binding protein caveolin with a bilayer enriched in

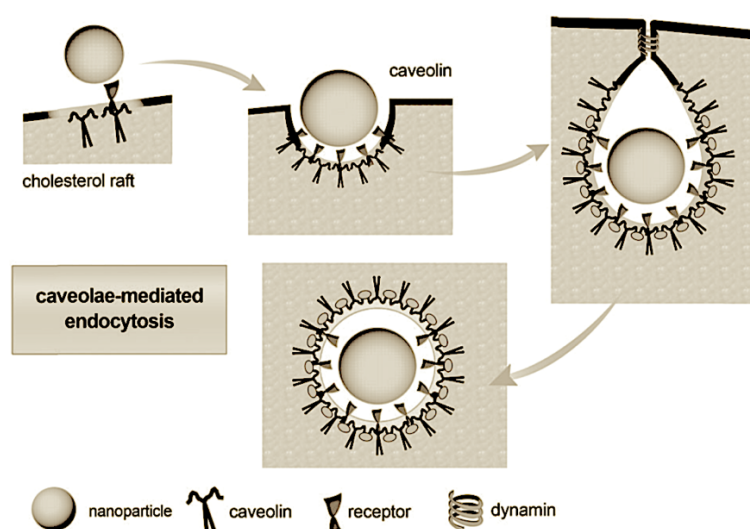


**Figure 9.** Caveolae-mediated endocytosis. Caveolin plays a major role in membrane curvature formation. Like in CME, the mitogen dynamin is involved for allowing vesicles to sprout and release into cells ([Taggart, 2001](#)).

cholesterol and glycolipids. It is interspersed with regions of the dense body that anchor the cytoskeleton, and is a repertoire of bottle-shaped membranes in epithelial and non-epithelial cells. The caveola form part of the cell membrane, increasing the surface area up to 75 % in non-epithelial cells (figure 9) ([Taggart, 2001](#)). In terms of drug delivery, NPs and associated drugs can escape lysosomal degradation into the cells when internalized *via* a caveolae-dependent mechanism. In some cases, viruses also use this internalization pathway to escape degradation ([Carver and Schnitzer, 2003](#)).

#### **1.3.1.4. Macropinocytosis**

The macropinocytosis is a non-specific, massive fluid cell ingestion process that involves the formation of large vesicles. It represents a unique pathway for endocytosis in mammalian cells. This actin-driven endocytic process is not directly coordinated by the presence of cargo, but can be induced when the growth factor signaling pathway is activated ([Kerr and Teasdale, 2009](#)). During the process, cytoskeletal rearrangements form large membrane extensions or folds that then fuse to the plasma membrane, producing large uncoated vesicles (0.2-5  $\mu\text{m}$ ) ([Kuhn \*et al.\*, 2014](#)). Macropinocytosis is important in many physiological functions, such as antigen presentation, and serves as an entry portal for microbial pathogens ([Norbury \*et al.\*, 1995](#)). Macropinocytosis is also thought to be involved in the uptake of large NPs that would not be able to enter cells *via* clathrin- or caveolae-dependent endocytosis ([Kuhn \*et al.\*, 2014](#)).

#### **1.3.1.5. Other pathways**

As discussed above, multiple pathways are responsible for cellular uptake of NPs. Pathways others than the ones we have described above have been proposed, including passive diffusion, hole formation, direct microinjection and electroporation (figure 10) ([Verma and Stellacci, 2010](#)). Wang *et al.* reported that penicillamine-coated QDs penetrate the plasma membrane of erythrocytes through a non-endocytic passive mechanism. This process does not affect the integrity of the entire membrane nor causes pore formation ([Wang \*et al.\*, 2012](#)). Microinjection techniques have been used to inject silver (20 nm) and metal oxide magnetite (8 nm) NPs directly into the cytoplasm of HeLa cells ([Candeloro \*et al.\*, 2011](#)). Electroporation is a physical method that promotes the entry of NPs into cells, based on the application of external high-voltage electrical pulses to cells to induce the formation of transient membrane pores. This method can eliminate the effects of extracellular biological factors (protein corona) ([Zhao \*et al.\*, 2011](#)).

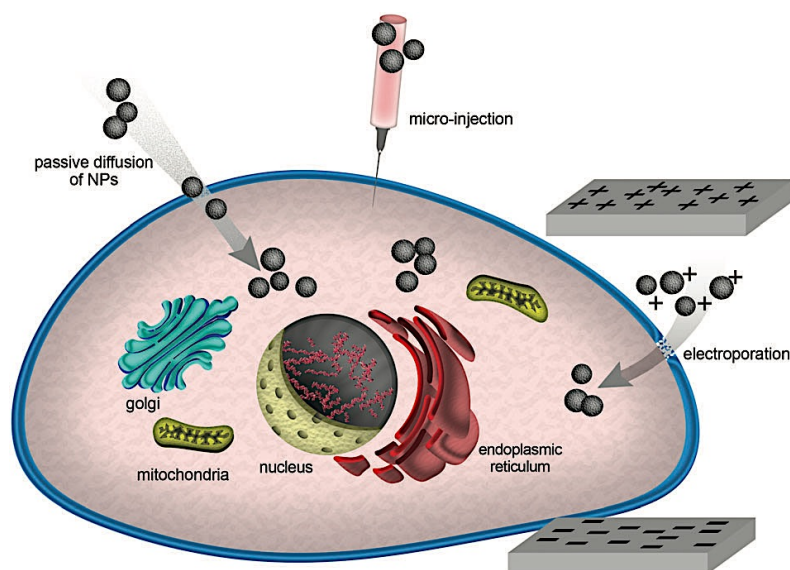


**Figure 10.** Schematic diagram depicting other non-endocytic cell entry pathways ([Verma and Stellacci, 2010](#)).

### 1.3.2. Intracellular fate of NPs

Once NPs have entered cells through endocytic vesicles, their ultimate fate is usually determined by intracellular sorting/transport mechanisms, primarily mediated by intracellular network. The intracellular transport/pathway of NPs is summarized in figure 11 ([Behzadi et al., 2017](#)). After cellular uptake, NPs usually first encounter early endosomes, which are the main sorting stations for endocytosis. In early endosomes, some NPs may be transported to the recirculating endosomes and subsequently excreted. The NPs retained in the early endosomes slowly move along the microtubules toward the inside of the cells and fuse with the late endosomes. Finally, the late endosomes may fuse with lysosomes. However, the lysosome is not necessarily the end of the pathway. Some endosomes undergo exocytosis and release their undigested contents by fusion with the plasma membrane. In pathways leading to multivesicular bodies or even lysosomes, a portion of NPs may escape from the vesicle compartment to the cytoplasm. In addition, some NPs may enter the cytoplasm through non-specific mechanisms. NPs in the cytoplasm or in vesicles can enter the nucleus, mitochondria, endoplasmic reticulum (ER) and Golgi apparatus (GA) through unknown mechanisms. In fact, vesicles containing NPs can fuse with ER, GA and other organelles. NPs entering the ER or GA can leave the cell by vesicles associated with conventional secretion systems. NPs located in the cytoplasm can exit the cell by re-entering the vesicle system or directly through non-specific mechanisms ([Behzadi et al., 2017](#)).



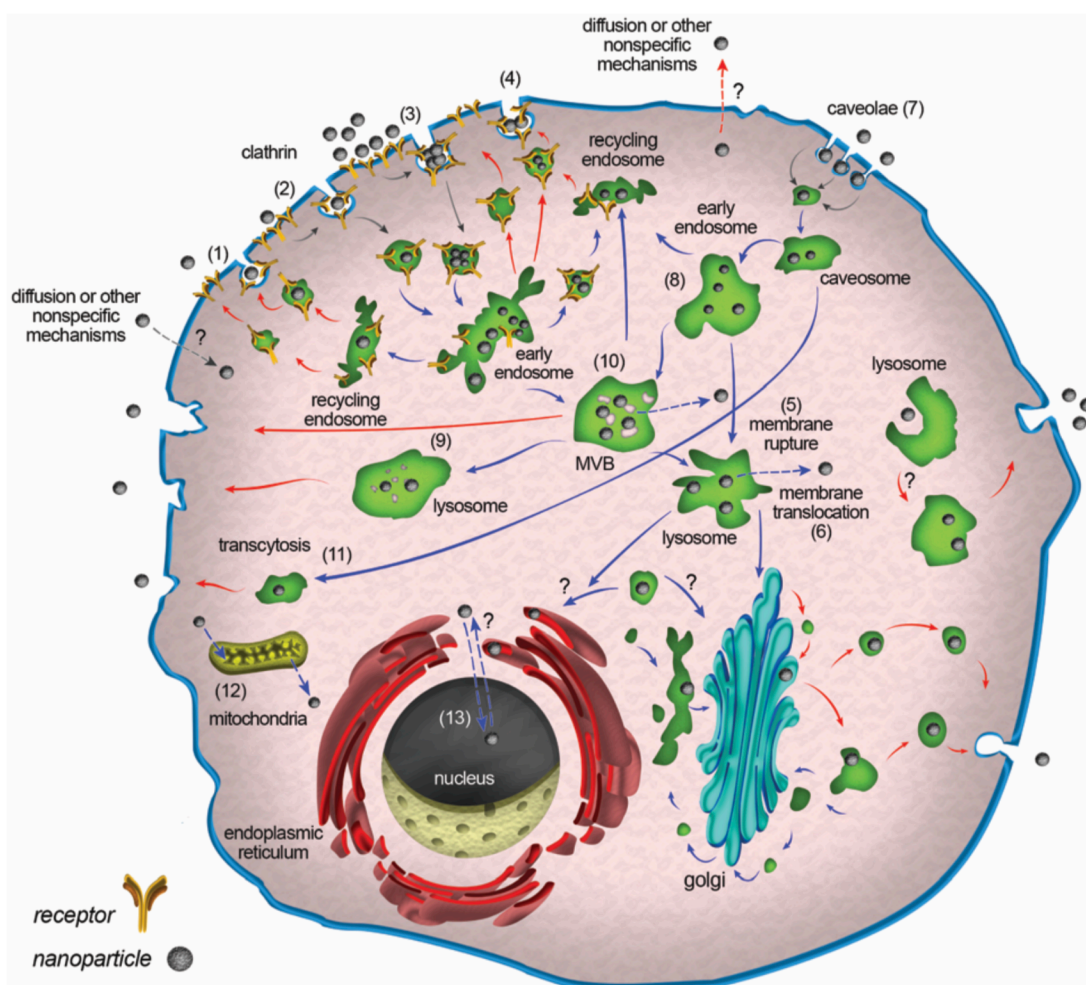


**Figure 11.** Schematic of intracellular transport/pathway of NPs ([Behzadi et al., 2017](#)).

Although the cell entering pathway may vary, the endosomes are the first intracellular compartment encountered by internalized NPs. Early endosomes are characterized by a lower intraluminal pH (~6-6.5, necessary for endosomal specific enzymatic activity), which has been used to trigger the release of pH responsive NPs into the cytosol. The polyamine-based carrier system can effectively achieve neutralization after protonation under acidic conditions in the endosome. This neutralization increases the pH of the endosomes, causing the transport of ions into the lumen of the endosome, resulting in swelling and release of endocytic NPs (proton sponge effect) ([Boussif et al., 1995](#)). Lysosomes are considered to be components of a cell machine for digestion or recovery because they contain cathepsin proteases. Degradation products produced by enzymatic activity on the cargo material are released into the cytoplasm to meet the nutritional needs of the cells. Tumor cells exhibit higher lysosomal cathepsin activity and release of cathepsin into the extracellular environment is associated with the promotion of tumor growth. The concept of dissolved basic

ingredients was introduced by Christian de Duve, who referred to hydrolase as a “suicide bag” ([De Duve, 1983](#)). Where endosomes or lysosomes are not the ultimate therapeutic target, it is necessary to design strategies for endosomal release and to protect the administered drug from degradation in the degraded lysosomal environment. This is achieved by encapsulating the drug into various NP-based DDs. These NPs not only protect sensitive drug molecules from degradation, but also release drugs in a time-dependent manner ([Kong et al., 2013](#)).

An alternative pathway to avoid cell entry in acidic pH and soluble lysosomal environments is the retrograde transport pathway, which results in endosomal cargo entering the GA and ER ([Tarragó-Trani and Storrie, 2007](#)). ER and GA are responsible for calcium homeostasis, folding of membrane and secreted proteins, and lipid biosynthesis. The retrograde transport pathway is involved in the recycling of certain receptors and is utilized by some toxins to localize and interfere with the function of ER ([Bitler et al., 2010](#); [Sandvig et al., 2010](#)). *In vitro*, PLGA based NPs ( $95 \pm 20$  nm) were found to accumulate mainly in the GA in the case of human bronchial epithelial and negative renal tubular cells, as revealed by immunofluorescence ([Cartiera et al., 2009](#)). Significantly more particles are localized in the GA compared to lysosomes. This study was unable to determine whether the NPs were in the GA or in the GA-associated vesicles of the late endosomes. In a later study, using Raman spectroscopy combined with optical microscopy, it was found that PEG-functionalized PCL and PLGA NPs were incorporated into the GA-associated vesicles of the late endosomes of human HeLa cells ([Chernenko et al., 2009](#)).

Mitochondria are unique organelles because they have a double membrane structure (internal and external mitochondrial membranes) and mitochondrial DNA is contained in the inner membrane. Mitochondrial dysfunction has been implicated in many diseases, including cancer, neurodegenerative and neuromuscular diseases, obesity and diabetes, and has been recognized as providing important therapeutic targets ([Fulda et al., 2010](#)). The synergistic effect of high density inner membrane (rich in saturated phospholipids) and high membrane potential (internal negative) results in highly controlled transport across the mitochondrial membrane compared to the plasma membrane ([Rin Jean et al., 2014](#)). Targeting and delivering therapeutic agents to mitochondria has been an insurmountable challenge due to the high selectivity and impermeability of mitochondrial membranes. It is generally accepted that cations target mitochondria mainly because of high membrane potential ([Reily et al., 2013](#)). Among the different cations, triphenylphosphonium (TPP) cations meet the prerequisite for transport with an adequate balance between delocalized positive charge and lipophilicity ([Lieberman et al., 1969](#)). TPP cations have been shown to successfully cross the barrier and reach the internal leaflets of the mitochondrial inner membrane. Therefore, TPP has been used as a carrier for delivering covalently bound small



molecule drugs to mitochondria ([Chalmers et al., 2011](#)). Interestingly, positively charged targeted NPs can escape from early endosomes and become confined to mitochondria, while negatively charged non-targeted NPs are still only found in endosomes after 4 hours of incubation. This observation may be due to the buffering effect of positively charged NPs, which prevents acidification of endosomal vesicles, which may increase ATPase-mediated influx of protons and counterions. The resulting osmotic swelling causes the endosomal membrane to rupture, resulting in the release of cargo in the cytosol ([Yameen et al., 2014](#)).

The nucleus is a double lipid bilayer-encapsulated organelle and has been an important therapeutic target for site-specific delivery of drugs and DNA. In most cases, the NPs deliver the drug into the cell, and the drug molecule diffuses through cytosol to reach the nuclear target. Caveolin-mediated endocytosis is of particular interest because this intracellular pathway transports endocytosed substances to lysosomal/cell membrane caveats with neutral pH, bypassing the acidity of lysosomes and enzymatic degradation. It is known to sort cargo into GA and ER near the nucleus and has been proposed to provide a safe pathway for access to the nucleus of cells ([Reilly et al., 2012](#)). With polymeric carrier systems, it has been reported that certain functional groups such as L-arginine and saccharides partially separate the polymer/DNA complex into GA and ER ([Fichter et al., 2012](#); [Li et al., 2013](#)). The glycofunctional strategy mimics the natural process of transporting glycosylated proteins from the ER to the nucleus ([Liao and Carpenter, 2007](#)). Further research has focused on developing this pathway by designing new polymers with glycosylation or arginine functional groups, which may provide a convenient method for caveolae-mediated nuclear targeting. After the plasma membrane barrier, the nuclear membrane poses another obstacle to nuclear delivery. The transport through the nuclear membrane occurs through a nuclear pore complex (NPC), which occurs in the nuclear membrane. Small ions and macromolecules (~9 nm) are transmitted through the nuclear membrane by passive diffusion of NPC, while macromolecules larger than 40 kDa (39 nm) are sorted by nuclear transport receptor-mediated active transport. Promoted by oligopeptide sequences that specifically bind to receptors, known as nuclear localization signals (NLS) ([Terry et al., 2007](#)). The combination of nuclear localization signals (NLS) and nanoparticle-based carrier systems has been shown to direct cargo to nuclear targets. Cheng *et al.* reported NPs from NLS functionalized PLGA NPs (~72 nm) and NLS functionalized QDs conjugated PLGA NPs (~168 nm) were localized in the nucleus of HeLa cells ([Cheng et al., 2008](#)). Similarly, NLS-functionalized DOX-loaded PLGA NPs (~226 nm) achieved higher drug concentration in the nucleus (MCF7 cells) compared to the free drug lacking NLS PLGA NPs ([Misra and Sahoo, 2010](#)).

## 1.4. Nanotoxicology and underlying mechanisms

When NPs are used for medical purposes, they should fulfill the intended function and, ideally, should not cause any unwanted side effect. In reality, nanomaterials, whether they are inert or not, have high activity due to the quantum size effect and large surface area to volume ratio. Furthermore, they do constitute a "foreign matter" with regard to biological systems, exhibiting potential toxicity to living organisms. Thus, a clear understanding of the toxicology of NPs is a prerequisite for developing applications in the field of nanomedicine.

In the last decades, scientists have recognized that nanoscale particles possess higher toxicity compared to larger ones of the same chemical composition ([Borm and Berube, 2008](#)). For example, in the respiratory tract, nanoscale (< 100 nm) and larger particles (> 500 nm) enter cells according to different internalization pathways and elicit different biological and toxicological effects. The particle-cell interactions are different and, as a consequence, so is their biodistribution ([Oberdörster, 2010](#)). Thus, in order to gain a deeper understanding of the toxic effects induced by NPs, especially in humans, a new domain in toxicology was proposed in 1984: nanotoxicology ([Donaldson \*et al.\*, 2004](#)). The assessment stages of toxicity of NPs, or nanotoxicity, can be summarized as in figure 12 ([Shin \*et al.\*, 2015](#)). The first step consists in the characterization of NPs, in order to assess the relevance of biological responses with respect to the properties of NPs. The second step is determination of the cytotoxicity of NPs, based on selected cell systems as *in vitro* evaluation platform. The final steps consist in evaluations performed in model animals. Whole body NP fate and organ toxicity are usually assessed at this stage ([Caballero-Díaz and Cases, 2016](#)).

In general, nanomedicine and nanotoxicology are complementary disciplines that aim at improving human health. The medical goals and risks brought by NPs are being well considered and studied in depth. Evaluation of human and environmental exposures, biodynamics or pharmacokinetics, identification of potential hazards, and

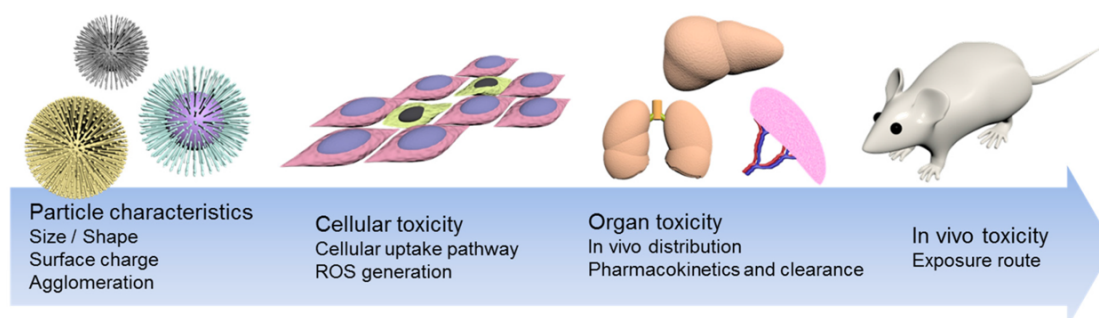


**Figure 12.** The main steps of nanotoxicity assessment. Nanotoxicity depends on particle size, charge, agglomeration state, *etc.* and can be evoked at the cell, organ or even systemic level in the body ([Shin \*et al.\*, 2015](#)).

biological persistence in cells and subcellular structures are required for meaningful risk assessment. Among them, dose, dose rate and biokinetics should be given priority. To date, the multidisciplinary collaboration of NP developers and toxicologists allows the elucidation of the toxicological risks associated with some of the most commonly used NPs ([Srivastava et al., 2015](#)).

In this paragraph, as toxicological risks associated with NPs, we will mainly focus on cellular toxicity of NPs and interaction of NPs with the immune system, as target organ.

### 1.4.1. NP cytotoxicity and underlying mechanisms

NPs may have several toxicological consequences at the cellular level. As shown in figure 13, nanomaterials can damage cell membranes through various processes leading to the formation of nanopores and thus to loss of membrane stability or integrity triggering cell leakage ([Elsaesser and Howard, 2012](#); [Ginzburg and Balijepalli, 2007](#)). The damage of cell membranes by NPs is species and concentration dependent ([Gou et al., 2010](#)). Mitochondria, as an energy center of cells, have been reported to be the main target of fullerenes and CNTs ([Foley et al., 2002a](#); [Zhu et al., 2006](#)). However, other NPs, such as titanium dioxide, polystyrene, or silver NPs, also appear to be able to affect mitochondrial function, leading to apoptosis ([Hussain et al., 2005a](#); [Xia et al., 2006a](#)). Another important target for NPs is the lysosome, the digestive system of cells.

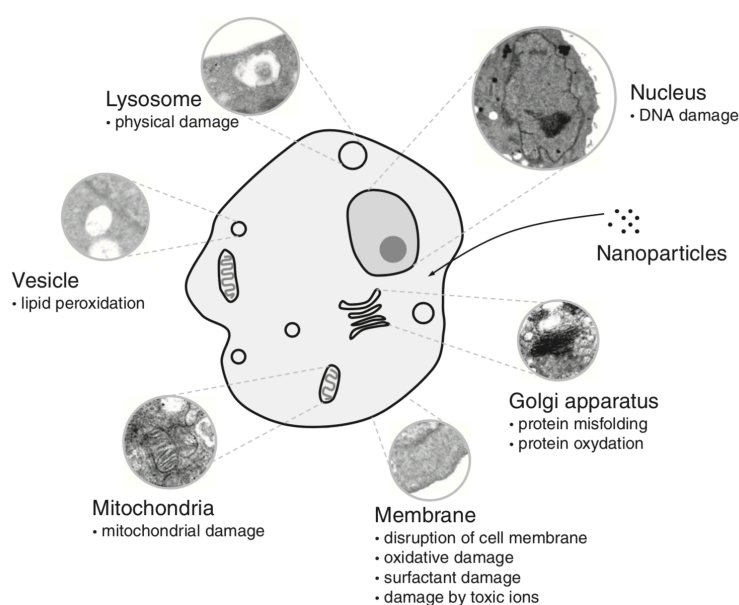


**Figure 13.** Schematic representation of the toxicological consequences of NPs in cells. NPs cause damage to the cell membrane and enter the cell, damaging various cellular components ([Elsaesser and Howard, 2012](#)).

After endosomes fusion with the lysosomes, the cells attempt to digest or excrete NPs ([Al-Rawi et al., 2011](#); [Greulich et al., 2011](#)). However, the effects of size, shape and material type on the ability of cells to accumulate or excrete NPs after accumulation in lysosomes are not fully understood ([Elsaesser and Howard, 2012](#)). Finally, NPs can induced DNA damages directly by entering the nucleus through the nuclear pores or by receptor-mediated transport or by inducing oxidative stress ([Elsaesser and Howard, 2012](#)). Oxidative stress is considered as the main mechanism involved in NP cytotoxicity, potentially leading to inflammation and cell death due to cell membrane, mitochondrial or DNA damage (figure 14). At the body levels, it is involved in numerous pathological conditions such as asthma, fibrosis or cancer, that may thus be potential health hazards associate to NPs. Oxidative stress results from an imbalance between the production of reactive oxygen species (ROS) and the ability of the organism to detoxify these reactive intermediates or repair the damages they induce. ROS include superoxide anion ( $O^{2-}$ ), hydrogen peroxide ( $H_2O_2$ ) and hydroxyl radical (OH). These species are by-products of aerobic metabolism and have inherent chemical properties that confer them reactivity towards various biological targets, and particularly proteins, phospholipids and DNA. In cells, ROS act as a signal transduction mechanism for adaptation to changes in environmental nutrients and redox regime ([Wood et al., 2003](#)). However, when produced at high levels, ROS can potentially damage lipids, proteins and DNA, and induce mitochondrial damage leading to cell death and pathological consequences ([Cross et al., 1987](#)).

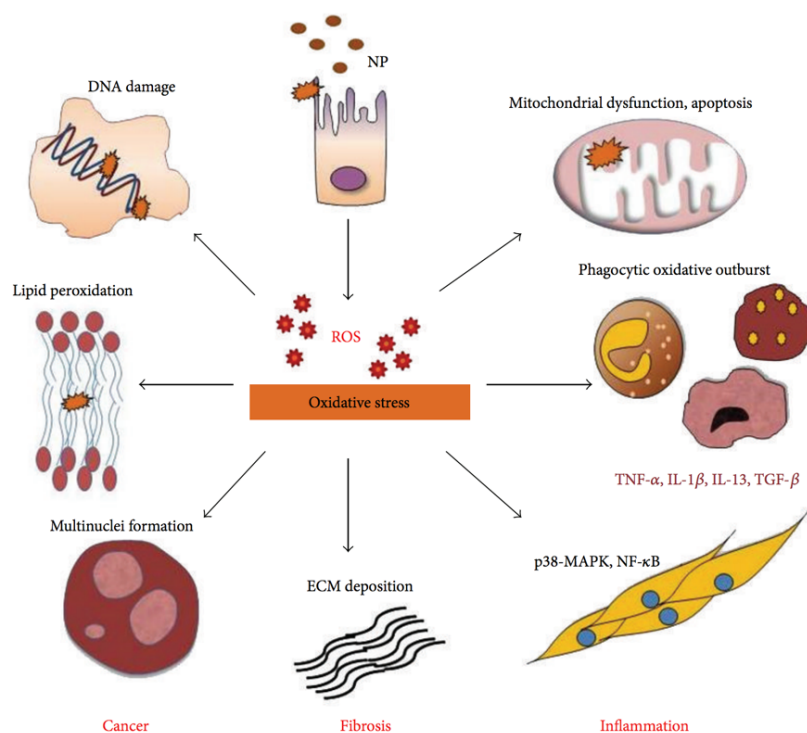


**Figure 14.** The main implications of oxidative stress in NP-induced toxicity ([Manke et al., 2013](#)).

To date, many studies have shown that NPs can trigger ROS production during biological interactions. For example, NPs, including titanium dioxide (TiO<sub>2</sub>), zinc oxide (ZnO), cerium oxide (CeO<sub>2</sub>) and silver NPs, induce signaling cascades that cause oxidative stress in cells after deposition on the cell surface or in subcellular organelles ([Buzea et al., 2007](#)). Phagocytes including neutrophils and macrophages produce large amounts of ROS after incomplete phagocytosis of NPs through the NADPH-oxidase system, and NP-induced ROS trigger inflammatory cascades of chemokines by activating cellular signaling pathways and cytokine expression. For example, CNT-induced oxidative stress triggers cell signaling pathways leading to increased expression of pro-inflammatory cytokines and chemokines ([Li et al., 2010b](#)). Shukla *et al.* reported toxicological studies on TiO<sub>2</sub> NPs. The data indicates that TiO<sub>2</sub> NPs have a slight cytotoxic potential. However, statistically significant induction of DNA damage was observed. TiO<sub>2</sub> NPs induce ROS leading to oxidative DNA damage and micronuclei formation ([Shukla et al., 2011](#)). Intrinsic properties of NPs such as surface charge, chemical composition, and particle size are key determining factors of ROS production and toxicity of NPs ([Shvedova et al., 2012](#)). Consequently, the production of ROS appears as a key element in the NP-induced toxicity (figure 14) ([Manke et al., 2013](#)). However, it is worth noting that ROS production is not the only mechanism of NP toxicity. According to some reports, some NPs produce toxicity in absence of ROS production ([Wang et al., 2010](#)).

### 1.4.2. NPs and the immune system

The immune system composed of the innate and adaptive immune systems is able to adapt to internal and external environmental changes, in order to protect the host against pathogens (bacteria, viruses). The interaction between foreign triggers and the immune system may produce undesirable immune responses ([Zolnik et al., 2010](#)), including inflammatory or autoimmune reactions, thereby increasing the host's susceptibility, e.g., to infection and cancer ([Shvedova et al., 2010](#)).

NPs as foreign substances may be recognized and taken up by immune cells, particularly phagocytes. Indeed, macrophages that are ubiquitous in barrier tissues such as the respiratory and gastrointestinal mucous membranes, and the skin, have the role of body surveillance and "cleaning". They detect and eliminate exogenous or endogenous abnormal factors, including exogenous microorganisms, their own senescent cells or misfolded proteins. However, in the case of extensive injury/invasion, resident macrophages can proliferate *in situ*, increase their number, and most importantly, generate an alert signal (e.g., a chemokine) that recruits neutrophils and trigger the production of inflammatory monocytes ([Boraschi et al., 2017](#)). Boraschi *et*

*al.* reported that NPs can regulate macrophage function in different ways. NPs can induce or inhibit the expression of genes involved in inflammation and repair responses, thereby driving polarization/reprogramming to the M1 or M2 functional phenotype. In addition, NPs can modulate innate memory of macrophages by reducing or enhancing responses to subsequent challenges, most likely through epigenetic changes (figure 15) (Boraschi *et al.*, 2017). Kedmi *et al.* analyzed the potential immunotoxicity of positively charged lipid NPs and found that these NPs lead to a significant increase in Th1 cytokine expression (IL-2, IFN- $\gamma$ , and TNF- $\alpha$ ), possibly through activation of toll-like receptor 4 (TLR4) (Kedmi *et al.*, 2010). An in-depth understanding of the interaction of NPs with the immune system can be helpful in designing nanomedical products (e.g., DDS) that not only can modulate immune responses, but also evade immune surveillance, thereby exerting more effectively their therapeutic potential.

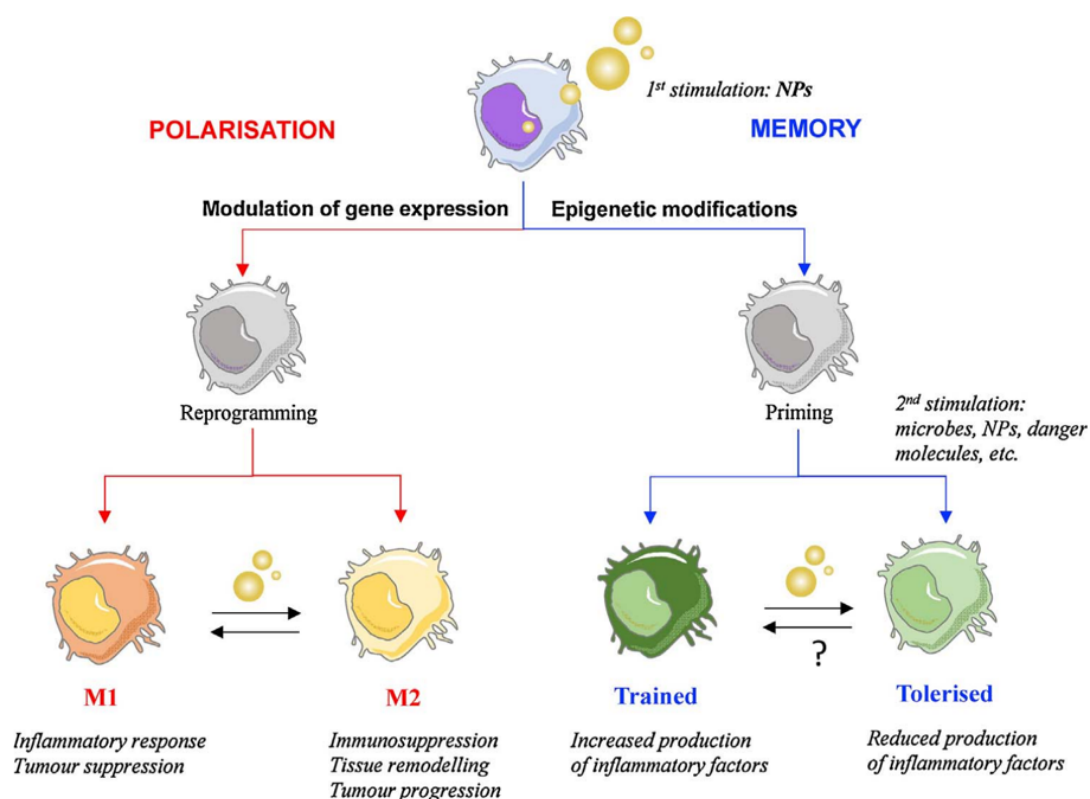


**Figure 15.** NPs modulate the function of monocytes/macrophages. NPs can induce or inhibit the expression of genes involved in inflammation and repair responses, thereby driving polarization/reprogramming to the M1 or M2 functional phenotype (Boraschi *et al.*, 2017).

### 1.4.3. Physicochemical characteristics that govern NP toxicity

The physicochemical characteristics of NPs are important factors for their intrinsic toxicity. These factors include mainly chemical composition, size, charge, shape, and surface chemistry.



### 1.4.1.1 Chemical composition and form

Chemical composition refers to the arrangement, type, and ratio of atoms that compose a material. It has been reported that the toxicity of nanomaterials and their chemical composition are related. It is mainly due to the different interactions between NPs and cells. Even when elementary composition is similar, differences in atom and molecule arrangements may result in differences in terms of cytotoxicity. For example, although graphene and SWCNTs are mainly composed of carbon, Zhang and colleagues showed that SWCNTs exhibit higher toxicity on PC12 cells compared to graphene, which was attributed to differences in the atom arrangement within the materials ([Zhang et al., 2010](#)). Sayes *et al.* prepared a set of nanocrystalline titania (nano-TiO<sub>2</sub>) samples of controlled phase composition and relied on *in vitro* cytotoxicity assays to compare their biological effects. The results show that the crystal structure affects cytotoxicity, as the anatase form of TiO<sub>2</sub> is slightly more toxic than the rutile form ([Sayes et al., 2006](#)). In addition, a subsequent study showed that amorphous TiO<sub>2</sub> NPs did exhibit significantly different toxicity compared to the anatase and rutile forms ([Braydich-Stolle et al., 2009](#)).

### 1.4.1.2 Size

*In vitro* and *in vivo* toxicological studies have shown that NPs have greater toxicological effects compared to corresponding bulk materials. It is generally believed that this is due to the high area-to-volume ratio of NPs. This view has been supported by some research. As examples, Margriet and colleagues compared the effects of silver NPs of increasing size (20, 80, 113 nm) in *in vitro* assays for cytotoxicity, inflammation, genotoxicity and developmental toxicity ([Park et al., 2011a](#)). The results showed that 20-nm sized NPs induce more pronounced effects on cellular metabolic activity and membrane integrity. Zhang and colleagues studied the toxicity of 5, 10, 30 and 60 nm PEG-coated gold NPs in mice. Biodistribution results show that 5 and 10 nm particles accumulate in the liver, 30 nm particles accumulate in the spleen, while 60 nm particles have a broader distribution with limited accumulation in the organs. This study indicated also size-dependent *in vivo* toxicity of PEG-coated gold NPs, 10 and 60 nm PEG-coated gold NPs being more toxic, and 5 and 30 nm particles having relatively low toxicity. ([Zhang et al., 2011](#)). To elucidate the effects of particle size on cellular uptake and biodistribution of NPs, He *et al.* have designed polymer NPs of size ranging from 150 to 500 nm. They found that NPs with larger size are more efficiently phagocytosed by murine macrophages and NPs of 150 nm in diameter are more prone to accumulate in tumors ([He et al., 2010a](#)).

### 1.4.1.3 Charge

All particle systems in aqueous media exhibit a surface charge, either positive or negative. Dissociation of acidic chemical groups on the surface of NPs will result in a negatively charged surface. Likewise, protonation of basic groups on the surface of NPs will result in a positively charged surface ([Berg \*et al.\*, 2009](#)). The zeta potential ( $\zeta$ ) measurements are used to estimate the charge of NPs relative to their surrounding conditions. However, zeta potential is not an actual measurement of the charge of a single particle. Rather, it is a measure of the electric double layer produced at the surface of a NP by the surrounding ions in solution ([Berg \*et al.\*, 2009](#)). Goodman *et al.* demonstrated that cationic Au NPs showed higher cytotoxicity than anionic counterpart, demonstrating the key role of surface charge on NPs cytotoxicity ([Goodman \*et al.\*, 2004](#)). Badawy *et al.* evaluated the toxicity of AgNPs of different charge, from negative to positive, on bacteria ([El Badawy \*et al.\*, 2010](#)). The toxicity of AgNPs was not only controlled by the charge of the particles, but also by the surface charge of the cell membrane of the tested bacillus. The more negative citrate-AgNPs were the least toxic, while the positively charged bPEI-AgNPs were the most toxic ([El Badawy \*et al.\*, 2010](#)). Schaeublin *et al.* investigated the effects of surface state (positive, neutral and negative) of Au NPs on a human keratinocyte cell line. The results indicated that all three NPs disrupted cell morphology and exhibited dose-dependent toxicity. However, surface charge determined how Au NPs affect cellular processes. Indeed, charged NPs induced cell death through apoptosis, whereas neutral NPs caused necrosis ([Schaeublin \*et al.\*, 2011](#)). Kim *et al.* found that surface charge is a key factor affecting lung inflammation in functionalized polymeric NPs, positively charged NPs causing acute lung inflammation ([Kim \*et al.\*, 2016](#)). Thus, the charge of NPs has been proposed as a valuable parameter for predicting the toxicity of NPs.

### 1.4.1.4. Shape

The shape of NPs plays a role in their toxicity. As an example of carbon nanomaterials, SWCNTs are more toxic than amorphous carbon black at the same mass dose in the lung of mice ([Lam \*et al.\*, 2004](#)). Yamamoto *et al.* examined the cytotoxicity of TiO<sub>2</sub>, Al<sub>2</sub>O<sub>3</sub>, ZrO<sub>2</sub>, Si<sub>3</sub>N<sub>4</sub> and SiC particles on mouse fibroblasts and macrophages. The results show that the dendritic particles have a higher level of cytotoxicity to macrophages than the spindle and spherical particles. The effect of the shape of NPs on their cytotoxicity could be attributed to the number of sharp edges that induced severe oxidative stress, but they also admitted additional evidence was needed to support this hypothesis ([Yamamoto \*et al.\*, 2004](#)). There are two problems in estimating the cytotoxicity caused by the shape. One is



cell sensitivity and phagocytosis. The other is related to the interaction forces between the NPs and the longitudinally oriented NPs that increase in proportion to their length. Therefore, the van der Waals force developed by rod-shaped NPs is larger than the one by spherical NPs ([Hsiao and Huang, 2011](#)).

#### 1.4.1.5 Surface chemistry

Surface functionalization is an effective way to customize NPs for specific therapeutic/diagnostic purposes. Synthetic and natural ligands are attached to the surface of the NPs to enhance stability/solubility and to incorporate targeting ligands and/or therapeutic agents ([Kanaras \*et al.\*, 2002](#); [Wang \*et al.\*, 2011a](#)). NPs can cause structural reconstruction and phase transition of the lipid bilayer of the cell membrane ([Jing and Zhu, 2011](#)). The direct interaction of surface functionalized NPs with cells can disrupt the integrity of the membrane structure, and the extent of leakage depends on the NP surface chemistry ([Lin \*et al.\*, 2010](#)). For example, the surface reactivity of the NPs may induce production of reactive oxygen species (ROS) and therefore potential damage to living cells ([Sasidharan \*et al.\*, 2011](#)). Besides, surface functionalization may give NPs greater advantages. [Slowing \*et al.\*](#) synthesized MSNs functionalized with 3-aminopropyl, 3-guanidinopropyl, 3-[*N*-(2-guanidinoethyl)guanidino] propyl, or *N*-folate-3-aminopropyl groups ([Slowing \*et al.\*, 2006](#)). The cell uptake efficiency, endocytosis mechanisms and biocompatibility of these NPs were then investigated by using human cervical cancer cells (HeLa). The results indicated that NPs cellular uptake and ability to escape endosomal entrapment depended on surface functional groups. Similarly, surface-functionalized NPs can elicit immune responses and immunotoxicity through several mechanisms ([Chang, 2010](#); [Zolnik \*et al.\*, 2010](#)). For example, [Wan-Kyu \*et al.\*](#) reported that amino-functionalized cationic silica-titania NPs are immunotoxic to macrophages ([Oh \*et al.\*, 2010](#)).

#### 1.4.4. Cell susceptibility to NP toxicity

Depending on the nature of NPs, the type of cells they interact with is also one of the factors affecting their toxicity profile. [Sohaebuddin \*et al.\*](#) have studied the effects of various NPs (TiO<sub>2</sub> and SiO<sub>2</sub> NPs, as well as MWCNTs) on 3T3 fibroblasts, RAW 264.7 macrophages, and telomerase-immortalized bronchiolar epithelial cells (hT cells) ([Sohaebuddin \*et al.\*, 2010](#)). Compared with fibroblasts and epithelial cells, macrophages exhibited higher responses to NPs thus suggesting that cell type is a critical determinant of intracellular response, degree of cytotoxicity and potential mechanism of toxicity of NPs. Indeed, different cell types may internalize the same

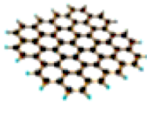
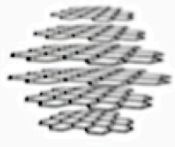

NPs through different pathways. Santos *et al.* used the HeLa, 1321N1 and A549 cell lines to study the endocytic pathway of carboxylated polystyrene NPs with diameters of 40 and 200 nm (Dos Santos *et al.*, 2011). They found that 132N1 cells mainly take up NPs through clathrin-mediated endocytosis, whereas A549 cells use caveolin-mediated pathways. Thus, the interaction between NPs and cells is a complex process and it is not possible to generalize conclusions from specific cell lines to all cell types. Therefore, the influence of cell type on NP fate and toxicity must be considered when studying NPs *in vitro* and *in vivo*.

## 1.5. Carbon dots

CDs are the last member of the carbon NP family and their discovery was an “accidental event”. Indeed in 2004, Xu *et al.* found this new carbon nanomaterial when using arc discharge techniques to prepare SWCNTs (Xu *et al.*, 2004). Since then, CDs have attracted considerable attention due to their important properties. These intrinsically fluorescent NPs have been briefly introduced earlier (1.1.4). In the following, they will be depicted into more details as they are the main purpose of my Ph.D. studies.

### 1.5.1. Structure

In fact, the carbon-based dots include carbon nanodots (CNDs), spherical "carbon quantum dots" (CQDs) and  $\pi$ -conjugated monolithic "graphene quantum dots" (GQDs). The term CDs used in this study refers to CNDs. Cayuela *et al.* summarize their nomenclature (figure 16) and structural characteristics by distinguishing their carbon atom arrangement, crystal structure, and dimension (Cayuela *et al.*, 2016). Amorphous, without quantum confinement, quasi-spherical nanodots are referred to in other publications as carbon nanoclusters, polymer dots or even carbon dots or C-dots (less than 10 nm in size). Evidence for distinguishing between CQDs and GQDs lies in the

GQDs (Graphene Quantum Dots)	CQDs (Carbon Quantum Dots)	CNDs (Carbon Nano Dots)
		
Graphene disc (2-20 nm)	Crystalline and spherical particle (< 10 nm)	Amorphous and quasi-spherical particles (< 10 nm)

**Figure 16.** Classification and nomenclature of carbon-based dots (Cayuela *et al.*, 2016).

precursors used for synthesis. In the case of GQDs (2-20 nm graphene disk), the precursor is mainly based on graphene materials, and CQDs (size less than 10 nm) can be prepared from other carbon nanomaterials having a crystal structure, such as carbon nanotubes, or by pyrolysis of organic molecules at high temperatures. CDs are typically quasi-spherical particles consisting of an amorphous nanocrystalline core, which is predominantly graphitic carbon ( $sp^2$ ), or graphene or graphene oxide sheets fused by diamond-like  $sp^3$  hybrid carbon insertions ([Baker and Baker, 2010](#); [Demchenko and Dekaliuk, 2013](#); [Lim et al., 2015](#); [Yang et al., 2009a](#)). There are many carboxyl and hydroxyl groups at the surface of carbon dots, imparting excellent water solubility and which are suitable reactive groups for further functionalization and surface passivation with various organic, polymeric, inorganic or biological materials. Besides, it is worth noting that surface passivation enhances the intrinsic fluorescence properties of CDs (*vide infra*).

## 1.5.2. Photoluminescent properties

Compared with conventional organic or inorganic fluorophores, the main advantages of CDs include non-flickering photoluminescence (PL) and excellent photostability. The underlying mechanisms of the tunable PL properties of carbon dots are not fully understood and the exact source of their fluorescence emission is still controversial and requires more research to draw a clear picture. Nonetheless, scientists have proposed two hypothetical fluorescence emission mechanisms for CDs. The first hypothesis involves a band gap transition caused by the conjugated  $\pi$ -domains, while the second refers to a more complex origin associated with surface defects in the CDs ([Lim et al., 2015](#)).

The absorbance and fluorescence spectra of organic fluorescent dyes generally display narrow absorption and emission bands, and Stokes shift depends on the type of dye considered. As shown in figure 17, the excitation spectrum of CDs extends from the UV region to the visible region (250-600 nm), enabling “single excitation and multiple emission” ([Sun et al., 2006a](#)). Sun *et al.* reported that surface decoration of non luminescent CDs with PEG<sub>1500N</sub> produced luminescent NPs. This study also suggests that the PL center of CDs may be derived from surface energy traps ([Sharma et al., 2018](#)). Many studies have shown that CDs with enhanced PL characteristics may be obtained through doping with various heteroatoms, including N, S, Si, P, B, Ga, halogen (Cl, Br, I), Se, Ge, Mg, Cu, Zn, Tb, Ru, and Mn ([Wu et al., 2017](#)).

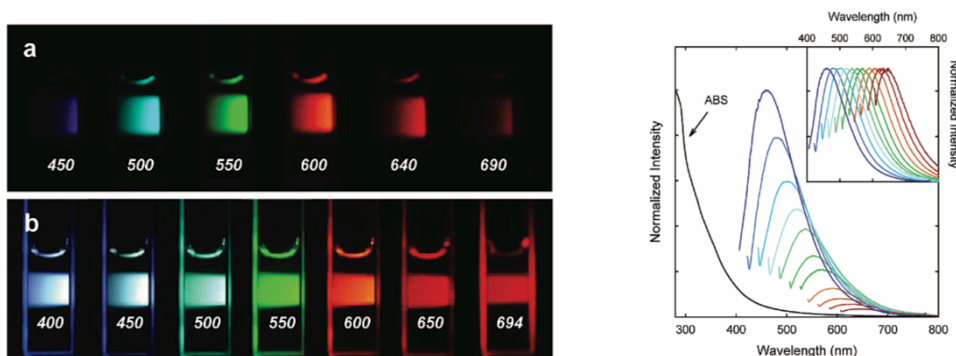


**Figure 17.** Left: Aqueous solution of CDs excited at 400 nm and photographed through a band pass filter at the indicated wavelength (nm) (a), and excited at the indicated wavelength and directly photographed (b). Right: Normalized absorption (black line) and luminescence emission spectra of CDs in aqueous solution, with increasing excitation wavelength from 400 to 800 nm, with 20 nm increment ([Sun et al., 2006a](#)).

### 1.5.3. Synthesis

CDs may be easily produced from inexpensive starting materials using various protocols that are based on either top-down or bottom-up approaches ([Himaja et al., 2015](#); [Lim et al., 2015](#); [Wang et al., 2017](#); [Zuo et al., 2016](#)). In the top-down approaches, CDs are produced by breaking down large carbon structures, while in the bottom-up approaches, they are built from small organic precursors. Due to the very large number of publications describing the preparation of CDs, I arbitrarily selected some examples to illustrate my point in what follows.

#### 1.5.3.1. Top-down approaches

CDs can be obtained by cutting macroscopic carbon structures such as carbon powders, carbon nanotubes, graphite columns, and graphene using different methods presented below. The disadvantage of these methods is that size distribution and morphology of the products cannot be precisely controlled because of the absence of selectivity of the chemical cutting processes involved. However, the diversification of the size and surface state of the CDs produced by the top-down approaches provides additional opportunity to explore CDs with tunable PL.

##### *Electrochemical synthesis*

Electrochemical synthesis of CDs was first reported by Zhou *et al.* ([Zhou et al., 2007](#)). The authors produced blue luminescent nanocrystals by electrochemical treatment of CNTs in acetonitrile containing 0.1 M tetrabutylammonium perchlorate as the supporting electrolyte. The colorless solution turned yellow to dark brown, indicating the formation of CDs peeled off from the nanotubes and their accumulation in the solution. Zhao *et al.*

reported the synthesis of CDs by electrochemical methods using graphite column electrodes as the carbon source ([Zhao et al., 2008](#)). In another report, Li *et al.* obtained special fluorescent characteristics of CDs by changing the electrolyte ([Li et al., 2010a](#)). They obtained a mixture of ultra-small CDs of different sizes and different emission colors. An advantage of electrochemical methods is their low cost and ease of operation.

### Chemical oxidation

Liu *et al.* obtained water-soluble fluorescent CDs from candle soot treated with oxidizing acid (30 % H<sub>2</sub>O<sub>2</sub>/AcOH 2:1, v/v). These CDs are stable for several months under ambient conditions and can be excited at a single wavelength to produce multiple color emission ([Liu et al., 2007](#)). Wang *et al.* used a modified nitric acid oxidation method to prepare photoluminescent CDs exhibiting excellent biocompatibility and interesting properties for *in vivo* fluorescence imaging and tumor cell tracking ([Wang et al., 2013a](#)). Chemical oxidation of carbon bulk material can provide CDs with various surface states and functional groups (introducing oxygen-containing functional groups -OH and -COOH at the NP surface) that are critical to their tunable emission. It is also a convenient and effective method to produce CDs without the requirement of sophisticated equipment.

### Solvothermal synthesis

Solvothermal synthesis is a widely used method for the preparation of NPs. For example, it allows precise control of the size, shape distribution and crystallinity of metal oxide NPs or nanostructures. In addition, characteristics of the NPs can be tuned by varying the reaction temperature, reaction time, solvent, surfactant (if any), and precursor. Liu *et al.* reported a simple solvothermal method to produce nitrogen-doped graphene quantum dots (N-GQDs) from graphene oxide (GO) as starting material ([Liu et al., 2013](#)). DMF was used both as a solvent and nitrogen source, and decomposes to dimethylamine and carbon monoxide at temperature above its boiling point (figure 18). Dimethylamine then reacts with GO to produce N-doped GQD.

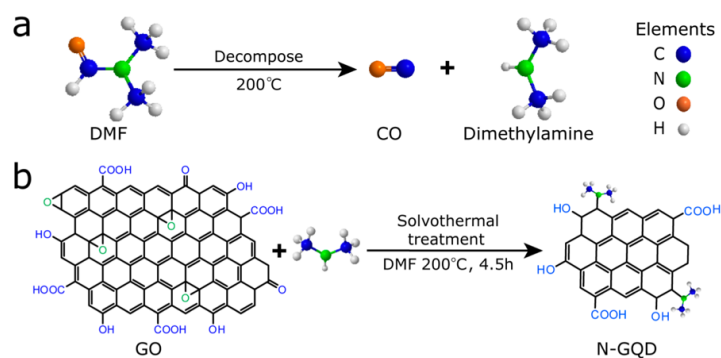


**Figure 18.** Production of N-doped CDs from graphene oxide (GO) in DMF. (a) Decomposition of DMF at high temperature. (b) Reaction of dimethylamine with GO according to Liu *et al.* ([Liu et al., 2013](#)).

### 1.5.3.2. Bottom-up approaches

Bottom-up syntheses refer to CD production using molecular precursors as carbon source. In addition to a wide variety of precisely defined molecular precursors (e.g., citric acid, glucose, oleic acid, phenylenediamine, EDTA, urea...), a number of “green” carbon sources have been described including biomass, eggs, hair, coffee grounds, pollen bees, and various other natural materials ([Zhang and Yu, 2016](#)).

#### *Carbonization under air atmosphere*

Carbonization generally occurs in bottom-up approaches, which is a chemical process that converts organic matter into carbon residues *via* pyrolysis reactions. Zhou *et al.* reported that fluorescent CDs were synthesized by low-temperature carbonization of watermelon rind ([Zhou et al., 2012](#)). The CDs have a small size (2.0 nm) and stable fluorescence properties with strong blue light emission. Liu *et al.* reported the synthesis of luminescent, water-soluble graphitized C-dots by one-step carbonization of ethylene glycol at 140 °C in the presence of concentrated sulfuric acid ([Liu et al., 2012b](#)). The CDs thus prepared showed blue PL emission in the presence of mercury ions in water. Dong *et al.* synthesized polyamine-functionalized CDs by carbonizing citric acid at low temperature (<200°C) using polyvinylamine as a passivating agent ([Dong et al., 2012](#)).

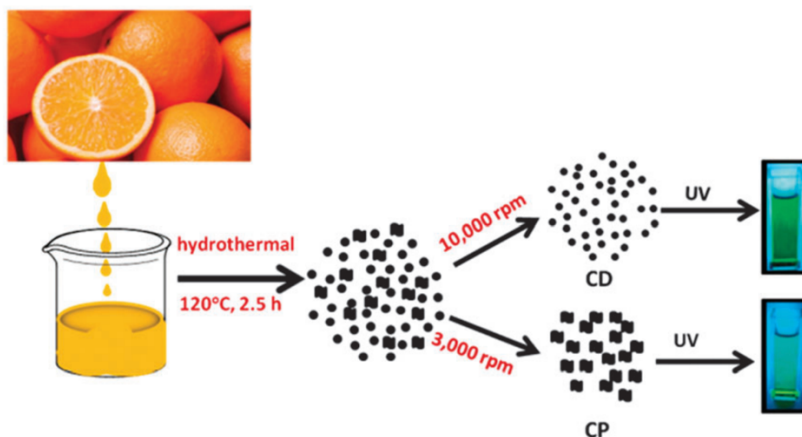


**Figure 19.** Hydrothermal synthesis of CDs from orange juice ([Sahu et al., 2012](#)).

#### *Hydrothermal synthesis*

Hydrothermal synthesis describes a chemical reaction in water under optimal temperature conditions (100-250 °C), and thus has usually to be conducted under high pressure in tightly sealed reactors. The hydrothermal route is considered to be a direct and efficient method to promote polymerization and carbonization of precursors. It is thus widely used in the synthesis of NPs due to easy control, low environmental damage and low energy consumption. Sahu *et al.* have prepared highly



photoluminescent CDs with a PL quantum yield of 26 % by a hydrothermal treatment of orange juice ([Sahu et al., 2012](#)). The mechanism for the formation of nanoparticles involves the hydrothermal carbonization of the main components of orange juice such as sucrose, glucose, fructose, citric acid and ascorbic acid. This synthesis process is illustrated in figure 19. Wu *et al.* used silkworms, a carbon source with high nitrogen content, as raw material to prepare photoluminescent nitrogen-doped CDs by a one-pot hydrothermal method ([Wu et al., 2013](#)). These CDs have a quantum yield of 13.9 %, show amphoteric properties, have high photostability, low toxicity, and are suitable for biological imaging. Li *et al.* synthesized luminescent CDs with controllable emission wavelength by the hydrothermal method starting from citric acid and urea ([Li et al., 2014](#)). The quantum yield was as high as 44.7 % and these CDs were used to prepare multicolor CD/polymer composites that exhibited blue, green, and even white emission.

#### *Microwave-assisted synthesis*

Microwave (MW) heating has several advantages over other conventional heating methods. For example, it allows reaching high temperatures very quickly and thus significantly reduces reaction time. MW heating is widely used for NP synthesis because it is simple, convenient, fast, energy-efficient and industrially scalable. That is probably why MW-assisted synthesis has become the more popular method to produce CDs. Wang *et al.* proposed a simple, economical, and green one-step MW-assisted synthesis of CDs ([Wang et al., 2011b](#)). The preparation requires carbohydrates (glycerol, glycol, glucose, sucrose, etc.) and a small amount of inorganic ions, and reaction can be completed in a few minutes. Zhai *et al.* reported a MW-assisted preparation of CDs through pyrolysis of citric acid in the presence of various amine compounds (1,2-ethylenediamine–EDA, diethylamine–DEA, triethylamine–TEA and 1,4-butanediamine–BDA) ([Zhai et al., 2012](#)). The authors showed that fluorescence of CDs was significantly improved by using primary amines. Pierrat *et al.* reported the production of cationic CDs by pyrolysis of citric acid and high molecular weight branched poly(ethyleneimine) (25 kDa, bPEI25k) under microwave irradiation ([Pierrat et al., 2015](#)). These CDs showed high efficiency in transfecting cells with DNA and siRNA.

#### **1.5.3.3. CDs functionalization**

As discussed above, many methods for preparing CDs have been developed. However, in some instances the “as produced” CDs require chemical modification at the surface to provide the NPs with additional specific properties. Shen *et al.* reported on functionalization of CDs for use in blood glucose testing ([Shen and Xia, 2014](#)). The

prepared CDs are directly functionalized with boric acid and do not require any additional surface modification for introduction of binding sites. The added glucose can selectively lead to the assembly of CDs based on covalent bonding between the *cis*-diol of glucose and the boric acid on the surface of the CDs. The boric acid-modified CDs obtained in this study proved efficient to titrate glucose in the range of 9-900  $\mu\text{M}$ . Yang *et al.* built up nuclear localization signal peptide (NLS)-functionalized CDs that are transported into the nucleus of cancer cells to enhance antitumor activity of loaded doxorubicin (DOX). In this structure, hydrazinobenzoic acid is used as a linker, and DOX is covalently conjugated to the NLS-functionalized CDs by a pH-sensitive hydrazone bond. The complex is effective for inducing apoptosis of human lung adenocarcinoma A549 cells and inhibiting tumor growth (Yang *et al.*, 2016). Eun *et al.* synthesized CDs by pyrolyzing citric acid in the presence of PEG diamine. Then, a hyaluronic acid (HA)-CD conjugate is produced by forming amide bonds between the amine groups of the CDs and the carboxyl groups of HA. *In vivo* real-time bioimaging of HA-CD conjugates revealed their targeted specific delivery to the liver, which cells express high levels of HA receptors. The MTS assay confirmed the cytocompatibility of the HA-CDs conjugate (Goh *et al.*, 2012).

#### **1.5.4. Biomedical applications**

A variety of applications have been suggested and tested for CDs. The vast majority of these applications have to do with the PL properties of CDs. Below are reviewed some applications related to the biomedical field, especially to drug delivery and bioimaging.

##### **1.5.4.1. CDs as drug delivery systems**

CDs are potential candidates for controlled drug delivery due to their high surface area to volume ratio, simple manufacturing and purification processes, excellent biocompatibility, low cytotoxicity, tunable physicochemical properties, and richness in reactive functional groups at their surface, appropriate for decoration with various compounds such as targeting moieties.

Lai *et al.* synthesized CDs with homogenous size distribution using glycerol as a single precursor and growing CDs in mesoporous silica.  $\text{SiO}_2$ -embedded CDs were further passivated *via* amino-PEG (PEG<sub>900N</sub>) anchoring. This material was proved to adsorb and controllably release doxorubicin (DOX) in HeLa cells (Lai *et al.*, 2012). Singh *et al.* reported the formation of hydrogels from DNA and CDs for targeted drug



release. The hydrogel was used as a container for DOX for sustained release. They found that the hydrogel was destroyed at an advantageous acidic pH, with apoptosis of HeLa cells as a result of DOX release ([Singh et al., 2017](#)).

#### 1.5.4.2. CDs for fluorescence bioimaging

CDs have received attention as diagnostic imaging probes, due to their rich photoluminescence, high light stability and low toxicity. They represent strong competitors and potential substitutes for the heavy metal semiconductor quantum dots (Qdots) currently in use. To illustrate this, I have selected a few applications from an extensive literature.

Qian *et al.* synthesized Si-doped carbon quantum dots (SiCQDs) and found that these SiCQDs exhibit enhanced visible fluorescence due to the introduced silicon atoms. Bioimaging experiments have demonstrated that these SiCQDs are well suited for bioimaging of human HeLa cells ([Qian et al., 2014](#)). Sun *et al.* produced CDs by laser ablation of carbon targets in argon. The results suggest that these CDs have great potential in the field of bioimaging because of luminescent emission stable against photobleaching and absence of blinking effect ([Sun et al., 2006b](#)). Yang *et al.* injected PEGylated CDs intravenously into mice and observed bright fluorescence in the urine after 3 hours, concluding that the excretion route of these NPs is mainly urine ([Yang et al., 2009a](#)). Khan *et al.* reported orange emissive CDs synthesized from urea and citric acid using a solvothermal synthesis that spontaneously localized within HeLa cell nuclei and specifically bind RNA ([Khan et al., 2018](#)). This study demonstrates the possibility of single-molecule imaging and super-resolution microscopy using fluorescent CDs. Zhang *et al.* synthesized “gold-carbon dots” (G-CDs) using the microwave-assisted method and demonstrated their potential in multiple applications ([Zhang et al., 2016](#)). Especially, these G-CDs exhibit amazing peroxidase-like activity and single excitation/dual emission properties. In another work, fluorescence ratio imaging was used to monitor Fe<sup>3+</sup> levels in normal rat osteoblasts ([Yang et al., 2018a](#)). Yang *et al.* prepared CDs from citric acid, urea and sodium fluoride using a one-step microwave-assisted pyrolysis method. They reported that CDs can achieve red-shifted PL emission by incorporation of electron-withdrawing fluorine atoms, allowing *in vivo* fluorescence imaging in nude mice injected intravenously (figure 20). After 12 hours, the fluorescence signal was mainly located in the tumor area. The results indicate that CDs can effectively accumulate in tumors due to the EPR effect. The mice remained healthy after injection, which demonstrates the biocompatibility of these CDs.

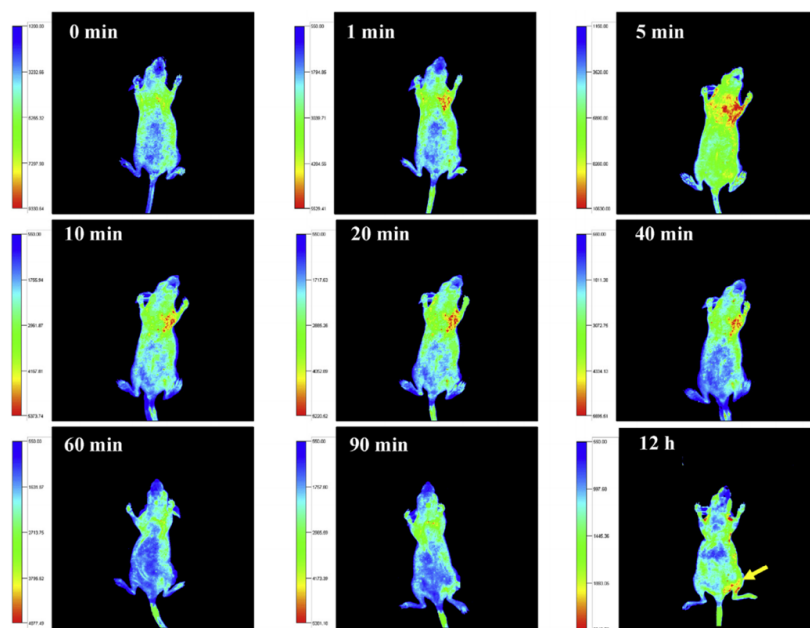


**Figure 20.** Fluorescence images in tumor-bearing mice injected with CDs at various time points (Yang *et al.*, 2018a).

#### 1.5.4.3. CDs for magnetic resonance imaging

CDs are widely used in bioimaging and also improved the prior art to some extent. For instance, gadolinium (Gd) is widely used in magnetic resonance imaging (MRI), a non-invasive imaging technique with high spatial resolution used in clinical diagnosis. However, gadolinium ions ( $Gd^{3+}$ ) have caused safety problems due to their high toxicity (Lim *et al.*, 2013). Xu *et al.* described CD-stabilized gadolinium hybrid nanoprobe (Gd-CDs) produced by hydrothermal treatment of a mixture of citric acid, ethylenediamine and  $GdCl_3$ . These CDs are simple to prepare, easy to functionalize, and furnish high contrast, thus providing an efficient non-toxic Gd-based MRI contrast agent (Lim *et al.*, 2013). Shi *et al.* reported CDs prepared under low temperature pyrolysis from citric acid and bPEI as a new bimodal bioimaging nanoprobe. These CDs were conjugated with cyclic diethylenetriamine pentaacetic acid dianhydride (cDTPAA) to obtain CD–DTPAA–Gd nanoprobe. The probe had negligible cytotoxicity as well as high sensitivity for fluorescence imaging and high spatial resolution MRI (Shi *et al.*, 2015).

#### 1.5.4.4. Theranostic applications

As mentioned above, the use of CDs as DDS and imaging tools has been extensively reported *in vitro* and *in vivo*. The combination of diagnostic and therapeutic capabilities into a single agent to provide a specific therapeutic regimen refers to

theranostic nanomedicine and CDs offer challenges and opportunities associated with this emerging technology (Xie *et al.*, 2010).

Huang *et al.* reported a phototriggered therapy based on chlorin e6-conjugated CDs (CDs-Ce6) (Huang *et al.*, 2012). PEG<sub>2000N</sub>-passivated CDs were conjugated with Ce6, a commonly used photosensitizer, through EDC-NHS coupling reaction. The resulting nanocarriers were confirmed to be non-cytotoxic, have good biocompatibility, and revealed effective in enhancing both *in vivo* photosensitizer fluorescence detection (PFD) and photodynamic therapy (PDT) of gastric cancer. Goh *et al.* reported the use of CDs for real-time bioimaging of target-specific delivery of hyaluronic acid (HA) derivatives (Goh *et al.*, 2012). The HA-CDs were specifically delivered to the liver with abundant HA receptors. Tang *et al.* reported on CDs featuring efficient Förster Resonance Energy Transfer (FRET) for real-time monitoring of drug delivery and imaging (Tang *et al.*, 2013). In this construction, CDs act as both excellent drug carrier (DOX) and FRET donor, whereas DOX was the acceptor. Pandey *et al.* reported CD-coated gold nanorods (CD@GNR) to which was conjugated DOX, for drug delivery, photothermal therapy and bioimaging applications.(Pandey *et al.*, 2013). This novel complex has been shown to allow a highly biocompatible thermochemotherapy for solid tumors. Zheng *et al.* reported a CD-based DDS for bioimaging and theranostic applications (Zheng *et al.*, 2014). CDs were synthesized under thermal pyrolysis conditions from citric acid (CA) as a carbon source and polyene-polyamine as a passivating agent. They obtained a supramolecular nanomedicine (CD-Oxa) by a condensation reaction between amino groups displayed at the surface of the CDs and the free carboxyl group of the anti-cancer drug oxaliplatin (Oxa(IV)) (figure 21).

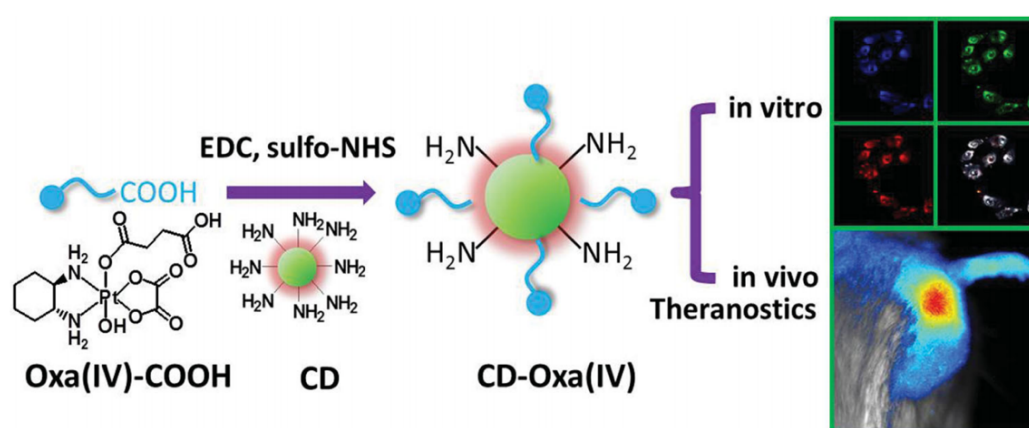


**Figure 21.** Schematic diagram of CD-Oxa as a theranostic platform. CD-Oxa integrates the optical properties of CDs and the anti-cancer function of oxaliplatin into one unit. The platform features include drug carriers, controlled drug release, and multicolor imaging capabilities (Zheng *et al.*, 2014).

### 1.5.5. Toxicology

Low toxicity and high biocompatibility are two necessary conditions for promoting biological applications of nanomaterials ([Zhao et al., 2015](#)). As discussed above, CDs possess physicochemical and photochemical stability, as well as non-blinking behavior. Their preparation methods are relatively simple, of low cost, and suitable for large scale preparation. The applications of CDs for *in vitro* and *in vivo* drug delivery or bioimaging have been increasingly reported. In contrast, toxicological properties of CDs have been less studied. Though CDs do not contain toxic elements, it must be recognized that their nanoscale dimension may pose potential risks to human health. Some of the published toxicological assessments of CDs, in which the researchers used CDs of different chemical composition produced by different methods and different biological models with different toxicological endpoints, reported inconsistent results ([Havrdova et al., 2016](#); [Lacerda et al., 2006](#); [Lewinski et al., 2008](#); [Singh et al., 2009](#); [Yang et al., 2009d](#)).

Yang *et al.* systematically evaluated the *in vitro* and *in vivo* toxicity of PEG<sub>1500</sub>-passivated CDs ([Yang et al., 2009c](#)). They showed that these PEG<sub>1500</sub>-CDs of 4 to 5 nm size had negligible effect on the proliferation ability and activity of human breast cancer MCF-7 and colorectal adenocarcinoma HT-29 cells. The concentrations of CDs used in these studies (1-200 µg/mL) were significantly higher than those required for potential applications such as live cell imaging. Wang *et al.* evaluated CDs (50 nm) prepared from commercially supplied carbon nanopowder and found that the cytotoxicity of CDs prepared from polyacrylic acid (PAA) and polyethyleneimine (PEI) as passivation reagent was significantly higher than the one induced by CDs prepared from poly(ethylene glycol) (PEG) and propionylethylene-imine-co-ethylene-imine (PPEI-EI) ([Wang et al., 2011c](#)). Jiang *et al.* successfully prepared CDs by a modified photo-Fenton reaction and a hydrothermal method using graphene oxide sheets as precursors ([Jiang et al., 2015a](#)). The potential toxicity of these CDs was assessed on zebrafish embryos and larvae by the CCK-8, LDH, ROS and Annexin-V apoptosis assays. The results indicated that internalization of low doses of CDs (12.5 and 25 µg/mL) does not induce significant cytotoxicity on HeLa cells ([Jiang et al., 2015a](#)). Fan *et al.* prepared CDs (2-4 nm) by a simple hydrothermal treatment using polyethylene glycol as the sole carbon source, and evaluated their *in vitro* toxicity in HepG2 cells. These CDs exhibited negligible cytotoxicity at concentration below 100 µg/mL. Cell loss was 51 % when the CD concentration reached 400 µg/mL. The results obtained suggest that these CDs are excellent two-photon probes for use in bioimaging applications due to their high cell uptake and absence of toxicity ([Fan et al., 2014](#)).

Li *et al.* reported that the chemical nature of the surface of CDs may affect their toxicity. They synthesized CD-based nanohybrids with polyhydroxy hyperbranched polyglycerol (HPG) shells by the "grafting" method with an anionic ring-opening polymerization technique. The size of pristine CDs and CDs-g-HPG was  $6.8 \pm 1.7$  nm and  $70.8 \pm 11.3$  nm, respectively, whereas zeta potential was  $-14.6 \pm 1.0$  mV and  $-15.0 \pm 1.5$  mV, respectively. Evaluation of *in vitro* toxicity showed that CDs-g-HPG had lower cytotoxicity than pristine CDs, indicating that HPG conjugation improved the biosafety of CDs (Li *et al.*, 2017). It is not clear however whether differences were due to conjugation or to size variation.

Liu *et al.* evaluated the effect of CDs (5 nm) on the growth of *Escherichia coli* (*E. coli*) (Liu *et al.*, 2015). The growth of the bacteria was increased when CD concentration was less than 5 mg/L, whereas it was inhibited at upper concentrations (10-200 mg/L). Sun *et al.* synthesized high-luminescence CDs by microwave-assisted pyrolysis of tris(hydroxy- methyl)aminomethane (Tris) and citric acid, and studied their toxicological properties in *Physa acuta* (*P. acuta*) (Sun *et al.*, 2016). The CDs did not have acute toxicity nor caused embryonic developmental malformations, but they exhibited chronic toxicity (Sun *et al.*, 2016). Xiao *et al.* investigated the safety of commercial CDs (4 nm, Jubang Science & Technology Co. Ltd., Beijing, China) on minnow (*Gobiocypris rarus*) embryos and found that high CD concentrations are developmentally toxic (Xiao *et al.*, 2016). Physiological abnormalities included decreased athletic ability and body length, increased heart rate, pericardial and yolk sac edema, curved tail/ridge, and reduced hatching rates. This developmental toxicity was attributed to oxidative stress leading to suppression of DNA function. Recently, Yang *et al.* evaluated biodistribution and toxicity of CDs upon inhalation in mice (Yang *et al.*, 2018b). Toxicity endpoints included histopathology and blood biochemical analyses. Biodistribution results indicated that the major target organs of CDs are lung and liver. At high CD concentrations (1.0 and 5.2 mg/kg), mice died, and lung and liver damage, including inflammation and necrosis, was observed.

In summary, a significant number of toxicological studies were conducted on CDs using diverse cell lines and animal models. But, due to the diversity of tested concentrations and models, a standardized evaluation system has yet to be established. Furthermore, CDs characteristics were not always provided, making comparisons between studies difficult. In addition, most of the toxicity studies were conducted in invertebrate or *in vitro* models, resulting in a lack of toxicity assessment in mammalian models, particularly upon repeated exposures. Due to the lack of sufficient evidence of safety, public concerns about the potential toxicity of CDs cannot be eliminated. What needs to be answered to explore the source of CDs is why in the cases discussed above, some of the CDs were toxic while others were not.



## **Part 2**

### **Objectives, materials, and methods**





## 2.1. Objectives of the thesis

One of the goal of the thesis is to address some of the challenges and knowledge gaps in nanotoxicology by using *in vitro* and *in vivo* models. With the proliferation of CD manufacturing and applicability research, toxicological assessments need to evolve to address related safety issues and ensure sustainability. Thus, using CDs as model NPs, we aimed to get a better understanding of the source of NPs toxicity. The second goal of our work is to evaluate the potential of CDs as gene carriers. More specifically, we aimed at studying the factors that influence the ability of cationic CDs to mediate the entry of genetic material into cells, with the goals to improve the efficacy of these NPs.

To achieve our goals, we thus established a library containing 34 CDs so as to investigate their toxicity *in vitro* and *in vivo*. Physicochemical properties of CDs, were characterized by measuring CDs size, surface charge and chemical composition (N, C, H). Toxicological evaluations consisted at first in investigating the viability loss triggered by the whole CDs library in a model of human macrophages, and in analyzing the obtained data with regard to the CD physicochemical characteristics. Secondly, we selected representative CDs in the library to conduct in-depth toxicological evaluations, including 1-assessment of viability loss induced by the representative CDs as a function of cell type or incubation time, 2-characterization of CD cellular uptake and its mechanism, and 3-investigation of CD-evoked inflammation, oxidative stress and mitochondrial perturbation. At last, was evaluated the lung inflammatory response induced by the selected CDs in mice.

With respect to CDs as gene carriers, an extended library containing 88 cationic CDs was established to carry out investigations on their transfection performance and identify structure-activity relationships. These specifically designed CDs were systematically evaluated in an *in vitro* transfection assay using a *Luciferase* reporter gene. Their cytotoxicity was also systematically determined in parallel. Throughout this research project, we studied the effects of various synthetic factors on transfection efficiency using a trial-and-error approach and sequentially improved our CD-based gene carriers determining the particular effect of 1-activation conditions; 2-stoichiometry of the reagents, and 3-nature of the passivation reagent, on transfection rate.

## 2.2. Materials

Citric acid, bPEI25k, bPEI600, 3-(4,5-dimethylthiazol-2-yl)-2,5-diphenyl tetrazolium bromide (MTT), hydrogen peroxide (H<sub>2</sub>O<sub>2</sub>), dimethyl sulfoxide (DMSO), and phorbol myristate acetate (PMA) were from Sigma-Aldrich (St Louis, MO, USA). Dialysis membranes were from Spectrum laboratories (Rancho Dominguez, CA, USA). Plasmid pCMV-GLuc (5.7 kbp, Nanolight Technology, Pinetop, Az, USA) was used as reporter gene to monitor *in vitro* DNA transfection activity. This plasmid encodes the *Gaussia princeps* luciferase gene. DNA concentration refers to phosphate content. Fetal bovine serum (FBS), culture media (Dulbecco's Modified Eagle Medium, DMEM) and supplements were from GIBCO-BRL (Cergy-Pontoise, France). Fungizone, penicillin–streptomycin mix (10,000 U/mL and 10,000 g/mL, respectively), trypsin, Hepes (1 M) and phosphate buffered saline (PBS) were from Invitrogen Corp. Lysis solution for luciferase activity monitoring was purchased from Promega (Charbonnières, France). Coelenterazine was from Alfa Aesar (Bisheim, France). ELISA kits for cytokine assays were purchased from R&D Systems (Lille, France) or eBiosciences (Le Pont de Claix, France). The Multi-Analyte ELISArray Kit was purchased from Qiagen. All CDs and buffer solutions were prepared with deionized water purified with an EMD Millipore Milli-Q™ integral system (resistivity  $\leq 18.2 \text{ M}\Omega\cdot\text{cm}$ ) and filtered through a 0.2  $\mu\text{m}$  polycarbonate membrane.

### 2.2.1. Preparation of the CDs

All the CDs used in this study were synthesised by my colleague Mickaël Claudel. Some of them were prepared according to an earlier work realized in the laboratory ([Pierrat \*et al.\*, 2015](#)). The nanoparticle structure diversity required for our studies was introduced through variations of the experimental conditions under which CDs were produced:

- Activation mode (solvothermal preparation, pyrolysis at atmospheric pressure, solvothermal microwave-assisted pyrolysis, microwave-assisted pyrolysis at atmospheric pressure...);
- Carbon source (citric acid, ammonium citrate, sodium citrate, ethyl citrate, glucose, mannitol...);
- Passivation agent (oligoamines: EDA, DMEDA, TETA, PEHA, various PEIs, various PEGs and mPEGs...);
- “Modifier” (HCl, H<sub>3</sub>PO<sub>4</sub>, H<sub>3</sub>BO<sub>3</sub>...);
- Stoichiometry of reagents (carbon source *vs.* passivation reagent);

- Processing temperature (100 to 230 °C);
- Processing time (depending on the activation mode).

Here, I will briefly introduce a few representative protocols that were followed to produce the CDs that I further used in my studies.

#### *Solvothermal preparations*

Citric acid (1.0 g), bPEI25k or bPEI600 (4.0 g), and H<sub>2</sub>O (50 mL) were mixed under vigorous stirring to form a homogeneous solution. The solution was then transferred into a reaction vessel fitted with a reflux condenser, and heated for 24 h at 100 °C. When cooled down to room temperature, the resulting solution was transferred into a dialysis bag (MWCO 1000) and was equilibrated for 12 h against 1 L HCl 0.1 N (dialysate was replaced at 1, 3, 9 h), and then against ultrapure water for an additional 12 h-period. Finally, the solution was filtered through a 0.22 µm PES membrane (Millex) and freeze-dried at -50°C for 24-36 hours.

#### *Solvent-free pyrolysis*

Citric acid (0.125 g) and bPEI25k or bPEI600 (0.500 g) were introduced into a 10 mL borosilicate glass vial without solvent and heated for 30 min in a Monowave 50 synthesis reactor. The residue was vigorously stirred with water (5 mL), centrifuged (10.000 rpm, 5 min), and the supernatant was dialyzed, filtered, and freeze-dried as described above.

#### *Pyrolysis under atmospheric pressure*

Citric acid (1.00 g) and bPEI25k or bPEI600 (4.00 g) were dissolved in water (5 mL) in a 25 mL borosilicate reaction flask. The flask was heated at 180 °C for 30 min under atmospheric pressure, using a heating mantle. During this first heating step, volatiles were integrally driven out of the reaction vessel. Then temperature was raised to and maintained at 225 °C for an additional period of 30 min. The resulting reaction mixture was treated as described above.

#### *Microwave irradiation under solvothermal conditions*

Citric acid (1.0 g) and bPEI25k or bPEI600 (4.0 g) were mixed in H<sub>2</sub>O (10 mL) under vigorous stirring to form a homogeneous solution. The solution was then transferred into a tightly sealed borosilicate glass vial and heated for 30 min at 100 °C using an Anton Paar Monowave 500 microwave reactor. The crude residue was purified by dialysis and freeze-dried as described above.

### *Microwave irradiation in a domestic oven*

Citric acid (0.125 g), bPEI600 (0.500 g), and HCl 0.1 N (5 mL) were mixed in an Erlenmeyer flask to form a homogeneous solution that was heated in a domestic microwave oven at 620 W for 180 sec. Noteworthy, using temperature measuring strips, the maximum temperature reached in the vessel was determined to be around 250 °C. The residue was stirred with HCl 1N (5 mL) for 15 min, centrifuged, and the supernatant was dialyzed and freeze-dried as described above.

## **2.2.2. Characterization of CDs**

Characterization of the CDs has been achieved by Mickaël Claudel. This included the determination of their elemental composition, absorption and photoluminescence spectra, and fluorescence quantum yield. The average particle size (hydrodynamic diameter) and zeta potential ( $\zeta$ ) of CDs or CD-nucleic acid complexes were measured by dynamic light scattering (DLS) on freshly prepared CD solutions or CD-nucleic acid complexes (in NaCl 1.5 mM pH 7.4, 25 °C). The primary shape and morphology of CDs were captured by transmission electron microscopy (TEM) using a bench top transmission electron microscope operating at 5 kV.

## **2.3. *In vitro* evaluation of CDs**

### **2.3.1. Cell culture**

#### *THP-1 cells*

The THP-1 cells (human acute monocytic leukemia cells, TIB-202<sup>TM</sup>), were obtained from the American Type Culture Collection (ATCC-LGC, Molsheim, France). They were grown in culture flasks at 37 °C in a 5 % CO<sub>2</sub> humidified incubator using RPMI-1640 culture medium supplemented with heat inactivated foetal bovine serum (FBS, 10 %), penicillin (100 IU/mL), streptomycin (100 µg/mL), L-glutamine (2 mM) and 2-mercaptoethanol (0.05 mM). The culture medium was changed every 3-4 days. Cells were subcultured when the culture concentration reached 100,000 to 120,000 cells/mL, by dilution in fresh medium. The starting cell density for subcultures was 3x10<sup>5</sup> cells/mL. Before each experiment, THP-1 cells were seeded in appropriate culture devices at the required density and differentiated into macrophages by overnight treatment with 10 ng/mL PMA. Before use, differentiated cells were gently washed with PBS.

### *A549 cells*

The A549 cells (human lung epithelial carcinoma cells; CCL-185™) were obtained from ATCC-LGC. They were grown in culture flasks at 37 °C in a 5 % CO<sub>2</sub> humidified chamber using DMEM/F-12 culture medium containing FBS (10 %), L-glutamine (2 mM), penicillin (100 IU/mL), streptomycin (100 µg/mL), and HEPES (5 mM). A549 cells were subcultured when cultures reached confluency. To do so, the cells were treated with 0.05 % trypsin-EDTA until their full detachment from the flasks. After trypsin inactivation by addition of complete culture medium and centrifugation of the cell suspension, cells were seeded in a new flask at a density of *c.a.* 2,500 cells/mL, or in appropriate culture devices for experiments.

### *Calu-3 cells*

The Calu-3 cells (human lung epithelial carcinoma cells; HTB-55™) were obtained from ATCC-LGC. They were grown in culture flasks in DMEM/F-12 culture medium supplemented with FBS (10 %), L-glutamine (2 mM), penicillin (100 UI/mL), streptomycin (100 µg/mL), and HEPES (5mM). The cells were subcultured when cultures reached confluency, as described above. They were then seeded in a new flask at a density of *c.a.* 25,000 cells/mL for subculturing, or in appropriate culture devices for experiments.

## **2.3.2 Viability assay after cell exposure to CDs**

Cell viability in response to CDs was assessed on the three cell lines, THP-1, A549 and Calu3 by the MTT assay. THP-1 cells were seeded in 96-well culture plates at a density of 100,000 cells/well in the presence of 10 ng/mL PMA to induce macrophage differentiation. A549 and Calu-3 cells were seeded at a density of 30,000 and 100,000 cells/well, respectively, without other treatment. At these respective densities, the two last cell lines were confluent at the time of CD treatment. The culture medium was used according to the cell type, as described above. The day after the cell plating, fresh CD solutions at the desired final concentrations (3, 6, 12, 25, 50, 100 and 200 µL/mL) were prepared in complete culture medium from a stock solution in water. Then, the cell culture medium was removed from each well, the cells were rinsed with PBS, and CD solutions at increasing concentrations or culture medium alone (control) were added to the wells. After 1, 4 or 24-h incubation, the culture medium was removed and stored at -20°C until cytokine assay (*vide infra*). The cells were then carefully washed with PBS before addition of a 1 mg/mL MTT solution prepared in complete culture medium, and incubated for 1 h. After dye incubation, culture medium was removed and cells were lysed by addition of DMSO (100 µL). Absorbance of the resulting samples was read at

570 nm with a correction at 690 nm or 540 nm using a Multiskan FC reader (Thermo Scientific). When possible, the values of the CD concentration effective in inducing 50% loss in viability ( $EC_{50}$ ) and the CD concentration effective in inducing 20% loss in viability ( $EC_{80}$ ) were calculated after logarithmic transformation of the concentration values and adjustment of the dose-response curve with the Hill equation, using the GraphPad Prism 6.0 software.

### 2.3.3. Assessment of CD internalisation

Confocal laser scanning microscopy (CLSM) and flow cytometry (FACS) were used to observe and quantify CD internalization in THP-1 and A549 cells.

For CLSM experiments, THP-1 cells were seeded into 8-well IbiTreat  $\mu$ -Slides (1.5 polymer coverslip, IBIDI<sup>®</sup>) at a density of 500,000 cells/well and differentiated into macrophages upon PMA treatment (*vide supra*). A549 cells were seeded in the same culture devices at a density of 75,000 cells/well without further treatment. One day later, cells were carefully washed with PBS and incubated with 25  $\mu$ g/ml CDs for 4 h. At the end of the incubation time, they were carefully washed with culture medium to remove non-internalized CDs. Then, the DSQ12S fluorescent probe (10 nM in PBS) was added to the samples for 5 min to label the cell membrane, and the intracellular distribution of CDs was immediately observed using a Leica SP2 microscope equipped with a 63x oil immersion objective (NA=1.2). CDs and the DSQ12S membrane probe were excited with 405 and 635 nm laser sources, respectively. The emission bands were detected with a photomultiplier. The position and the width of the detection channels were adjusted for each dye.

For FACS experiments, THP-1 cells were plated in 24-well plates at a density of 500,000 cells/well and differentiated into macrophages with PMA. For A549 cells, 180,000 cells/well were seeded in the plates. After 24 h, the cells were washed with PBS and CDs (25  $\mu$ g/mL) were added to the cells for 4 h. After CD treatment, cells were washed carefully with PBS to remove non-internalized CDs. Then, cells were detached from the plates with Trypsin-EDTA, pelleted by centrifugation, re-suspended in culture medium without serum and kept on ice until analysis using the LSRFortessa X-20<sup>™</sup> flow cytometer (BD Biosciences) controlled by the FACSDiva<sup>™</sup> software (BD Biosciences). The samples were excited using a 405 nm laser with emission signal detected at 450 nm, or at 355 nm laser with emission signal detected at 515 nm. The analysis of the results was carried out with the FlowJo software. Events of very small size and very high granularity (debris) were excluded from the analysis. For A549 cells, cell doublets (approximately 20 % of events, identified on a FSC-H/SSC-W cytogram) were also excluded.

In some FACS experiments, cells were pretreated with pharmacological inhibitors or incubated at 4 °C in order to investigate the CD uptake mechanisms. The tested pharmacologicals include:

- NaN<sub>3</sub> (50 mM) to inhibit energy-dependent NP internalization,
- Chlorpromazine (25 μM) to inhibit clathrin-dependent uptake,
- Cytochalasin (25 μM) to inhibit phagocytosis and macropinocytosis,
- Nystatin (50 μM) to inhibit caveolins,
- Fillipine III (2.5 μM) to inhibit caveolins,
- Monodansylcadaverine (100 μM) to inhibit clathrins.

The cells were pre-incubated with the different inhibitors for 30 min prior to addition of CDs. Besides the use of the above described inhibitors, cell incubation at 4 °C was used to inhibit active and passive transports. Thus, 30 mins prior to exposure to CDs, the cells were placed in a refrigerator at 4 °C. They were kept in this condition for another 3.5 hour after CD addition. CD cell uptake was then analyzed by FACS according to the protocol described above.

### **2.3.4. Measurement of mitochondrial membrane potential in response to CDs: JC-10 assay**

The changes in mitochondrial membrane potential evoked by CDs were measured in THP-1 and A549 cells using the JC-10 probe, according to the kit instructions (Ref: MAK160, Sigma). This probe enters the mitochondria, where it is retained in its multimeric (red) form in membrane polarized mitochondria (functional), and is converted into the monomeric (green) form into mitochondria which membrane is depolarized (non-functional).

THP-1 cells were seeded in 96-well plates at a density of 100,000 cells/well in the presence of 10 ng/mL PMA to induce macrophage differentiation. A549 cells were seeded at a density of 30,000 cells/well without other treatment. The day after the cell plating, the cell culture medium was removed, the cells were carefully rinsed with PBS, and CD solutions at increasing concentrations (3, 6, 12, 25, 50, 100 and 200 μL/mL) or culture medium alone (control) were added to the wells for 4 h. After CD treatment, the cell culture supernatant was removed and the JC-10 probe (100 μL) was added to the cells. After incubation for 1 h, fluorescence of the samples was measured at  $\lambda_{ex}540$  nm/ $\lambda_{em}590$  nm (functional mitochondria) and at  $\lambda_{ex}490$  nm/ $\lambda_{em}525$  nm (non-functional mitochondria) using a Varioskan multimode reader (Thermo Scientific). The ratio of fluorescence at 525 nm to fluorescence at 590 nm was calculated for each sample. Then,

data for each sample were expressed as the percentage relative to the fluorescence ratio of control cells.

### **2.3.5. Measurement of oxidative stress in response to CDs: determination of reduced glutathione**

Oxidative stress was assessed by measuring changes in cellular levels of reduced glutathione (GSH) evoked by CDs in THP-1 and A549 cells, using the 2,3-naphthalenedialdehyde probe (NDA). THP-1 cells were seeded in 24-well plates at a density of 500,000 cells/well, in the presence of 10 ng/mL PMA to induce macrophage differentiation. A549 cells were seeded at a density of 180,000 cells/well without other treatment. The day after the cell plating, the cell culture medium was removed, the cells were carefully rinsed with PBS, and CD solutions at increasing concentrations (3, 6, 12, 25, 50, 100 and 200  $\mu\text{L}/\text{mL}$ ) or culture medium alone (control) were added to the wells for 4 h. After CD treatment, the cells were washed with 5 mM EDTA, 40 mM  $\text{NaH}_2\text{PO}_4$ , 110 mM  $\text{Na}_2\text{HPO}_4$ , pH 7.4 and lysed with 0.1 % triton X100. Then, proteins were denatured and precipitated by addition of a 0.1 M hydrochloric acid and 50 % sulfosalicylic acid (1:1) mixture before sample centrifugation (10,000 g, 15 min, 4  $^\circ\text{C}$ ). Cell lysates diluted in lysis buffer (60  $\mu\text{L}$ ) or GSH standards (0  $\mu\text{M}$  to 16  $\mu\text{M}$ ) were then incubated with the NDA probe (20  $\mu\text{L}$  of a 1 mg/mL solution) for 25 min at 4  $^\circ\text{C}$ , before fluorescence measurement ( $\lambda_{\text{ex}}$ : 485 nm;  $\lambda_{\text{em}}$ : 528 nm) using a Varioskan multimode reader. Besides, protein concentration in cell lysates was determined using the bicinchoninic assay (BCA, Sigma). To do so, cell lysates (25  $\mu\text{L}$ ) were incubated with 200  $\mu\text{L}$  of BCA reagent for 30 min at 37  $^\circ\text{C}$  before absorbance measurement at 570 nm using a Multiskan FC reader. GSH amount in samples was expressed in nmol of GSH per mg of protein.

### **2.3.6. Cytokine assays**

Cell culture medium collected at the end of the viability assays were used to quantify IL-8 and IL-1 $\beta$  production by the cells in response to CDs using specific enzyme-linked immunosorbent assays (ELISA). The assays were conducted according to the manufacturer's instructions (R&D Systems). Absorbance was read at 450 nm with a correction at 570 nm using a Multiskan FC reader. Calibration curves were used to calculate the cytokine concentrations in unknown samples, expressed in pg/mL.

Likewise, samples were used to simultaneously screen the production of up to 12 cytokines or chemokines, including tumor necrosis factor- $\alpha$  (TNF- $\alpha$ ), IL-1 $\beta$ , IL-6, IL-



12, IL-17A, IL-8, monocyte chemoattractant protein 1 (MCP-1), Regulated on Activation, Normal T cell expressed and Secreted (RANTES), macrophage inflammatory proteins MIP-1A and MIP-1B, macrophage-derived chemokine (MDC) and eotaxin, using the Multi-Analyte ELISArray Kit (QIAGEN). This assay was performed according to the manufacturer's instructions. Absorbance was read at 450 nm using a Multiskan FC reader. Data for ELISArray were expressed as fold change compared to control samples (cells non exposed to CD).

### **2.3.7. Evaluation of CD transfection efficiency**

Transfection efficiency of CDs was assessed in A549 cells using the pCMV-GLuc plasmid (5.7 kbp, Nanolight Technology, Pinetop, Az, USA) as reporter gene. This plasmid encodes the *Gaussia princeps* luciferase. After expression in the transfected cells, this luciferase is secreted and its activity can be measured in the cell culture supernatant.

#### *Preparation of CD/pDNA complexes*

The CD/pDNA complexes formulated at various weight ratios (w/w) were prepared by mixing equal volumes of stock solutions of CDs and pDNA prepared at the adequate concentration in ultrapure water. The complexes were allowed to form for 30 min at room temperature without handling. The mixture was homogenized by pipetting up and down and subsequently incubated with cells. In these experiments, bPEI25k was used as a gold standard *in vitro* transfection reagent. bPEI25k/pDNA complexes were prepared from bPEI25k solutions according the same protocol as for CD/pDNA complexes.

#### *Transfection assay*

A549 cells were seeded in 96-well culture plates at a density of 6,000 cells/well. Twenty-four hours later, freshly prepared CD/pCMV-GLuc complexes (typically 10  $\mu$ L containing 0.4  $\mu$ g pDNA) were added to each well of the plates. Then, cells were placed in the incubator for 24 h. At the end of the incubation time, *Gaussia* luciferase expression was measured by monitoring light production on an aliquot of culture supernatant (20  $\mu$ L of a 1/100<sup>th</sup> dilution of supernatant prepared in non-supplemented culture medium) for 1 sec upon addition of the coelenterazine substrate (50  $\mu$ L at 1.5  $\mu$ M) using a luminometer (Berthold Centro LB960 XS, Thoiry, France). Data were expressed as RLU/well as a function of the different ratio of CD/DNA complexes tested. Value for each sample was the mean of a triplicate determination. Transfection assays were systematically coupled to MTT assays.

## **2.4. In vivo evaluation of CDs**

### **2.4.1. Animals**

Specific pathogen-free nine-week-old male BALB/c mice were purchased from Charles River Laboratories (Saint-Germain-sur-l'Arbresle, France). They were housed in polycarbonate exhaust ventilated cages with bedding made from spruce wood chips. The animal room was maintained under controlled environmental conditions with a temperature of 20 °C, a relative humidity of 50 ± 10 % and a 12 h/12 h light/dark cycle according to the EU guidance. Food and tap water were available *ad libitum*. The animals were acclimated for 1 week before use. Animal experimentation was conducted with the approval of the government body that regulates animal research in France (agreement number: #4674).

### **2.4.2. Animal exposure to CDs**

Mice were exposed to CDs according to an acute protocol. They received a single intrapulmonary administration of CDs and were sacrificed 24 h later. The doses of CDs were set at 25, 50 and 100 µg. They were delivered in the lungs of the mice by intranasal instillation of CD suspensions prepared in isotonic sodium chloride. Intranasal instillation was used because it is non-invasive procedure that allows effective delivery of substances into the lungs of small animals with reproducibility. Mice were anaesthetized by i.p. administration of 50 mg/kg ketamine (Imalgen®, Merial, Lyon, France) and 3.33 mg/kg xylazine (Rompun®, Bayer, Puteaux, France). Then, mice were handled in a vertical position to promote lung delivery through breathing while 25 µL of CD solution were gently deposited in their nostrils (12.5 µL per nostril). After administration, animals were kept in a 60° inclined supine position until full recovery from anesthesia.

### **2.4.3. Bronchoalveolar lavage fluid collection**

The previous experiment was terminated by the lethal injection of ketamine (240 mg/kg) and xylazine (15 mg/kg). The trachea was cannulated and lungs were lavaged by injecting through the cannula 6 x 0.5 mL of ice-cold saline containing 2.6 mM EDTA (saline-EDTA). The first milliliter of recovered bronchoalveolar lavage fluid (BALF) was centrifuged (200 g, 5 min at 4 °C), and the resulting supernatant was stored at -20 °C until cytokine determination. The cells recovered from the whole BALF were collected together and immediately processed (*vide infra*) to count and characterize cells present in the animal airways.

#### **2.4.4. Evaluation of lung inflammation evoked by CDs**

Lung inflammation induced by the CDs was evaluated by determining total and differential cell counts, and by assaying cytokines in BALF.

##### *Total and differential cell counts*

BALF were centrifuged to pellet cells, and erythrocytes were lysed by hypotonic shock. Cells were then resuspended in ice-cold saline-EDTA, and total cells were counted using a Neubauer's chamber. Cytologic preparations were obtained by cytocentrifugation (Cytospin 4, Thermo Scientific, France) of diluted BALF (200  $\mu$ L of a cell suspension at 250,000 cells/mL in ice-cold saline-EDTA) to determine differential cell counts. These preparations were stained with hematoxylin/eosin and determinations were made by counting at least 400 cells for each preparation. Eosinophil, neutrophil, lymphocyte and macrophage counts were expressed as absolute numbers from total cell counts.

##### *Cytokine assays*

Interleukin-6 (IL-6), keratinocyte-derived chemokine (KC) and monocyte chemoattractant protein-1 (MCP-1) were measured in BALF by ELISA according to the manufacturer's instructions (eBiosciences, Le Pont de Claix, France, for IL-6 and MCP-1; R&D Systems, Lille, France, for KC).

#### **2.5. Statistical analysis of the results**

Data are presented as box-and-whiskers graphs, scatter-plots, dose-response curves or histograms. In the box-and-whiskers graphs, statistical differences between groups were determined by the non-parametric Kruskal-Wallis test, when possible. In the scatter plot graphs, statistical differences between groups were determined by the Student's t-test. Calculation of the Pearson's correlation coefficient was used to test correlation between two parameters in the scatter plot representations. In the dose-response curve and histogram representations, data are means  $\pm$  SEM. Dose-response curves were obtained after data logarithmic transformation and fit with Hill's equation. Then, the Hill slope was used to calculate the EC<sub>50</sub> and EC<sub>80</sub>, when possible. Statistical differences between curves (*i.e.* overall shape of the curve) were determined by one-way analysis of variance (ANOVA) followed by the Tukey's test with the "Main column effect" parameter. In the histogram representations, statistical differences between groups were determined by ANOVA followed by the Dunnett's test. All analyses were done with the GraphPad Prism 6.0 software. Data were considered as significantly different when *p* was less than 0.05.



## **Part 3**

### **Results and discussion**



## 3.1 Safety evaluation of CDs in *in vitro* and *in vivo* models

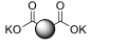
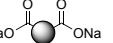
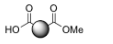
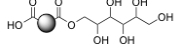
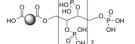
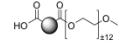
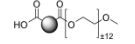
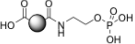
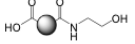
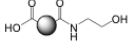
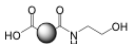
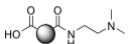
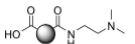
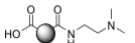
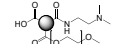
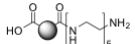
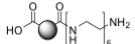
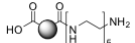
### 3.1.1 Presentation of the CD library

Our aim was to produce CDs with different characteristics of size, charge and surface chemistry, in order to study the impact of these characteristics on the toxicity of NPs. As mentioned earlier, Mickaël Claudel was in charge of the synthesis of CDs for this research program. He thus produced more than 300 samples. From this collection, we selected 34 CDs to frame a CD library for our toxicological studies. The selection was achieved so as to give a representative picture of the original NPs collection and support the full range of diversity of the CDs that were produced. The CDs were produced using various protocols (*vide supra*) so as to expand the structural diversity even when the same starting materials were processed. Another determinant of diversity was the reagent stoichiometry (w/w ratio of carbon source and passivating reagent).

The selected CD library is presented in Table 1. In terms of surface chemistry, the CDs are “decorated” with various functional groups such as carboxylates, alcohols, polyols, phosphates, PEG, methyl esters, amides, amines (primary, secondary, and tertiary), and linear or branched polyamines (primary, secondary, and tertiary) of various molecular weight.

All the CDs in the library have been characterized from a physical (size and charge) and chemical (N, C and H content) point of view. Their charge was determined by zeta potential measurements using DLS, in saline solution, pH 7.4. Worth to note, as most of the selected CDs are decorated with ionizable functional groups, zeta potential was systematically measured from CD solutions at pH 7.4. The size of the NPs was measured both by DLS (in saline and in the culture media corresponding to the conditions of exposure of the cells in our toxicological studies) and transmission electron microscopy. The chemical composition was obtained by elemental analysis. However, this technique is based on the heating of a precise quantity of material and can present limits in the study of the composition of the CDs. Indeed, because of the highly hygroscopic nature of CDs, it is really difficult to accurately weight mg amounts of CDs without capturing water. Nevertheless, the analyzes were done in duplicate, and offered acceptable reproducibility.

**Table 1.** Description of the CD Library

Structure	Synthesis process			Physical characterization				Chemical composition			Biological effect			
	Synthesis mode	Passivation agent	Ratio (w/w)	Zeta potential (mV)	Size TEM (nm)	Size DLS (nm)	Aggregation state in CM	N (%)	C (%)	H (%)	Maximal toxicity (%)	IC50 ( $\mu\text{g/mL}$ )	IC80 ( $\mu\text{g/mL}$ )	
<b>CD (-)</b>														
MC056		MW	-	-	-40.0	28.5	24.7	Dispersed	9.5	39.6	6.06	8.7	NA	NA
MC070		MW	-	-	-19.4	14.1	63.2	Dispersed	4.1	23.6	3.55	4.1	NA	NA
MC095		Post-F	-	-	-16.3	36.1	39.1	Dispersed	2.7	20.2	3.05	19.1	NA	NA
MC165		Pyrolysis	-	1:3	-16.8	28.9	45.2	Dispersed	0	45.7	6.31	6.8	NA	NA
MC177		Post-F	-	-	-44.1	14.1	21.7	Dispersed	0	7.17	2.28	4.8	NA	NA
MC142		Pyrolysis	PEG550	-	-17.6	15.9	80.7	Dispersed	0.4	48.8	8.66	14.1	NA	NA
MC154-2		Post-F	PEG550	-	-20.2	16.1	67.2	Dispersed	1.1	48	7.83	13.7	NA	NA
MC174		Post-F	EA	-	-23.69	15.9	36.5	Dispersed	4.1	9.3	3.95	8.2	NA	NA
MC108		Post-F	EA	-	-9.7	-	90.7	-	12.5	23.3	7.83	17.5	NA	NA
MC140		Post-F	EA	-	-10.9	14.4	283.7	-	10.4	31.7	6.71	3.2	NA	NA
<b>CD (+)</b>														
MC125		Pyrolysis	EA	1:3	+11.4	16.0	157.8	Aggregated	11.1	43.4	5.68	16.7	NA	NA
MC086		Post-F	DMEDA	-	+13.7	23.9	79.2	Dispersed	12.4	26.2	7.48	32.5	NA	54.7
MC107		Post-F	DMEDA	-	+20.7	13.6	39.8	Dispersed	11.2	24.4	7.86	40.2	NA	33.7
MC131		Pyrolysis	DMEDA	1:3	+21.3	12.6	43.8	Aggregated	12.8	35.6	6.99	37.2	NA	43.2
MC148		Pyrolysis	DMEDA PEG550	1:3:3	+26.9	16.3	17.7	Dispersed	2.4	49	8.48	5.9	NA	NA
MC124		Post-F	PEHA	-	+23.9	12.4	20.8	Dispersed	13.9	27	7.30	35.3	NA	64.3
MC136		Pyrolysis	PEHA	1:4	+18.6	17.9	36.4	Dispersed	12.3	26.9	7.35	28.3	NA	124.0
MC175		Pyrolysis	PEHA	1:4	+18.4	15.0	13.3	Dispersed	14.0	31.4	7.56	4.7	NA	NA



**Table 1.** Description of the library (*continued*).

	Structure	Synthesis process		Physical characterization				Chemical composition			Biological effect			
		Synthesis mode	Passivation agent	Ratio (w/w)	Zeta potential (mV)	Size TEM (nm)	Size DLS (nm)	Aggregation state in CM	N (%)	C (%)	H (%)	Maximal toxicity (%)	IC50 ( $\mu\text{g/mL}$ )	IC80 ( $\mu\text{g/mL}$ )
MC167		Pyrolysis	PEHA PEG550	1:3:3	+27.2	17.5	29.0	Dispersed	7.2	43	7.90	25.6	NA	NA
MC168		Pyrolysis	PEHA PEG5000	1:3:3	+21.1	13.4	21.1	Dispersed	0.7	49.1	8.74	10.2	NA	NA
MC242-3		MW	bPEI600	1:2	+36.1	-	10.2	Aggregated	14.9	32.4	6.90	97.6	19.5	7.5
MC242-4		MW	bPEI600	1:4	+41.4	19.9	18.6	Aggregated	13.9	54.2	5.94	84.9	103.0	18.8
MC225		MW	bPEI600	1:4	+26.4	39.5	10.1	Aggregated	14.6	29	7.37	98.1	34.2	10.2
MC161-2		Pyrolysis	bPEI600	1:4	+26.8	14.2	15.2	Dispersed	14.1	29.4	7.30	78.9	92.2	21.2
MC185		Pyrolysis	bPEI600	1:2	+30.0	18.9	17.0	Dispersed	15.1	36.7	6.96	97.4	49.5	13.4
MC239-1		ST	bPEI600	1:2	+18.7	14.6	47.9	Dispersed	12.5	25.3	7.58	16.8	NA	NA
MC240-1		ST	bPEI600	1:5	+22.7	14.1	74.4	Dispersed	14.8	27	7.32	0	NA	NA
MC246-2		MW-ST	bPEI600	1:2	+24.6	-	15.8	Dispersed	13.1	26.2	7.29	0.3	NA	NA
MC246-3		MW-ST	bPEI600	1:4	+24.3	16.5	36.2	Dispersed	14.1	27	7.36	0.7	NA	NA
MC217		MW	bPEI25k	2:1	+23.1	14.6	136.5	Aggregated	11.7	32.1	6.66	97.6	53.4	14.0
MC224		MW	bPEI25k	1:2	+31.1	13.9	10.3	Aggregated	15.4	28.3	7.43	97.2	16.1	5.8
MC222		MW	bPEI25k	1:4	+36.0	-	27.9	Aggregated	13.5	39	6.46	96.7	35.3	11.3
MC068-2		ST	bPEI25k	2:1	+12.4	5.5	7.4	Aggregated	12.1	28.9	7.19	97.7	20.9	6.2
MC034		ST	bPEI25k	2:1	+22.7	19.1	7.2	Aggregated	11.8	26.6	6.95	98.4	18.1	5.9

Notes: 1) CD(+) is “cationic CD” and CD(-) is “anionic CD”; MW: microwave, ST: solvothermal synthesis, Post-F: post functionalization; NA: not available.

2) In this table, all CDs were prepared from same carbon source (citric acid), and “Ratio” refers to citric acid : passivation agent (w/w).

3) “Biological effect” refers to PMA-activated THP-1 cells exposed to CDs.

### 3.1.1.1 Analysis of the factors involved in the synthesis of CDs

To obtain our library, different mode of synthesis (microwave irradiation–MW, solvothermal conditions–ST, solvent-free pyrolysis–Pyrolysis, post-functionalization–Post-F), passivating agent and reagent stoichiometry (w/w ratio of carbon source and passivating reagent) were used. In order to avoid any skew in the subsequent analysis of the determinants of CDs toxicity, we first checked that taken individually, each of this factors had no direct influence on the size and charge of the produced NPs. To address this issue, we draw a series of box-and-whiskers graphs where CD charge and size were plotted as a function of mode of synthesis of CDs, type of passivation agent, or stoichiometry of the carbon source *vs.* passivation agent (figure 22). Analysis was conducted on the whole library. In some representations, data for cationic and anionic CDs were plotted separately. Negatively charged CDs were obtained from three modes of synthesis, namely under microwave irradiation, through post-functionalization, and by solvent-free pyrolysis. For these CDs, there is no significant difference in the zeta potential (figure 22A) or the size (figure 22D) of the NPs produced according to MW and Post-F synthesis modes. The number of CDs obtained by pyrolysis ( $n = 2$ ) is too small for statistical analysis (figure 22A and 22D). It may also be noted that there is no effect of the passivation agent used on the zeta potential or the size of the cationic CDs (figure 22B and E) and that the stoichiometric ratio does not appear as a decisive influencing factor (figure 22C and F). It is not possible to represent and analyze the influence of the nature of the passivation agent or the stoichiometric ratio of reagents on the size and charge of anionic CDs due to the small number of NPs. Cationic CDs were obtained by four different modes of synthesis, namely microwave irradiation, post-functionalization, solvent-free pyrolysis, and solvothermal reaction. Again, there is no significant impact of the mode of synthesis on the zeta potential or the size of these CDs (Figures 22A and 22B). If the passivation agent also does not significantly impact the size and charge characteristics of the positive CDs, it can be noted that PEHA makes it possible to obtain CDs of uniform charge and size compared to the other passivation reagents (figure 22B and E). Finally, from a statistic point of view, the stoichiometric ratio of reactants does not affect significantly the size and charge of the cationic CDs (figure 22C and F), although a better homogeneity of size is observed for the ratios 1:2 and 1:4.

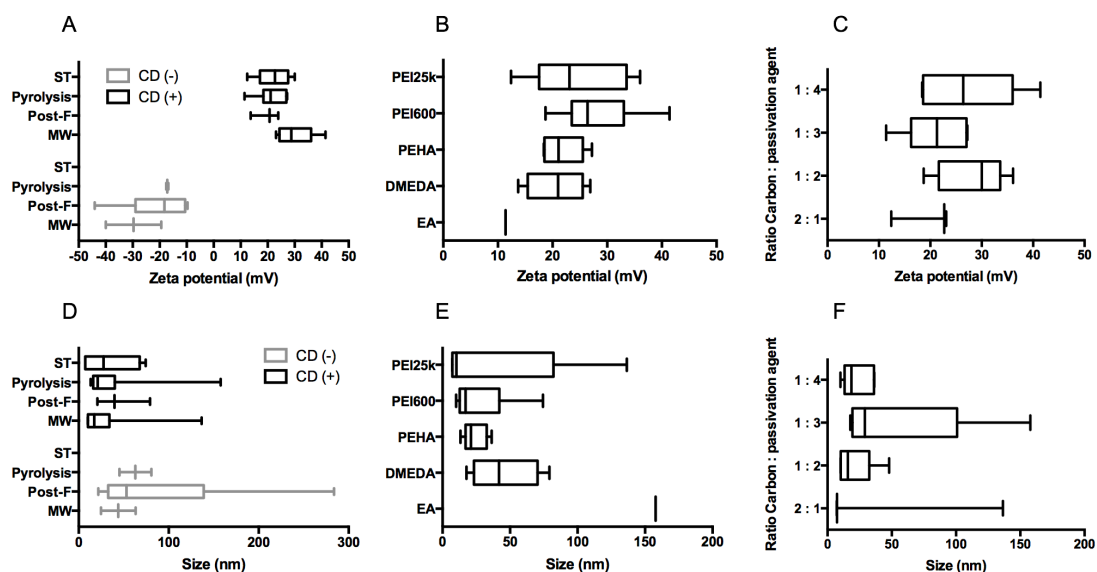


**Figure 22.** Analysis (DLS) of the CD charge (A to C) and size (D to F) as a function of mode of synthesis of CDs (A and D), type of passivation agent (B and E), and stoichiometry of the carbon source vs. passivation agent (C and F). Analysis was conducted on the whole library. Data ( $n = 2$  to 9, according to the groups) are presented as box-and-whiskers (with whiskers min to max). In panels A and D, data for cationic (black boxes) and anionic (gray boxes) CDs were plotted separately. Statistical differences were tested with the non-parametric test Kruskal-Wallis, when possible. ST: solvothermal synthesis; Post-F: post-functionalization; MW: microwave-assisted pyrolysis; Pyrolysis: solvent-free pyrolysis.

So we found, that taken individually the factors that are involved in the synthesis of CDs are not influencing the size and the charge of the produced NPs. Thus, in the subsequent stages of the library analysis, we considered that any variation of size or charge could be attributed to a variation in these factors.

### 3.1.1.2. Relationship between the charge and size of CDs

Two approaches allowed us to determine the size of the CDs, TEM and DLS. These determinations were conducted in aqueous medium. The size determination by TEM shows that the CDs have fairly homogeneous size ranging from 5.5 to 39.5 nm with an average of 17.4 nm, whereas analysis by DLS gives greater heterogeneity with size values between 7.2 and 283.7 nm (table 1) and an average of 48.4 nm. We plotted size values determined by DLS as a function of size values determined by TEM (figure 23A), and found no correlation between the two series of values. However, during the

preparation of TEM grids, capillary forces tend to provoke aggregation of the NPs, so analysis of CD size from TEM images was only performed on fields where the objects were visually well dispersed. In this way, aggregates that form at the time of TEM grid drying were not taken into account in the size determination, as were aggregates that were initially present in the sample. This could explain absence of correlation between the two series of values. Consequently, whereas TEM provides a more accurate size for non-aggregated CDs, DLS overestimates it while giving a valuable overview of the NP aggregation state.

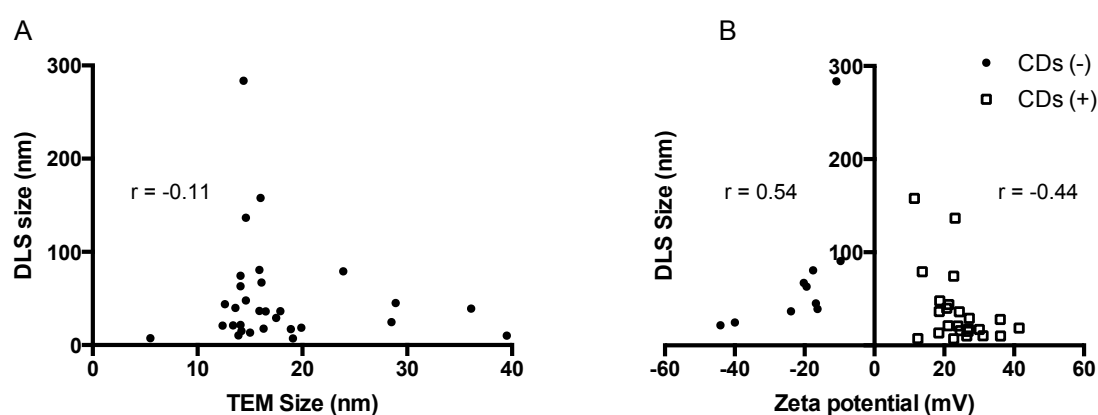


**Figure 23.** Correlation between CD size assessed by DLS and TEM (A) and between CD size (DLS) and charge (B). In panel A, analysis was conducted on  $n = 30$  CDs and in panel B, different symbols were used to plot data of cationic (open square,  $n = 24$ ) and anionic (black dots,  $n = 10$ ) CDs. Statistical correlations were tested with the determination of Pearson's correlation coefficients.

To analyze the relationship between the size and the charge of CDs, we plotted size values determined by DLS as a function of zeta potential values (Figure 23B). For the 10 anionic CDs of size ranging from 21.7 to 283.7 nm, there is a correlation between their size and their charge (Pearson's coefficient  $r = 0.54$ ). Thus, the most negatively charged particles have the smallest size (around 20 nm), while the less charged particles have larger size, suggesting the formation of aggregates in an aqueous medium for these less charged objects. The size of the 24 cationic CDs ranges from 7.2 to 157.8 nm. In contrast to anionic CDs, for these NPs, there is no significant correlation between size and charge (Pearson's coefficient  $r = -0.44$ ). This suggests that a zeta potential greater than +10 mV may be sufficient to provide the samples with colloidal stability and obtain dispersed objects in a saline aqueous medium.

The surface charge is known as a key factor for colloidal stability of NPs. However, there is relatively little information on the relation between surface charge and colloidal stability of CDs in the literature. Moreover, it is important to note that most often pH at which measurements are realized is not mentioned in the publications, which is especially problematic for CDs displaying titratable chemical groups (carboxylic acid, amine...) at their surface. For some types of NPs, such as metal oxide NPs, the NPs size has been claimed to be related to the surface charge density: that is, the larger the surface charge, the smaller the particle size ([Abbas \*et al.\*, 2008](#)). For example, Yamanaka *et al.* reported a greater surface charge density of 30 nm silica NPs compared to 60 nm silica NPs ([Yamanaka \*et al.\*, 2004](#)). Likewise, Sonnefeld *et al.* showed that silica NPs with a diameter of 8 nm have a higher surface charge density compared to 40 nm silica NPs ([Sonnefeld, 1995](#)). Though this is consistent with colloidal stability versus charge, some literature reports contradictory results. Indeed, Kobayashi *et al.* reported no significant difference in surface charge density between 30, 50 and 80 nm silica NPs ([Kobayashi \*et al.\*, 2005](#)). Likewise, Ridley *et al.* found similar charge densities for 4 and 100 nm anatase NPs ([Ridley \*et al.\*, 2006](#)). In summary, the relationship between size and charge of NPs is still uncertain. We believe that the size and charge of each type of NPs should be systematically investigated in details. Here, we analyzed the relationship between the size and the surface charge of CDs for the first time. We found that "the higher charge, the smaller size" applies to anionic CDs, but not to cationic ones. Therefore, our results may indicate that the surface charge is not sufficient for inferring the overall trend of CD size.

### **3.1.2. Analysis of factors contributing to CD cytotoxicity using the whole library**

#### **3.1.2.1. Assessment of CD cytotoxicity in a human model of macrophages**

To be able to carry out a physicochemical characteristic-toxicity relationship analysis, we assessed loss of cell viability evoked by the whole CD library in PMA-activated THP-1 cells, as a model of human macrophages. The cells were exposed for 24 hours to increasing concentrations of CDs (3 to 200 µg/mL) and cell viability was assessed by mitochondrial activity measurements (MTT assay). Each sample was tested

at least in triplicate (biological triplicate on independent cell cultures). We then draw dose-response curves for each of the CDs (figure 24) and determined toxicity values at the highest dose tested (200  $\mu\text{g/mL}$ , maximal toxicity), as well as the doses inducing a 50 % ( $\text{IC}_{50}$ ) and a 20 % ( $\text{IC}_{80}$ ) decrease in cell viability, when the determination was possible. These data are listed in Table 1 (biological effect) and are represented on figure 24. The 34 CDs induced a dose-dependent loss in viability, but to different extent. Thus, 19 CDs induced low toxicity (viability remaining higher than 80 % at 200  $\mu\text{g/mL}$ , representative dose-response curve in green), 5 CDs triggered medium toxicity (viability between 60 and 80 % at 200  $\mu\text{g/mL}$ , representative dose-response curve in orange) and 10 CDs provoked high toxicity (viability less than 40 % at 200  $\mu\text{g/mL}$ , representative dose-response curve in red).

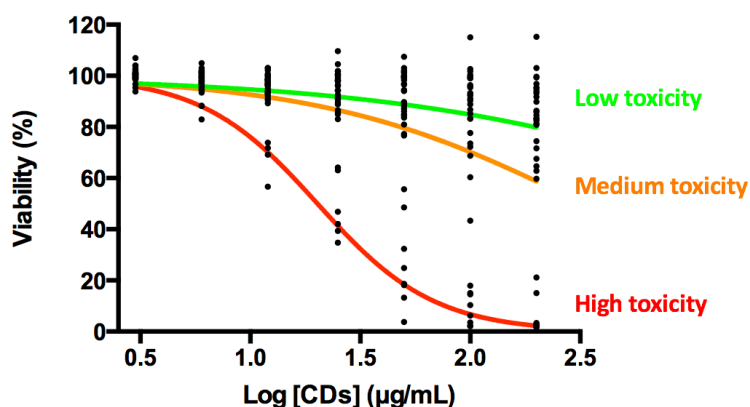


**Figure 24.** Toxicity of the CD library on THP-1 cells. PMA-activated THP-1 cells were treated with increasing concentrations (3-200  $\mu\text{g/mL}$ ) of the CDs for 24 h and viability was assessed with the MTT assay. Results are expressed as percentage of control (untreated cells) and are means  $\pm$  SEM of  $n = 3$  experiments. The CDs can be discriminated as NPs inducing low, medium and high toxicity according to the viability at 200  $\mu\text{g/mL}$  of CDs. Low toxicity : viability remaining higher than 80 at 200  $\mu\text{g/mL}$  of CDs ; Medium toxicity : viability between 60 % and 80 % at 200  $\mu\text{g/mL}$  of CDs ; High toxicity : viability less than 40 % at 200  $\mu\text{g/mL}$  of CDs.

### 3.1.2.2. Influence of the charge on the toxicity

To analyze the relationship between NP charge and toxicity, we plotted the percentage of toxicity of CDs at 200  $\mu\text{g/mL}$  (as determined above) as a function of CD zeta potential. Among the 34 CDs of the library, 10 have a negative zeta potential, with

values ranging from -44.1 mV to -9.7 mV (figure 25). For each of these CDs, the toxicity remains below 20 %. Positive CDs (n=24) have a zeta potential ranging from +11.4 to +41.4 mV. Among these CDs, we can distinguish NPs that induce a loss of viability less than 20 % (8/24), NPs that induce a loss of viability ranging between 20 and 40 % (6/24) and those inducing a loss of viability greater than 40 % (10/24). There is a positive correlation between zeta potential and toxicity (Pearson's correlation coefficient:  $r=0.45$ ), revealing a general trend according to which increasing zeta potential is associated with higher toxicity. Nevertheless, for the same charge, some cationic CDs induce maximal toxicity while others do not. For example, for the same charge of approximately +25 mV, MC246-3 induces 0.7 % toxicity at 200  $\mu\text{g/mL}$  while MC217 induces a toxicity of 97.6 %. Thus, a positive charge does not systematically translate into cytotoxicity.

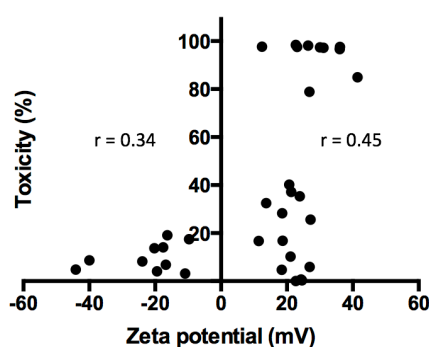


**Figure 25.** CD toxicity as a function of their charge, as assessed on the whole NP library. THP-1 cells were treated with increasing concentrations (3-200  $\mu\text{g/mL}$ ) of CDs for 24 h and cell viability was assessed with the MTT assay. Toxicity evoked by 200  $\mu\text{g/mL}$  of anionic (n=10) and cationic (n=24) CDs was plotted as a function of zeta potential. Statistical correlations were tested with the determination of Pearson's correlation coefficients.

In fact, the relationship between toxicity and surface charge of NPs remains controversial. According to some reports, the toxicity of NPs may be linked to their surface charge. For example, cationic ZnO, silica, silica-titanium dioxide hollow and gold NPs have been shown to be more cytotoxic in non-phagocytic cells than negative variants of similar size ([Baek et al., 2011](#); [Bhattacharjee et al., 2010](#); [Goodman et al., 2004](#); [Oh et al., 2010](#); [Ruizendaal et al., 2009](#)). However, the relationship between charge and cytotoxicity does not appear with all types of NPs. Thus, Mura *et al.*, using positive, negative and neutral NPs obtained by coating the surface of commercial PLGA NPs with

chitosan, poloxamer or poly(vinyl alcohol), respectively, found that the charge has no significant effect on the cytotoxicity of these NPs in Calu-3 cells ([Mura et al., 2011](#)). Yu *et al.* working on macrophages, lung cancer cells and human erythrocytes, found that the porosity of SiO<sub>2</sub> NPs is more important for their cytotoxicity than their surface charge ([Yu et al., 2011](#)). Recently, Havrdova *et al.* compared the *in vitro* toxicity of negative pristine CDs derived from candle soot, neutral CDs coated with PEG, and cationic CDs coated with PEI, in mouse fibroblasts ([Havrdova et al., 2016](#)). Their results showed that positively charged CDs have higher cytotoxicity than negatively charged CDs, which is consistent with our results. However, they found that neutral and negatively charged CDs caused viability loss of more than 40 % when the concentration reached 200 µg/mL, whereas viability loss evoked by our negatively charged CDs was less than 20 %. This difference between our study and the one of Havrdova *et al.* could result from variations in cell model or cell culture density, which may impact toxicity level. Difference in the source of CDs is another important variation between the two studies.

All together, these data suggest that the surface charge is an important but not a decisive factor for CD cytotoxicity, and that surface chemistry may also be an important factor, as we will see later on in this report.

### **3.1.2.3. Influence of size and aggregation state on the toxicity**

In this part of our work, we wondered whether CD size could influence their toxicity. Size of the whole CD population ranged from 5.5 and 39.5 nm as assessed by TEM, and 7.2 and 283.7 nm as assessed by DLS. When these values were plotted as a function of percentage of maximal CD toxicity (as determined above), we found no statistically significant correlation between these two parameters, whatever the method used to determine the CD size (figure 26 A and B).

When introduced into physiological fluids, NPs are subjected to electrolytes and biomacromolecules, such as proteins and lipids that may influence their colloidal stability ([Moore et al., 2015](#)). Thus, NP may aggregate, which will significantly alter their body fate, cell uptake and toxicity. Using DLS, we assessed the colloidal stability of our CDs in complete culture medium (culture medium containing 10% foetal bovine serum) which corresponds to the biological media used for *in vitro* experiments, by assessing possible changes in CDs size. We then identified two CDs populations, one



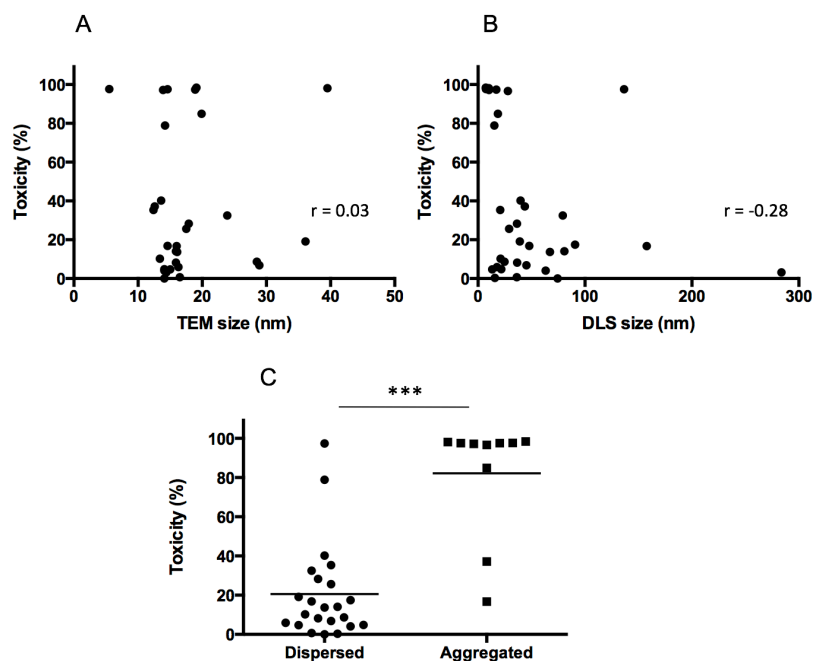


**Figure 26.** CD toxicity as a function of their size and aggregation state, as assessed on the whole library. THP-1 cells were treated with increasing concentrations (3-200  $\mu\text{g/mL}$ ) of CDs for 24 h and cell viability was assessed with the MTT assay. Toxicity evoked by 200  $\mu\text{g/mL}$  CDs was plotted as function of CD size as assessed TEM ( $n=30$ ), of CD size, as assessed by DLS ( $n=34$ ) (B), of CD aggregation state in complete culture medium ( $n=33$ ) (C). (A) and (B): statistical correlation was tested with the determination of Pearson's correlation coefficient. (C): statistical differences were tested with the Student t-test.

population which size remained measurable by DLS and generally close to the size measured in saline, and one population which formed particles with non measurable size (table 1). We qualified these last CDs as “aggregated”, although they still formed stable dispersions. Then, we plotted cytotoxicity of the entire CDs population as a function of their “aggregation” state. As revealed on figure 26C, 10 out the 34 NPs formed aggregates in complete culture medium, and the aggregation state of the CDs in the cell's exposure media has a marked impact on their toxicity. Thus, CDs that aggregate induce more toxicity than well dispersed CDs ( $p < 0.001$ ).

All together we found that the size of CDs, in the size range tested by TEM (5.5 – 39.5 nm) or DLS (7.2 – 283.7 nm), does not directly affect their toxicity, which is inconsistent with some reports on other NPs. For example, Pan *et al.* tested the cytotoxicity of Au NPs on four cell lines representing major functional cell types with barrier and phagocytic function: connective tissue fibroblasts, epithelial cells, macrophages, and melanoma cells. The results showed that 1.4 nm Au NPs were highly cytotoxic, whereas 15 nm Au NPs

were non-toxic at up to a 60-fold concentration ([Pan et al., 2007](#)). Similarly, Napierska *et al.* found that the cytotoxicity of silica NPs is size-dependent on endothelial cells ([Napierska et al., 2009](#)). The smallest NPs (14 to 16 nm in diameter) exhibited high cytotoxicity, while larger NPs (104 and 335 nm) induced very low cytotoxic responses. Inconsistency between our data and these studies could stem from differences in the chemical composition of the particles and/or their behavior in biological media. It should be noted that all our CDs form stable dispersions in saline as well as in culture medium.

### 3.1.2.4. Influence of chemical composition on the toxicity

The chemical nature of NPs is critical to determine their toxicity. Indeed, depending on their chemical nature, NPs can exhibit different cellular uptake, subcellular localization, and ability to catalyze the production of reactive oxygen species ([Xia et al., 2006b](#)). Thus, we then looked for a possible correlation between the chemical composition, especially the carbon (C), hydrogen (H), and nitrogen (N) contents of CDs and their toxicity. As shown on the correlation plots presented on figure 27A and B, no apparent link was found between the carbon (Pearson's coefficient:  $r=0.06$ ) or the hydrogen (Pearson's coefficient:  $r=0.12$ )

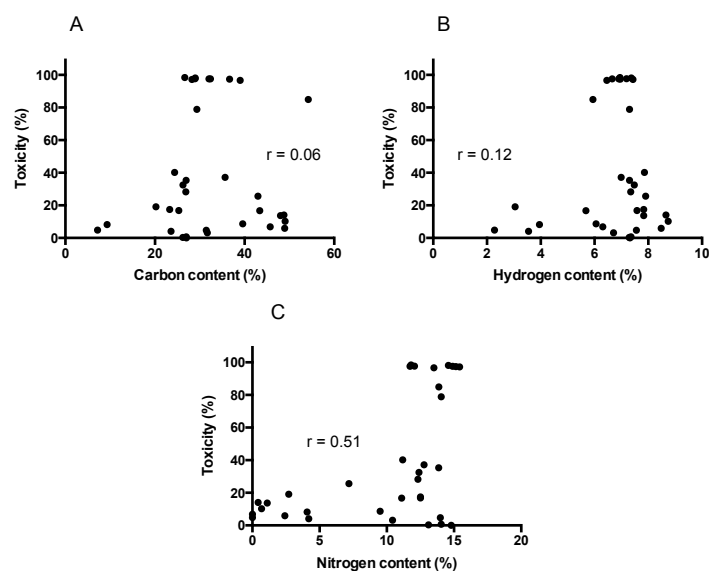


**Figure 27.** Cytotoxicity of CDs as a function of their chemical composition, as assessed on the whole library. THP-1 cells were treated with increasing concentrations (3-200  $\mu\text{g/mL}$ ) of CDs for 24 h and cell viability was assessed with the MTT assay. Toxicity evoked by 200  $\mu\text{g/mL}$  CDs was plotted as function of CD carbon (A), hydrogen (B) or nitrogen content (C) ( $n=34$ ). Statistical correlations were tested with the determination of Pearson's correlation coefficients.

content of the CDs and their toxicity. On the contrary, some correlation appears between nitrogen content of the NPs and their toxicity (Pearson's coefficient:  $r=0.51$ ) (figure 27 C). Thus, the CD toxicity increases with the nitrogen content.

### 3.1.2.5. Influence of the synthesis modalities on the toxicity

As we have seen above, various synthesis processes have been used to produce our CD library, involving variations in activation mode, passivation agent, or mass ratio between the carbon source and additives. So, we have studied to what extent these variables could influence the toxicity of CDs. In terms of activation mode, as shown by figure 28A, the CDs produced under microwave irradiation exhibited significantly higher cytotoxicity compared to those obtained through post-functionalization ( $p<0.05$ ) or by solvent free pyrolysis ( $p<0.05$ ). These results suggest that the activation mode used to produce CDs may be a factor affecting the cytotoxicity of CDs. Regarding passivation reagent, we found that the use of PEI (bPEI600 or bPEI25k) leads to toxic CDs compared to shorter amines ( $p<0.001$ , compared to EA, DMEDA or PEHA) (figure 28B). This is consistent with other reports, as PEI is often used for surface functionalization of nanomaterials to install positive charges and improve permeabilization of plasma membranes ([Havrdova et al., 2016](#)).

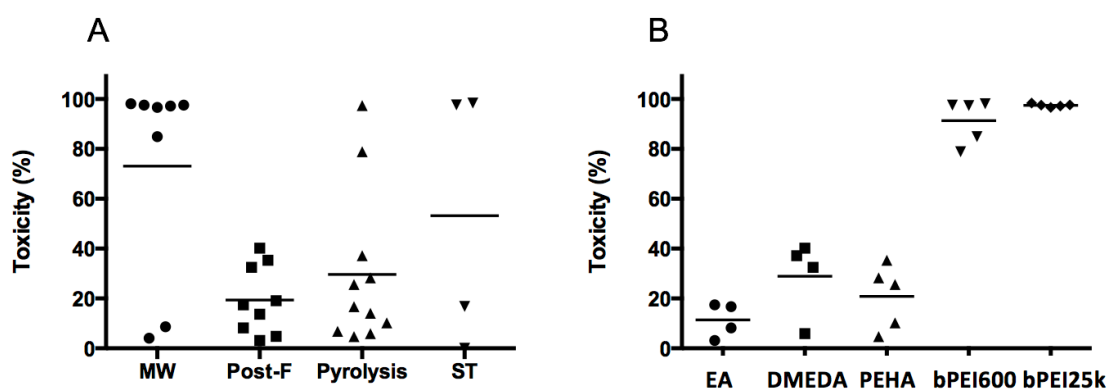


**Figure 28.** CD toxicity as a function of the method of synthesis (A,  $n=32$ ), and the nature of the passivating agent (B,  $n=23$ ), as assessed on the whole library. THP-1 cells were treated with increasing concentrations (200  $\mu\text{g/mL}$ ) of CDs for 24 h and cell viability was assessed with the MTT assay. Toxicity evoked by 200  $\mu\text{g/mL}$  CDs was plotted in the graphs. Statistical differences were tested with the ANOVA followed by the Tukey's test. ST: solvothermal reaction; Post-F: post-functionalization ; MW: microwave-assisted pyrolysis; Pyrolysis: solvent-free pyrolysis. For the clarity of the figure, significance between groups was not represented (please see the text).

### 3.1.2.6. Influence of the PEGylation on the toxicity

Surface coatings can alter the toxicological profile of NPs. Indeed, toxic particles can become non-toxic or less toxic depending on chemical groups that are introduced to decorate their surface. For example, experiments with hamsters have shown that the formation of blood clots is more pronounced when the surface of i.v. administered polystyrene NPs is aminated ([Nemmar \*et al.\*, 2002](#)). Likewise, toxic CdSe QDs have been shown to become non-toxic when properly coated ([Derfus \*et al.\*, 2004](#)). In the literature, decoration of NP surface with PEG groups has been reported to effectively reduce NP toxicity ([Hanot \*et al.\*, 2015](#); [Luo \*et al.\*, 2014](#); [Mendonça \*et al.\*, 2016](#)). In our library, PEG<sub>550</sub> and PEG<sub>5000</sub> were introduced on cationic CDs prepared from DMEDA and PEHA. Toxicity of the obtained CDs was compared to the one evoked by non-decorated CDs. Size and charge of the compared CDs are summarized in table 2. The TEM size of these CDs (12.6 – 17.9 nm) is similar and all NPs are positively charged (+18.6 to +27.2 mV). As shown on figure 29, the introduction of PEG decoration leads to a decrease in CD toxicity (figure 29A). The length of the PEG chain has a marked impact on the biological response, since a sharper decrease in toxicity is observed for longer PEG (figure 29B). Difference in toxicity between decorated and non decorated CDs can be attributed to the decoration, as size and charge were similar among the compared NPs.

Taken as a whole for this section, CD library analysis showed that zeta potential plays a role in the toxicity of CDs, with no toxic effect for negatively charged CDs. Nevertheless, a positive surface charge alone cannot explain the toxicity of CDs. Thus, other factors such as the propensity to aggregate in biological media, the nitrogen content, and the nature of the (branched) amino chain was shown to impact the toxicity of CDs. In addition, PEGylation of cationic CDs reduces their toxicity.

**Table 2.** Description of the CDs.

Sample	Passivation agent	TEM size (nm)	DLS size (nm)	ζ (mV)
MC131	DMEDA	12.6	43.8	+ 21.3
MC148	DMEDA + PEG <sub>550</sub>	16.3	17.7	+ 26.9
MC136	PEHA	17.9	36.4	+ 18.6
MC167	PEHA + PEG <sub>550</sub>	17.5	29.0	+ 27.2
MC168	PEHA + PEG <sub>5000</sub>	13.4	21.1	+ 21.1

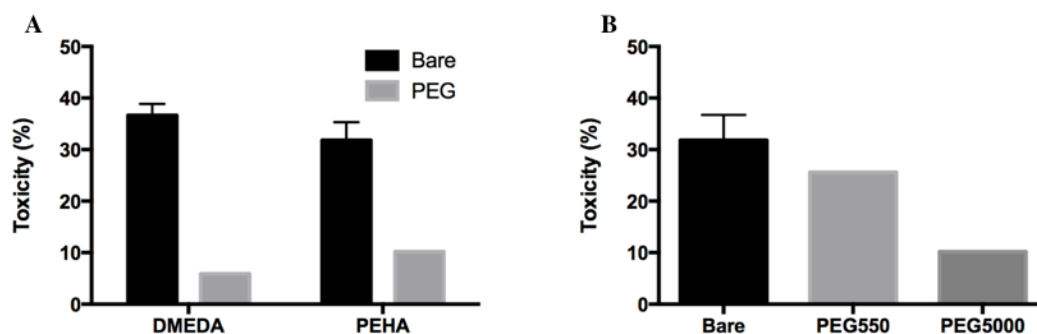


**Figure 29.** Impact of PEGylation on the toxicity of positively charged CDs. CDs were prepared from citric acid, *N,N*-dimethylethylene diamine (DMEDA), and PEG<sub>550</sub> (1:3:0 or 1:3:3, w/w) by solvent-free pyrolysis (A). CDs were prepared from citric acid, pentaethylene hexamine (PEHA), and PEG<sub>550</sub> or PEG<sub>5000</sub> (1:3:3, w/w) by solvent-free pyrolysis (B). THP-1 cells were treated with increasing concentrations (3-200  $\mu\text{g}/\text{mL}$ ) of CDs and cell viability was assessed at 24 h with the MTT assay ( $n=1$  to 3). Toxicity evoked by 200  $\mu\text{g}/\text{mL}$  CDs was plotted in the graphs.

### 3.1.3. In-depth toxicity study on a focused CD library

To get additional insight into the toxicity of CDs in relation to their characteristics, we carried our further investigations on a focused CD library (*vide infra*) using both *in vitro* and *in vivo* models. *In vitro*, three cell lines were used as models to investigate the cytotoxicity of the focused library members and determine whether this cytotoxicity is cell type and time-dependent or not. Then, we investigated cell internalization of these CDs as well as the potential pathways for cell uptake. Thirdly, we studied the mechanisms of action of the selected CDs at the cellular level, by measuring inflammatory markers, oxidative stress, and mitochondria perturbation. *In vivo*, we investigated the lung toxicity of the CDs in the focused library, using mice and inflammatory markers.

#### 3.1.3.1. Presentation of the focused CD library

The CDs that were selected for these in-depth toxicological evaluations are presented in table 3. These CDs were selected according to the following criteria:

- 1) *Cytotoxicity level*. We chose highly toxic CDs, MC34 and MC225, moderately toxic CDs, MC131 and MC138, and non toxic CDs, MC56 and MC148.
- 2) *Surface charge*. As shown in 3.1.2.1, negatively charged CDs do not cause cytotoxicity. Therefore, we selected only one anionic CD. MC56 was chosen as it has a clearly negative zeta potential (-40.0 mV). The other CDs in this library are cationic.

**Table 3.** Description of the “focused” CD library.

	Synthesis process			Physical characterization				Chemical composition			Biological effect		
	Activation mode	Passivation agent	Ratio (w/w)	Zeta potential (mV)	Size TEM (nm)	Size DLS (nm)	Size DLS (nm)	N (%)	C (%)	H (%)	Maximal toxicity (%)	IC50 ( $\mu\text{g/mL}$ )	IC80 ( $\mu\text{g/mL}$ )
<b>CD (-)</b>													
MC056	MW	-	-	-40.0	28.5	24.7	Dispersed	9.5	39.6	6.06	8.7	NA	NA
<b>CD (+)</b>													
MC131	Pyrolysis	DMEDA	1:3	+21.3	12.6	43.8	Aggregated	12.8	35.6	6.99	37.2	NA	43.2
MC148	Pyrolysis	DMEDA/mPEG550	1:3:3	+26.9	16.3	17.7	Dispersed	2.4	49	8.48	5.9	NA	NA
MC136	Pyrolysis	PEHA	1:4	+18.6	17.9	36.4	Dispersed	12.3	26.9	7.35	28.3	NA	124.0
MC225	MW	bPEI600	1:4	+26.4	39.5	10.1	Aggregated	14.6	29	7.37	98.1	34.2	10.2
MC034	ST	bPEI25k	2:1	+22.7	19.1	7.2	Aggregated	11.8	26.6	6.95	98.4	18.1	5.9

Note: 1) CD(+) is for cationic CDs, and CD(-) for anionic CDs; MW: microwave, ST: solvothermal synthesis, Post-F: post functionalization; NA: not available.

2) All CDs were prepared from same carbon source (citric acid), the w/w ratio refers to citric acid:passivation agent.

3) “Biological effect” refer to CDs exposed to PMA-activated THP-1 cells.

3) *Type of passivation agent.* We selected representative CDs prepared with various passivation agents: MC34 (bPEI25k), MC224 (bPEI600), MC131 (DMEDA) and MC148 (DMEDA + mPEG<sub>550</sub>), MC136 (PEHA).

### **3.1.3.2. Cell viability loss evoked by the focused CD library as a function of cell type and incubation time**

The cytotoxicity of the CDs in the “focused” library was investigated on three cell lines, namely THP-1 cells which are, as previously mentioned, a model of human macrophages, and A549 and Calu-3 cells, which are human lung epithelial cells, a cell type that forms the lung barrier *in vivo*.

At first, we compared the toxicity of the different CDs on the 3 cell lines upon a 24 h exposure. To do so, cells were exposed to increasing concentrations of NPs (3 to 200 µg/mL) and cell viability was assessed by mitochondrial activity measurements (MTT assay). On the three cell types, we found the following effects (figure 30):

- MC034 and MC225, passivated with polyamines, is the most toxic CDs within the library;
- MC131 and MC136, passivated with short oligoamines, is moderately toxic or non-toxic according to the cell type;
- MC056 (negatively charged) and MC148 (positively charged and PEGylated) are non-cytotoxic, whatever the cell type.

The toxic effects of the CDs evoked on A549 and Calu-3 cells are lower in intensity when compared to those observed on THP-1 cells (figure 30 B and C). Cell ranking is as follow: THP-1 > A549 > Calu-3.

However, the toxicity ranking of the CDs does not change with cell type and is as follow: MC34 > MC225 > MC131 > MC148.

Our results suggest that cytotoxicity of CDs is cell type-dependent, which is consistent with data from other reports. For example, hydroxyapatite NPs exhibit cell type-dependent cytotoxicity, and BEAS-2B (an immortalized human bronchial epithelial cell line) is more sensitive than RAW264.7 (an immortalized mouse macrophage cell line) ([Zhao et al., 2013](#)). Similarly, cell type-dependent cytotoxicity is applicable to Au NPs ([Coulter et al., 2012](#)). All in all, this study may provide a guide to the toxicity analysis of CDs and highlights that cell types also should be considered.



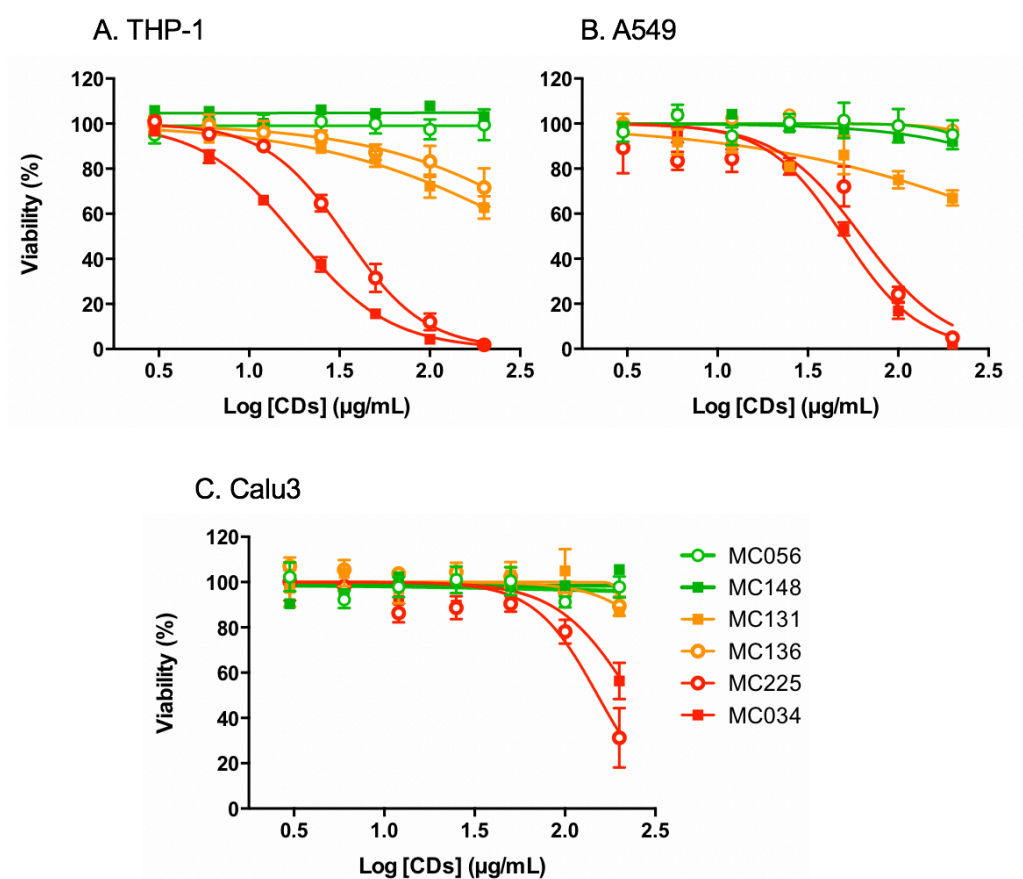


**Figure 30.** Toxicity of CDs in THP-1 (A), A549 (B) and Calu-3 (C) cells. Cells were treated with increasing concentrations (3-200 µg/mL) of the CDs for 24 h and viability was assessed with the MTT assay. Results are expressed as percentage of viability when compared to controls (untreated cells). They are means  $\pm$  SEM of n=3-6 experiments. Statistical differences when compared to control were determined by ANOVA followed by the Dunnett's test.

To analyze the influence of exposure time on CD toxicity, THP-1 and A549 cells were exposed for 1, 4 or 24 h to increasing concentrations of the two more toxic CDs, MC34 or MC225, and cell viability was assessed at the end of exposure using the MTT assay (figure 31). It was then observed that the cytotoxic effects of the two CDs are time-dependent in the two cell types and appear from the first hour of incubation. In THP-1 cells, cytotoxicity is even almost maximal at 1 h. Thus, the acute toxic effects of CDs occur within a very short time, which is very interesting, because it is quite rapid relative to other types of NPs. So far, the underlying mechanism for the acute toxicity of CDs is unclear. Only few reports describe the toxicity *vs.* exposure time of NPs, and data are inconsistent with our results on CDs. For example, toxicity of metallic



NPs was shown to be a relatively long process as it involves dissolution of the NPs inside the cell and release of toxic ions ([Meng et al., 2007](#)). Toxic effects of CuO and ZnO NPs were thus observed after 24 hours exposure ([Kim et al., 2017](#)). Our study suggests that toxic CDs produce deleterious effects within 1 hour, which may reveal the time the cells are taking up these CDs. Therefore, acute toxicity of CDs should be considered when biomedical applications are intended.

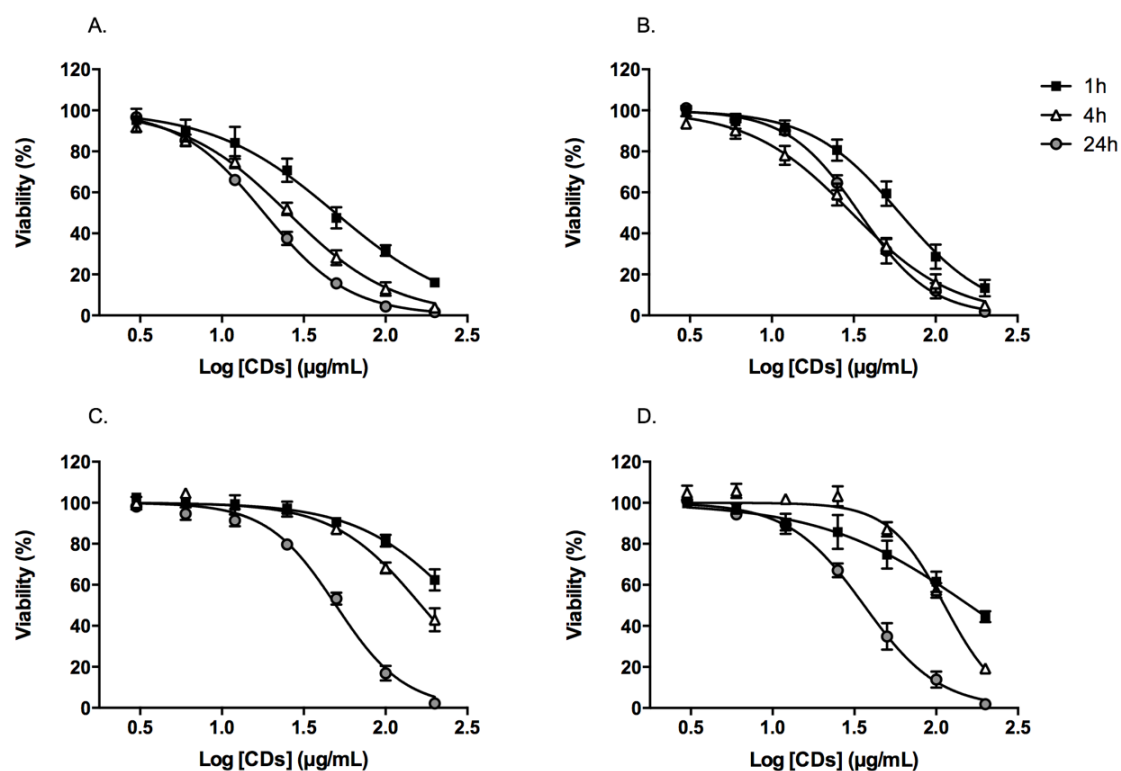


**Figure 31.** Toxicity induced by MC34 (A and C) and MC225 (B and D) in THP-1 (A and B) and A549 cells (C and D) as a function of time. Cells were treated with increasing concentrations (3-200 µg/mL) of the CDs for 1, 4 or 24 h. Results are expressed as percentage of viability when compared to controls (untreated cells). They are means  $\pm$  SEM of n=3-6 experiments. Statistical differences were determined by ANOVA followed by Tukey's test.

### 3.1.3.3. Cell internalisation of the selected CDs

Internalization of CDs and its mechanisms have been studied on THP-1 and A549 cells by flow cytometry (FACS analysis) and/or confocal laser scanning microscopy (CLSM) thanks to the intrinsic fluorescence properties of CDs.

### 3.1.3.3.1. Fluorescence properties of the CDs

To determine the fluorescence settings to be used to track CDs by CLSM and FACS, we characterized the fluorescence properties of our NPs. CD fluorescence excitation and emission spectra were recorded between 250 and 600 nm and 365 and 615 nm, respectively. As shown of figure 32A, the six CDs in the focused library are excitable between 300 and 500 nm, with an excitation maximum near 350 nm for MC225 and MC056 and around 420 nm for MC034, MC136 and MC148. MC131 has a maximal excitation at 525 nm, but is still excitable at lower wavelengths. Based on these data, we characterized CD emission at the two excitation wavelengths that are available in the CLSM and FACS facilities we intended to use for our experiments, namely 355 and 405 nm.

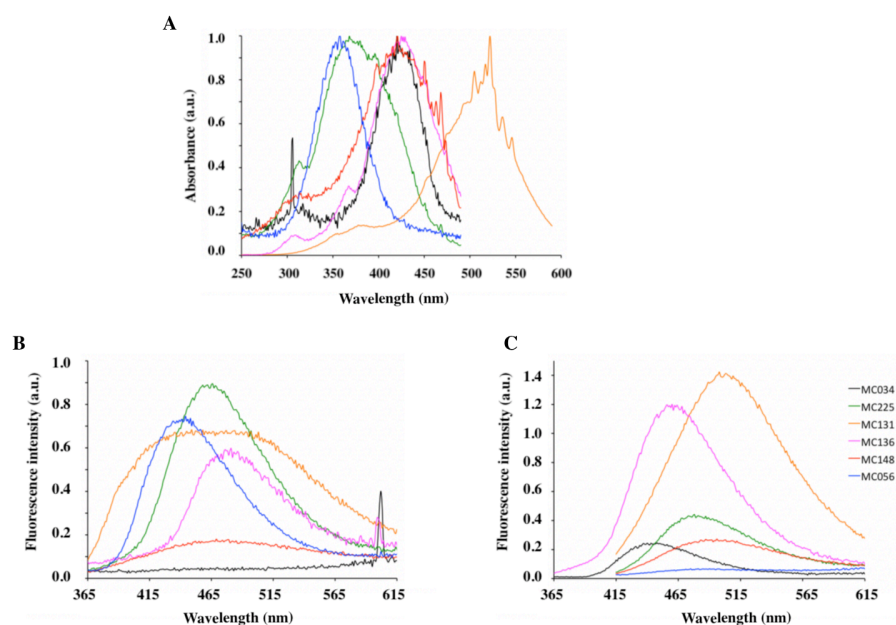


**Figure 32.** Fluorescence excitation (A) and emission (B:  $\lambda_{\text{ex}} = 355$  nm; C:  $\lambda_{\text{ex}} = 405$  nm) spectra of the selected CDs. Fluorescence data are presented in arbitrary units.

### 3.1.3.3.2. Internalization of the CDs

To characterize cell internalization of CDs in the focused library, THP-1 and A549 cells were exposed to NPs (25  $\mu\text{g}/\text{mL}$ ) for 4 hours and analyzed for fluorescence using a LSRFortessa X-20TM flow cytometer or a Leica SP2 microscope equipped with a 63x oil immersion objective (NA=1.2) after cell staining with the membrane probe DSQ12S exhibiting green fluorescence.

Figure 33 shows the strategy that was followed to analyze data obtained by FACS. First, cell morphology analysis according to size (FACS) and granularity (SSC) was used to exclude cell debris and doublets (figure 33A). Second, on the cell population that was conserved, the fluorescence intensity of the CDs was collected as a function of exposition condition (control or CDs), using two possible excitation wavelengths, namely 355 and 405 nm (figure 33B). Then, internalization data were expressed as percentage of cellular fluorescence intensity in the presence of CDs when compared to control.

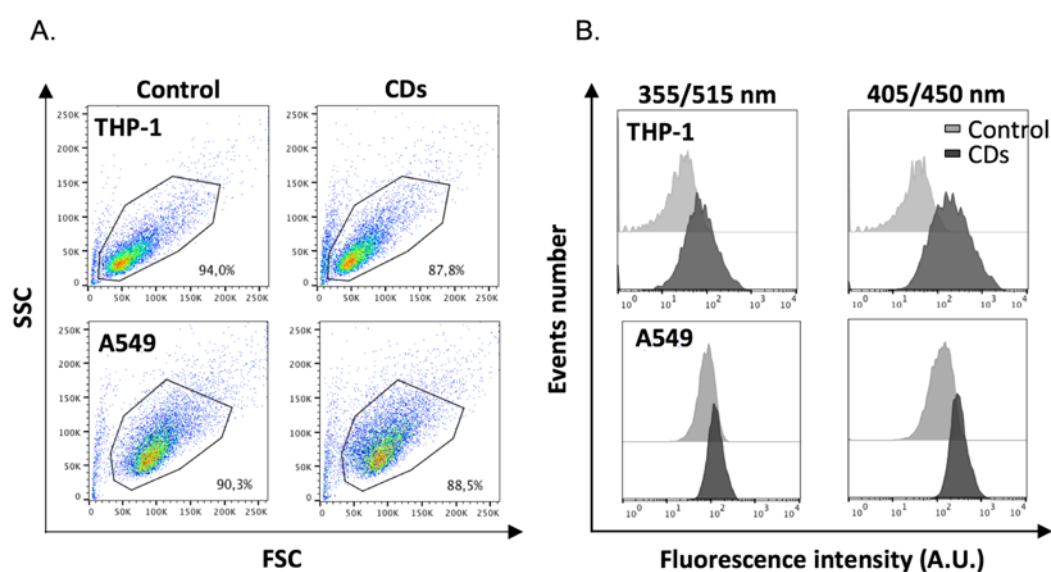


**Figure 33.** Analysis of CD internalization by FACS in THP-1 and A549 cells. Cells were exposed to CDs (25  $\mu\text{g}/\text{mL}$ ) for 4 h and cell fluorescence was analyzed using a LSRFortessa X-20TM flow cytometer. The samples were excited with a 355 nm laser with emission signal detected at 515 nm (355/515 nm) or a 405 nm laser with emission signal detected at 450 nm (405/450 nm). (A) Dot-plots showing cell morphology (granularity (SSC) versus size (FSC)) as a function of exposure condition (control or CDs) and cell type (THP-1 or A549) with percentage of cells conserved for analysis. (B) Fluorescence intensity as a function of exposure condition (control or CDs) and cell type (THP-1 or A549).

The CD internalization results measured by FACS are shown in figures 34A and 34B. Cells treated with the two more cytotoxic CDs (MC034 and MC225) exhibit the highest fluorescence intensity, indicating that these two CDs are highly internalized. This signal is stronger in THP-1 cells than in A549, suggesting that THP-1 cells are more capable of internalizing these CDs than A549 cells. MC-131 is also internalized, and internalization is comparable in the two cell lines. In contrast, no significant fluorescence signal is observed for MC136, MC148 and MC56 at any wavelength and

in the two cell types, indicating that these three CDs are not internalized by cells. Figure 24C shows representative images of cells exposed to the different CDs, as obtained by CLSM. These images confirm data obtained by FACS, the blue labeling due to CD fluorescence being observed in cells treated with MC131, MC225 and MC034, for the two cell lines, but not in cells treated with MC148 and MC056.

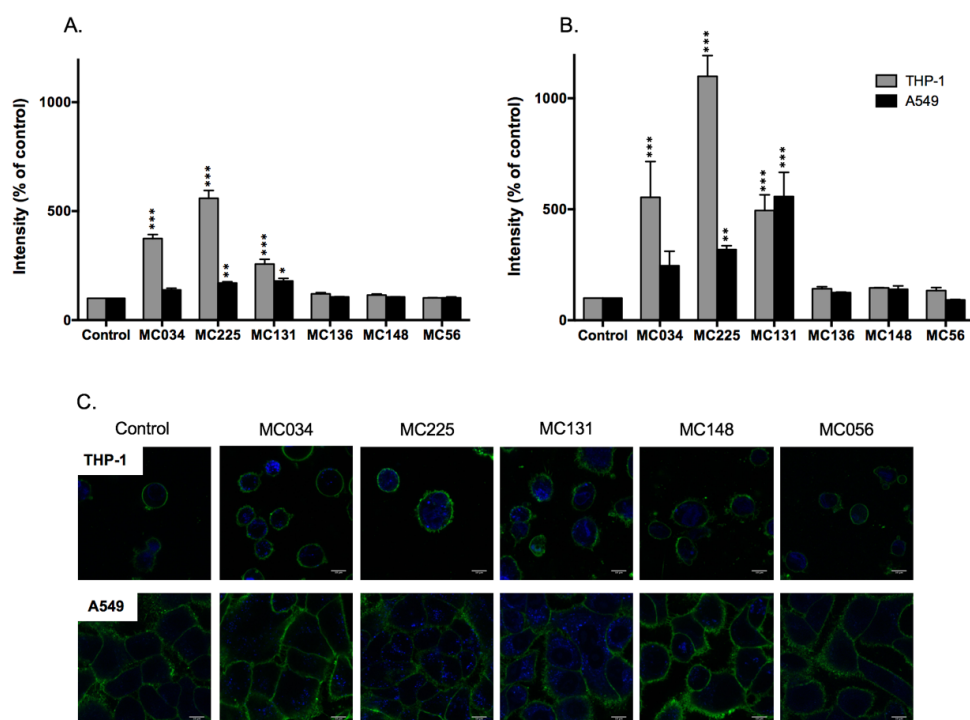


**Figure 34.** CD internalisation in THP-1 and A549 cells as assessed by FACS (A and B). Cells were exposed to CDs (25  $\mu\text{g}/\text{mL}$ ) for 4 h. (A and B) Cell fluorescence was analysed using a LSRFortessa X-20TM flow cytometer, after sample excitation with (A) a 405 nm laser (emission signal detected at 450 nm), or (B) a 355 nm laser (emission signal detected at 515 nm). Results are expressed as percentage of fluorescence intensity when compared to control (untreated cells). They are means  $\pm$  SEM of  $n=3$  experiments. Statistical differences when compared to control were determined by ANOVA followed by the Dunnett's test. (C) CD internalization in THP-1 and A549 cells as evidenced by CLSM using an excitation wavelength of 405 nm. On these images, blue fluorescence represents CDs, whereas green fluorescence represents cell membrane labeled with the membrane probe DSQ12S. Pictures are representative of 1-3 experiments.

Our results thus indicate that CDs can be internalized by cells and show potential for imaging applications, which is consistent with other reports ([Jiang et al., 2015b](#); [Pan et al., 2015](#); [Yang et al., 2009b](#); [Zheng et al., 2015](#)). However, the working concentrations of CDs are inconsistent in these reports, and even vary widely. For example, Jing *et al.* reported the use of non-toxic CDs (prepared from glycerol) for cell imaging at a concentration of 5 mg/mL ([Wang et al., 2015a](#)), which is much higher than

the concentrations we used (25 µg/mL). CDs are still rarely considered along with their toxicity when they are applied as imaging tools. Here, we found that the internalization of CDs is consistent with their cytotoxicity, that is, the most internalized CDs (MC34, MC225) showed the highest toxicity, whereas less/non-internalized CDs have low or no toxicity.

### **3.1.3.3.3. Mechanisms of CD internalization**

The mechanisms of CD internalization were studied on the most extensively internalized CDs, namely MC225, and in the two cell types (THP-1 and A549) by FACS. To do so, various treatment conditions and inhibitors were used to block internalization pathways, as indicated in table 4. Both cell lines were exposed to CDs under the same conditions. Cells were pre-incubated with each inhibitor for 30 minutes prior to the addition of CDs and then placed in the cell incubator for 3.5 hours. For the 4 °C treatment, cells were placed in a refrigerator at 4 °C for 30 minutes before exposure to CDs and they were kept for another 3.5 hours at 4 °C after the addition of the CDs.

At 4 °C, internalization rate of CDs was reduced by 77% of the control in THP-1 cells and 43% in A549 cells. This suggests that CDs are primarily internalized by passive and active pathways. NaN<sub>3</sub>, which inhibits the active pathways, reduced CD uptake by 36 % and 22 % in THP-1 and A549 cells, respectively. Interestingly, the inhibition rate by NaN<sub>3</sub> is half that observed at 4 °C, which may suggest that active and passive pathways have similar contributions in the internalization of CDs. The inhibition rate of internalization by cytochalasin-D reached 46 % for THP-1 cells, but only 13 % for A549 cells. This indicates that A549 cells differ from THP-1 cells in that they are less prone to CDs internalization *via* macropinocytosis or phagocytic pathways. Substantially, similar results were obtained with chlorpromazin, suggesting that THP-1 cells rely heavily on caveolae-dependent pathways to internalize CDs (59 %) while A549 cells use this pathway to a lesser extent (6 %). Internalization of CDs through the caveolae-dependent pathway was also acknowledged when using filipin-III and genistein as inhibitors. Using methyl-β-cyclodextrine, we found that the lipid rafts pathway is involved in CD internalization by THP-1 cells (23%), whereas it is not when considering A549 cells (no uptake inhibition).

All together, this study shows that highly internalized CDs (MC34, MC225) and moderately internalized CDs (MC131) are positively charged, whereas negatively charged CDs (MC56) and positively charged PEGylated CDs (MC148) are not internalized. This suggests that positive surface charge may necessary but not directly dominate the internalization of CDs. Besides, the size of the six selected CDs is less than *ca.* 40 nm, as consistently measured by TEM and DLS. Based on these results, the size and surface charge of CDs may not be sufficient predictive indicators of CDs internalization. Interestingly, some reports suggest a direct relationship between NP size and cell uptake, as is the case with latex beads internalized by non-phagocytic B16 cells ([Rejman \*et al.\*, 2004](#)). Also, smaller Au NPs (10 nm) showed more prominent internalization than larger counterparts (50 nm) (Tomić *et al.*, 2014). Besides, our data showed that the internalization pathway of CDs is cell-type dependent. Specifically, CDs uptake by THP-1 cells is higher than internalization by A549 cells (figure 34), and the pathways involved in the two cell models are not the same (table 4). Thus, our data provide a better insight into the cell internalization of CDs. In addition to considering the size and charge of CDs, cell type also needs to be considered.

**Table 4.** Mechanisms of internalisation of MC225 in THP-1 and A549 cells (FACS analysis). Cells were pre-treated with pharmacological inhibitors of endocytosis pathways or incubated at 4°C to inhibit active and passive transports and then exposed to 25 µg/mL MC225 for 4 h. Results are expressed as percentage of inhibition of fluorescence intensity when compared to control (untreated cells). They are means ± SEM of n=3 experiments. Statistical differences when compared to control were determined by ANOVA followed by the Dunnett’s test.

Condition(inhibitor) Target internalization pathway	Inhibition (% of control)	
	THP-1	A549
4°C		
<i>Active and passive process</i>	77 ± 6 <sup>***</sup>	43 ± 7 <sup>***</sup>
NaN <sub>3</sub>		
<i>Active process</i>	36 ± 3 <sup>***</sup>	22 ± 4
Cytochalasin D		
<i>Macropinocytosis, phagocytosis</i>	46 ± 6 <sup>***</sup>	13 ± 7
Chlorpromazin		
<i>Clathrin-dependent way</i>	59 ± 6 <sup>***</sup>	11 ± 5
Nystatin		
<i>Caveolae-dependent way</i>	34 ± 7 <sup>**</sup>	6 ± 4
Filipin III		
<i>Caveolae-dependent way</i>	25 ± 13	8 ± 3
Genistein		
<i>Caveolae-dependent way</i>	23 ± 7	No inhibition
Methyl-β-Cyclodextrin		
<i>Lipid rafts way</i>	23 ± 4	No inhibition

### 3.1.3.4. Mechanisms involved in the cellular responses to the selected CDs

The mechanisms of the toxic action of the six CDs were studied on the two more “responsive” cell types, THP-1 and A549 (study carried out on five CDs only, MC136 was not tested in these experiments). To do so, we assessed CD-induced inflammation, oxidative stress and mitochondrial perturbation.

#### 3.1.3.4.1. Inflammation

The pro-inflammatory effect of the CDs was first evaluated by assaying the pro-inflammatory cytokine IL-8 in the supernatant of THP-1 and A549 cells exposed for 24 hours to increasing concentrations of CDs (figure 38). The IL-8 is a potent chemoattractant and neutrophil activator whose transcription is dependent on NF- $\kappa$ B. It can be secreted by any cell that express Toll-like receptors involved with the innate immune response ([Hoet \*et al.\*, 2004](#)).

The amount of IL-8 secreted by the two cell lines significantly increased with the concentration of the two cytotoxic CDs, namely MC34 and MC225, up to 50  $\mu$ g/mL (figure 35). At concentrations of 100 and 200  $\mu$ g/mL, IL-8 secretion by THP-1 cells starts to decrease, most probably due to a significant loss in cell viability at these concentrations (figure 35A). IL-8 production by A549 cells appears to be less affected by CD concentration, even at 100 and 200  $\mu$ g/ml (figure 35B). Thus, consistent with our previous cytotoxicity data, we confirm that A549 cells are more tolerant to CDs when compared to THP-1 cells. Besides, secretion levels of IL-8 were almost 10 times higher in THP-1 cells compared to A549 cells. The main reason for this may be that macrophages are the major producers of TNF- $\alpha$ , which plays an important role in regulating cytokine production ([Parameswaran and Patial, 2010](#)). Our results suggest that IL-8 production is cell-type and dose-dependent and is involved in the mechanism of cytotoxicity caused by CDs. Moreover, we found that there is no absolute correlation between CDs particle size or surface charge and inflammation. For example, MC34 (+22.7 mV, 19.1 nm) induces IL-8 production in THP-1 and A549 but no IL-8 production was found after treatment with MC148 (+26.9 mV, 16.3 nm). This is inconsistent



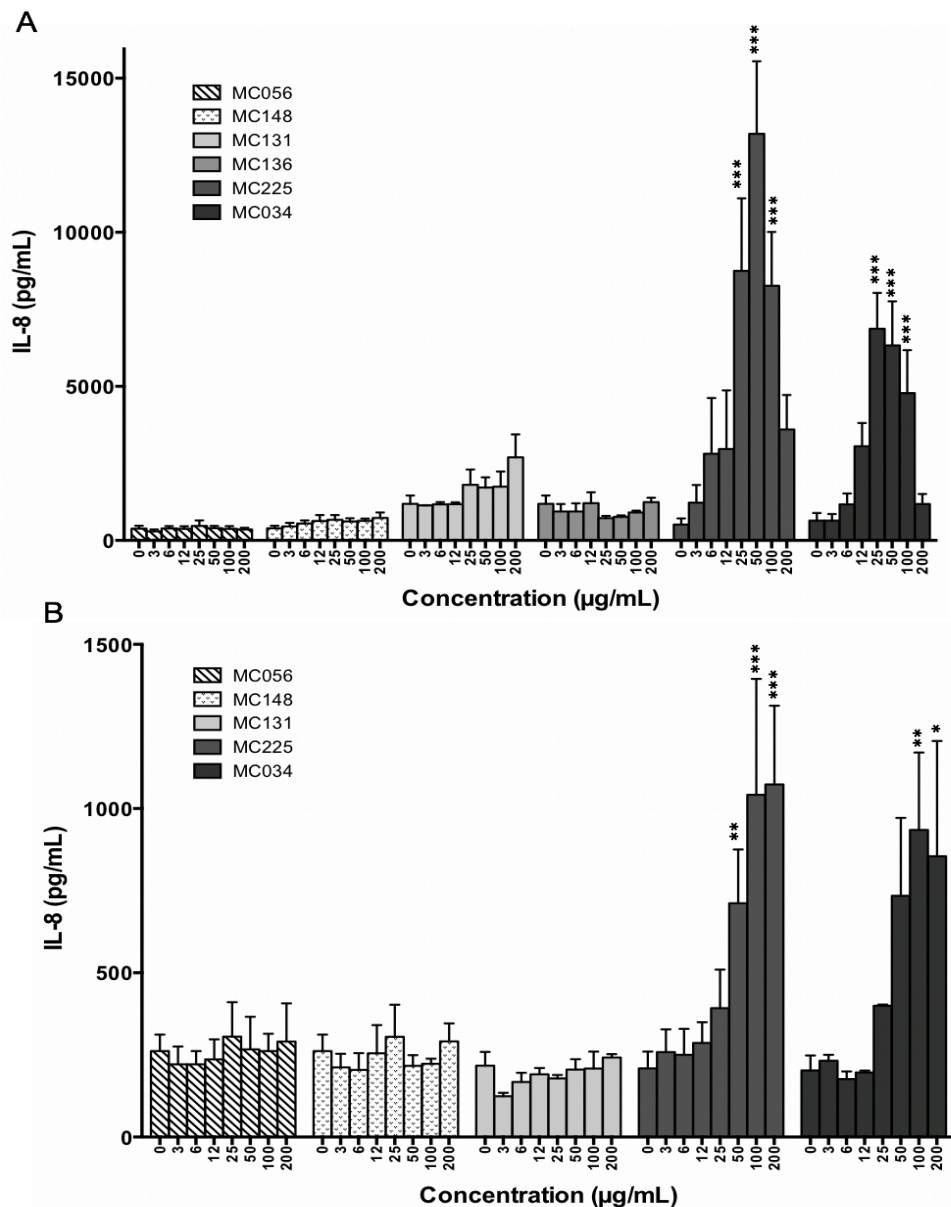


**Figure 35.** IL-8 production induced by selected CDs in THP-1 (A) and A549 (B) cells. Cells were treated with increasing concentrations (3-200  $\mu\text{g/mL}$ ) of the CDs for 24 h and IL-8 release was quantified by ELISA. Results are expressed as absolute IL-8 release (pg/mL). They are means  $\pm$  SEM of  $n=3-6$  experiments. Statistical differences when compared to control were determined by ANOVA followed by the Dunnett's test.

with results obtained with other NPs. For example, 20 nm Ag NPs induce much higher inflammation levels in RAW 264.7 macrophages compared to larger particles (80 nm or 113 nm) with the same composition ([Park et al., 2011b](#)).

To further characterize the inflammatory response evoked by CDs, we used a inflammatory cytokine multi-analyte ELISArray allowing the simultaneous assessment of 12 cytokines/chemokines. This assay was conducted on supernatant samples of THP-1



cells exposed to 200 µg/mL CDs. As shown in table 5, some cytokines (TNF- $\alpha$ , IL-6, IL-12, IL-17 and eotaxin) remain non detectable or in the background signal (non-exposed cells) after treatment with CDs. The release of MDC remained unchanged whatever CDs the cells were exposed to. The two more toxic CDs MC225 and MC34 evoked increases in IL-1 $\beta$ , MIP-1 $\alpha$ , MIP-1 $\beta$ , and MCP-1 release that were estimated to be more than 5-fold those observed in non-exposed cells. Although less pronounced, some increase in MIP-1 $\alpha$  and MIP-1 $\beta$  production was also observed in the supernatant of cells exposed to MC131 and, to a lesser extent, to MC148. Besides, MC131 evoked a significant release of MCP-1. At last, no increase in the release of detectable cytokines was observed in response to MC56. Thus, IL-8 was not the only pro-inflammatory cytokine produced in response to CDs, and once again, the evoked cytokine release correlates with the viability loss induced by the CDs.

	MC056	MC148	MC131	MC225	MC034
TNF- $\alpha$	nd	nd	nd	nd	nd
IL-6	nd	nd	nd	nd	nd
IL-12	nd	nd	nd	nd	nd
IL-17	nd	nd	nd	nd	nd
Eotaxin	nd	nd	nd	nd	nd
MDC	-	-	-	-	-
IL-1 $\beta$	-	-	-	+++	++
MIP-1 $\alpha$	-	-	+	+++	++
MIP-1 $\beta$	-	+	+	+++	++
MCP-1	-	-	+++	++	+++

**Table 5.** Cytokine induction in response to CDs in THP-1 cells. Cells were treated with CDs (200 µg/mL) for 24 h and cytokine release was assessed in cell culture supernatant using an inflammatory cytokine multi-analyte ELISArray. nd: non detectable. (-) : No change. (+): 1.5 < OD < 5-fold of the negative control or 0.10 < OD < 0.25-fold of the positive control; (++) : 5 < OD < 10-fold of the negative control or 0.25 < OD < 0.75-fold of the positive control. (+++): OD > 10-fold of the negative control or OD > 0.75-fold of the positive control.

The use of an inflammatory cytokine multi-analyte ELISArray thus allowed us to identify IL-1 $\beta$  as a cytokine secreted in response to our most toxic CDs. IL-1 $\beta$  is an important proinflammatory cytokines that activates monocytes, macrophages, and neutrophils, and induces Th1 and Th17 adaptive cellular responses. It is secreted as an inactive precursor called pro-IL-1 $\beta$  which processing depends on cleavage by proteases that are activated by cytosolic multiprotein platforms called inflammasomes, in response to endogenous or exogenous danger signals. Among inflammasomes, the NLRP3 inflammasome is responsible for the maturation of the

cytokine IL-1 $\beta$  upon cleavage by caspase-1. To further characterize IL-1 $\beta$  secretion in response to CDs, we conducted a dose-response study using the two more cytotoxic CDs, MC34 and MC225, in the THP-1 model and assessed IL-1 $\beta$  secretion using an ELISA. As shown on figure 36, the two CDs induced a dose-dependent production of IL-1 $\beta$  suggesting that both NPs are capable of activating the NLRP3 inflammasome. Here again, a decrease in the cytokine production was observed at the highest CD concentrations tested. However, this is probably a result of cell death caused by CDs at high concentration.

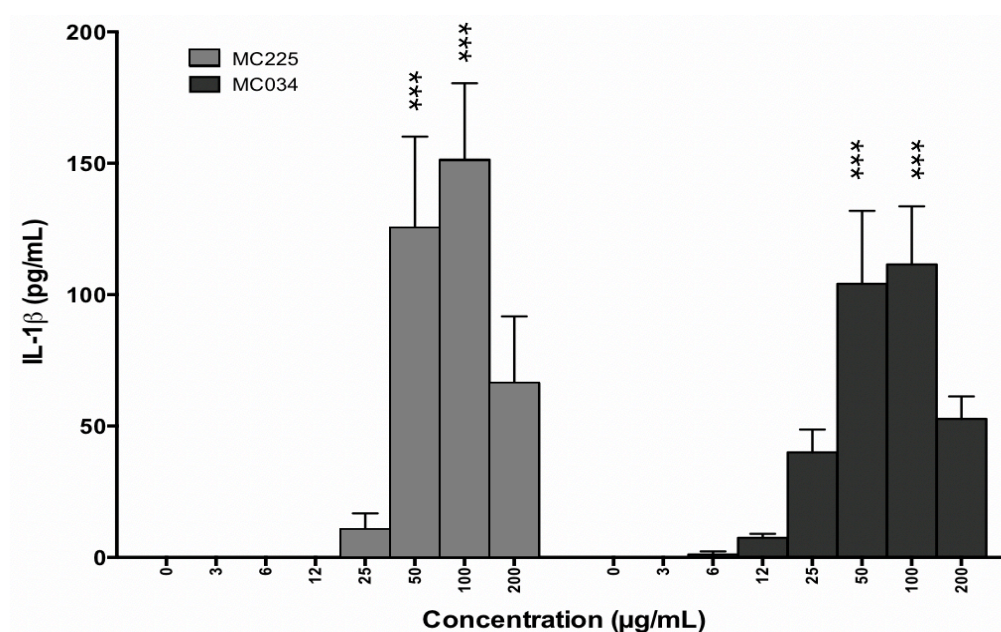


**Figure 36.** NLRP3 inflammasome activation induced by MC34 (grey bars) and MC225 (black bars) in THP-1 cells. Cells were treated with increasing concentrations (3-200  $\mu\text{g/mL}$ ) of the CDs for 24 h. NLRP3 inflammasome activation was assessed quantifying IL-1 $\beta$  in cell culture supernatant by ELISA. Results are expressed as absolute IL-1 $\beta$  release (pg/mL). They are means  $\pm$  SEM of n=3 experiments. Statistical differences when compared to control were determined by ANOVA followed by the Dunnett's test.

### 3.1.3.4.2. Oxidative stress

Oxidative stress results from an imbalance between production of reactive oxygen species (ROS) and levels of cellular anti-oxidant agents, among which reduced glutathione (GSH). It may trigger inflammation, and is considered as one of the main causes of NPs toxicity ([Hussain et al., 2009](#); [Marano et al., 2011](#)). To balance ROS levels and other free radical production which cause DNA damage, apoptosis,

inflammation and cellular fibrosis, cells possess enzymatic and non-enzymatic antioxidant systems among which reduced glutathione (GSH), which can be used as an index of oxidative stress. Indeed, levels of this anti-oxidant decrease in case of oxidative stress. To investigate oxidative stress in response to CDs, we thus measured intracellular GSH levels in THP-1 and A549 cells exposed to increasing concentrations of the NPs (figure 37). GSH consumption was observed in both THP-1 and A549 cells exposed to MC-34 and MC-225, revealing the involvement of oxidative stress in the cytotoxicity of the CDs. In contrast, negligible changes for GSH were observed in response to the non-cytotoxic CDs, MC56, MC131, MC136, and MC148.

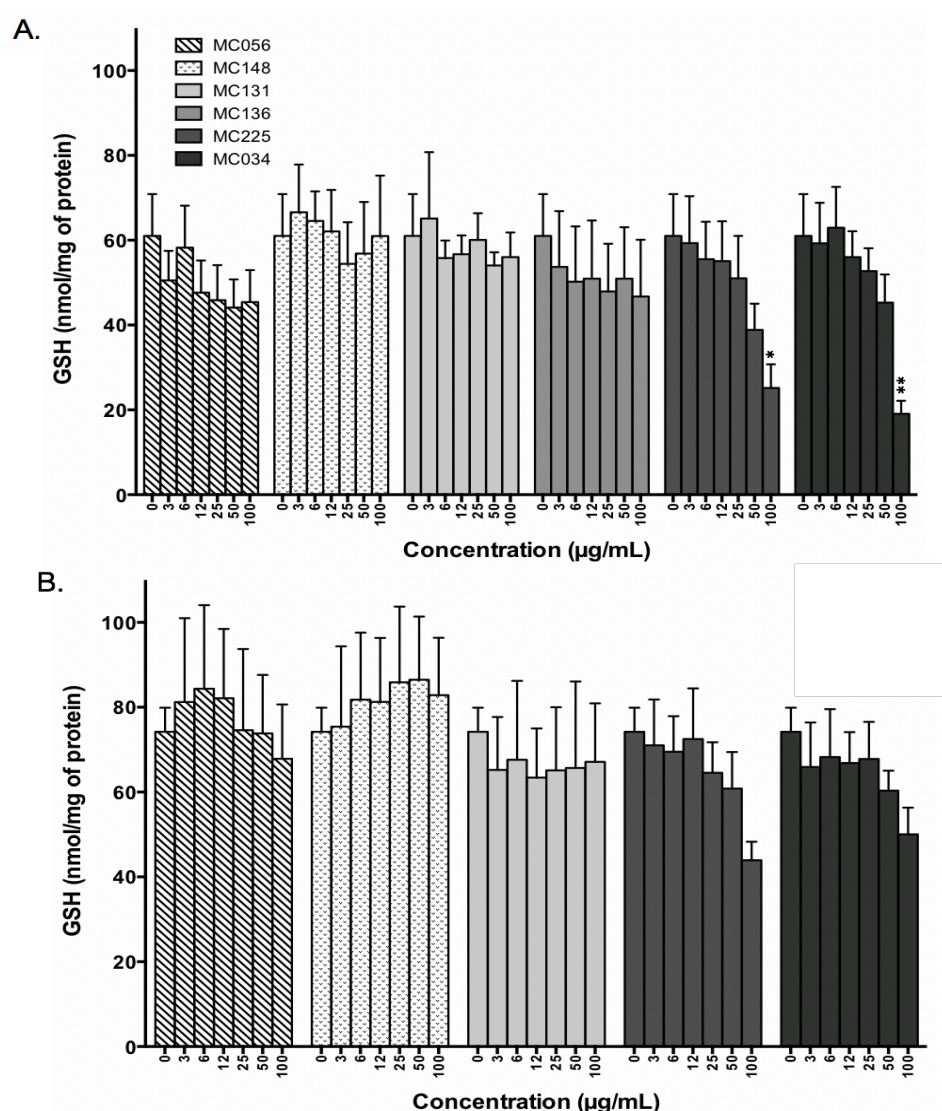


**Figure 37.** Oxidative stress induced by selected CDs in THP-1 (A) and A549 (B) cells. Cells were treated with increasing concentrations (3-200  $\mu\text{g/mL}$ ) of CDs for 4 h. Then, cell content in reduced glutathione (GSH) was assessed using the NDA probe. Results are expressed as absolute values (nmol/mg of protein). They are means  $\pm$  SEM of n=3 experiments. Statistical differences when compared to control were determined by ANOVA followed by the Dunnett's test.

Our study showed that the ROS may get involved into the mechanisms of CDs cytotoxicity. So far, we still don't know the reason. According to some reports, the larger surface area of NPs may respond for the ROS production ([Stone et al., 1998](#); [Wilson et al., 2002](#)). Since CDs can alter the function of mitochondria (see below), another possibility would be that CDs enter mitochondria and cause physical damage, leading to oxidative stress, which is consistent with some earlier studies ([Li et al., 2003](#); [Xia et al., 2006b](#)). In addition, the oxidative stress was higher in THP-1 cells compared to A549 cells, which may result from the lower uptake of CDs by the A549 cells.

#### **3.1.3.4.2. Mitochondria perturbation**

Some manufactured NPs can be transported through the cell membrane, particularly to the mitochondria ([Foley et al., 2002b](#)). However, whether NPs directly target mitochondria or enter the organelles following oxidative damage is still controversial ([Li et al., 2003](#)). NP-induced mitochondrial disturbances have important biological effects, including the onset of apoptosis and the reduction in ATP production, which can lead to cell necrosis ([Hiura et al., 2000](#)). A study in BRL3A cells confirmed these deleterious effects, in particular NPs increased ROS production and GSH consumption, and decreased mitochondrial membrane potential ([Hussain et al., 2005b](#)). We thus investigated the effects of our CDs on the potential of the mitochondrial membrane in THP-1 and A549 cells using the JC-10 probe (figure 38). This probe enters the mitochondria where it is retained as a multimer in functionally polarized mitochondria, and is converted to monomeric form in depolarized mitochondria. As it can be observed on figure 38, the two more cytotoxic CDs, MC034 and MC225, are capable of inducing a loss in mitochondrial membrane potential in the THP-1 model. In connection with the previous results, in this cell model, the two CDs induce a level of oxidative stress that could be responsible for damage to the mitochondria. Some weak mitochondrial perturbation was measured in response to MC131, but no mitochondrial effect was observed with the non-toxic CDs MC56, MC136, and MC148. In A549 cells, no mitochondrial effect was detected regardless of the CDs, including the “toxic” MC34 and MC225. Our results suggest that mitochondria effects are involved in the cytotoxicity of CDs in THP-1 cells, but not in the A549 cell line at the CDs concentration tested. The higher sensitivity of THP-1 cells when compared to A549 cells is consistent with the previously collected cytotoxicity data.



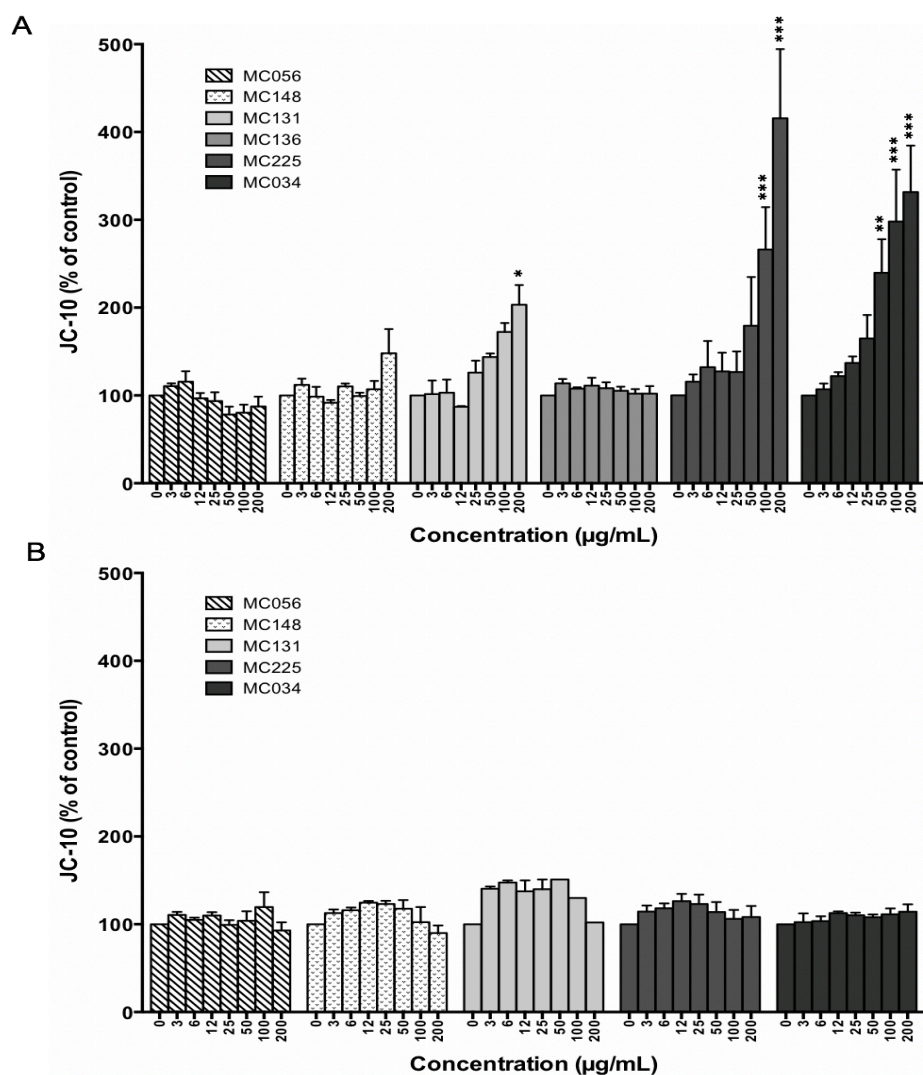


**Figure 38.** Mitochondrial perturbation induced by selected CDs in THP-1 (A) and A549 (B) cells. Cells were treated with increasing concentrations (3-200 µg/mL) of CDs for 4 h. Then, perturbation in mitochondrial membrane potential was assessed using the JC-10 probe. Results are expressed as percentage when compared to controls (untreated cells). They are means ± SEM of n=3 experiments. Statistical differences when compared to control were determined by ANOVA followed by the Dunnett's test.

Overall, we investigated the toxicity mechanisms of CDs by measuring three different endpoints: inflammation, oxidative stress, and mitochondrial perturbation. This study was carried out in the THP-1 and A549 cells. Basically, we found that inflammation, ROS and mitochondrial perturbation can be triggered by highly toxic CDs on THP-1 at the CD concentrations tested, whereas in the A549 cell line, IL-8 and ROS production were relatively low and no mitochondrial perturbation was found. These results are consistent with our previous cytotoxicity and internalization results, which suggested A549 cells are less sensitive to CDs.

### **3.1.3.5. *In vivo* lung toxicity of the selected CDs**

The study on lung toxicity of CDs was conducted in two steps. First, a dose-response study was carried out on the two CDs that had given the most potent effect *in vitro*, namely MC034 and MC225. This allowed us to select a dose of interest to then conduct a comparative study on the six CDs of the focused library. In the two part of the study, animals received a single administration of CDs in the lung, and toxicity were measured 24 h later. Assessment of pulmonary toxicity of CDs was performed by analysing the inflammation induced by CDs in bronchoalveolar lavage fluids (BALF) collected from mice. To do so, we measured total and differential cell counts (neutrophils, lymphocytes and macrophages) and levels of interleukin-6 (IL-6), keratinocyte-derived chemokine (KC) and monocyte chemoattractant protein-1 (MCP-1). By investigating the *in vivo* toxicity of CDs, we did hope to obtain a better and comprehensive understanding of the toxicity profile of CDs.

#### **3.1.3.5.1. Dose-response toxicity study with MC034 and MC225**

In this dose-response study, the animals were exposed to a single dose of 25, 50 or 100 µg of MC034 or MC225 and the effects were analyzed 24 h after administration (figure 39). The two CDs induce a dose-dependent inflammatory response characterized by an increase in total cell number due to neutrophil infiltration and an increased production of pro-inflammatory cytokines (IL-6, KC and MCP-1) in the lung, as measured in BALF (figure 39). These effects are statistically significant for the CD dose of 50 µg (cytokines), or 100 µg (neutrophils). By examining cells recovered in BALF from CD-exposed animals by optic microscopy after cell staining with hematoxylin/eosin, we observed the presence of punctuations in macrophages, and this for the two CDs (not shown). At low image resolution, we can not be certain that these punctuations correspond to internalized CDs. However, CLSM and FACS experiments conducted by M. Weiss and C. Ronzani on BALF cells from CD-exposed animals did confirm our interpretation (data not shown). Based on this dose-response study on MC034 and MC225, we selected the dose of 100 µg for the following comparative study on the six CDs.

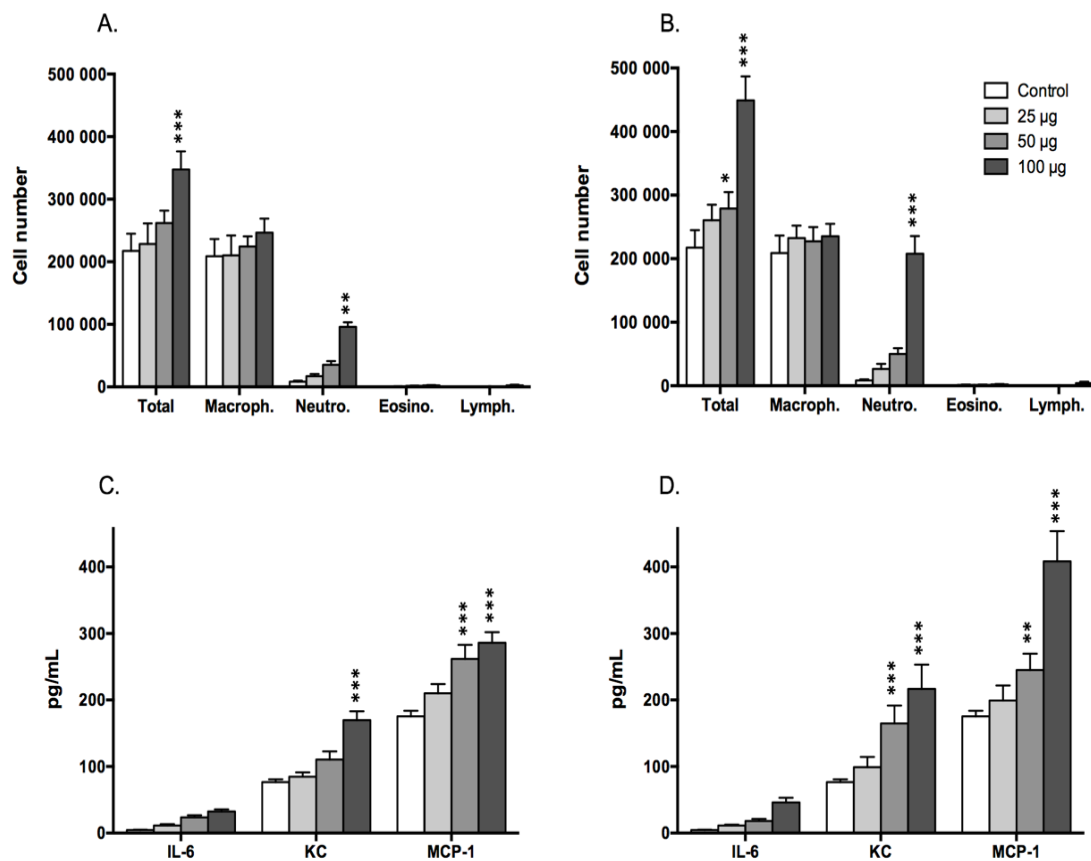


**Figure 39.** Dose-dependent lung inflammation induced by MC34 (A and C) and MC225 (B and D) in mice after acute exposure. Mice received a single lung administration of CDs (25, 50 or 100 µg) by intranasal instillation and were euthanized 24 h later. Total and differential cell number (A and B) and cytokine (IL-6, KC and MCP-1) levels were evaluated in BALF. Results are expressed as absolute values. They are means  $\pm$  SEM of n=6 experiments. Statistical differences when compared to control were determined by ANOVA followed by the Dunnett's test.

### 3.1.3.5.2. Single dose toxicity study on the focused CD library

In this comparative study, the animals were exposed to a single dose of 100 µg of one of the selected CDs and the effects were analyzed 24 h after administration (figure 40). As expected from the dose response study, MC034 and MC225 induce an inflammatory response characterized by an infiltrate of neutrophils and an increase in pro-inflammatory cytokine production (IL-6, KC and MCP-1). The other four CDs tested (MC131, MC136, MC148 and MC56) did not induce any significant pro-inflammatory effect. A slight infiltrate of neutrophils in the presence of MC136 is noted, but it has no statistical significance. The toxicity ranking observed in this *in vivo* study reflected the one observed *in vitro*, particularly in THP-1 macrophages.

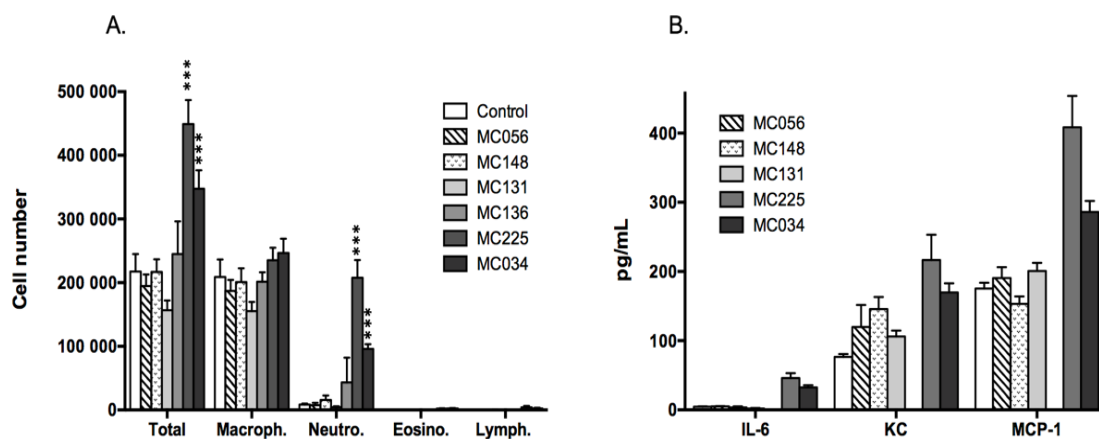


**Figure 40.** Lung inflammation induced by the selected CDs in mice after acute exposure. Mice received a single lung administration of 100  $\mu\text{g}$  CD by intranasal instillation and were euthanized 24 h later. Total and differential cell number (A) and cytokine levels (B) were evaluated in BALFs. Results are expressed as absolute values. They are means  $\pm$  SEM of  $n=6$  experiments. Statistical differences when compared to control were determined by ANOVA followed by the Dunnett's test.

As a summary, we assessed the *in vivo* toxicity of CDs based on their physicochemical characteristics. The results obtained in mice confirm *in vitro* evidence as only CDs that are cytotoxic to cultured cells induce pulmonary inflammatory responses characterized by infiltration of neutrophils and macrophages, and production of cytokines in the lung. We also show that the inflammation induced by these CDs is dose-dependent. CDs are widely reported in the field of biomedical applications, especially as *in vivo* imaging contrast agents and drug carriers, and emphasis is very much on their biocompatibility and low toxicity. However, fundamental studies of the *in vivo* toxicity of CDs are still lacking, and most reports only focus on those "non-toxic" CDs. Yang *et al.* (Yang *et al.*, 2009e) found that PEGylated CDs appeared to be non-toxic after intravenous administration in mice, which is consistent with our results. Subsequently, they found CDs in the liver, kidneys and spleen, and observed no significant toxicity, little accumulation of CDs and renal clearance within 24 hours. Similarly, Wang *et al.* investigated the acute toxicity, subacute toxicity and genotoxicity of CDs (prepared by nitric acid oxidation of raw soot) in mice (Wang *et al.*, 2013b). They found that CDs were non-toxic to mice at any dose (up to 51 mg/kg, which is around 10 times higher than ours 5mg/kg), and no significant toxic effects were observed in the animal organs, *i.e.*, no abnormality or damage (Wang *et al.*, 2013b). In our *in vivo* toxicity studies in mice, we highlighted the inflammation produced by CDs.



We have found that according to their composition CDs may cause safety problems *in vitro* and *in vivo*, which may cause researchers to pay more attention to the potential toxicity of CDs rather than to emphasize the non-toxic properties of CDs.

### 3.1.4. Conclusions

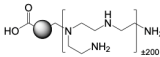
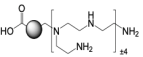
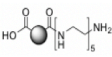
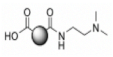
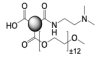
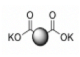
In the first part of our study dedicated to the safety of CDs, we investigated the toxicity of a library of 34 CDs exhibiting different physicochemical properties, in both *in vitro* and *in vivo* models. Analyzing the acute cytotoxicity of the whole NP library on THP-1 cells, we found that the 34 CDs exhibit either high, moderate or no toxicity. For CDs with the higher toxicity, we have demonstrated that toxicity is important at early time point such as 1 hour, and that it almost reaches a maximum at 4 hours. In addition, this toxicity is accompanied by a dose-time-dependent secretion of cytokines, a marker of inflammatory response. In the case of particles with moderate or no toxicity, this inflammatory response is absent. Analysis of the relationship between cytotoxicity and physicochemical characteristics of CDs indicates that highly or moderately cytotoxic NPs are invariably positively charged (e.g., MC225 and MC131), while non-cytotoxic nanoparticles are negatively charged (MC056). However, some positively charged CDs were found to be non-cytotoxic, especially when manufacturing process involved PEG, a polymer known for its steric exclusion properties, which tends to mask the charge on the surface of the NPs (e.g., MC-148). Although the size of NPs plays an important role in their toxicity, in the present study, in the range of NP size tested, it is not a predictor of CD toxicity. By contrast, the charge, aggregation state and the surface chemistry largely determine the interaction between the NPs and the biological medium and therefore their inherent toxicity.

Six CDs were selected in the different toxicity groups and were the subject of a thorough descriptive and mechanistic comparative study on different cell lines (table 6). From this work, it was found that the cytotoxicity level of NPs and their ability to induce inflammatory responses depend on the cell type. Thus, epithelial cells (A549 and Calu-3 cells) proved to be significantly less sensitive than THP-1 cells, which are immune cells with phagocytic activity. Cell internalization studies

by FACS and CLSM showed that only cytotoxic particles are internalized, and that the mechanism of this internalization depends on the cell type. Thus, if in THP-1 cells, internalization of the CDs involves an active process and several endocytic pathways, no clear major endocytosis mechanism was identified in A549 cells. To complete this comparative study, we have demonstrated that, unlike moderately toxic or non-toxic CDs, cytotoxic CDs induce oxidative stress and disrupt mitochondrial function, both of which may explain their cytotoxicity. The data from this comparative *in vitro* study (summarized in table 6) suggest that the positive net charge of the particles is not sufficient to predict their toxicity, but that the density of protonatable (titratable) amino groups at their surface could, in turn, be a determining factor.

In the last part of our safety study, we evaluated the *in vivo* toxicity of selected CDs. The results obtained in the mice lung confirmed *in vitro* evidence, as only CDs that are cytotoxic to cultured cells induce lung inflammation characterized by infiltration of neutrophils and production of cytokines in mice. We also show that the inflammation induced by these particles is dose-dependent. Thus, *in vitro* data, particularly the ones obtained in THP-1 cells, perfectly translate *in vivo*.

**Table 6.** Data from the in-depth comparative cytotoxicity study conducted on 6 CDs representative of initial NP sampling.

	MC-34	MC-225	MC-136	MC-131	MC-148	MC-56
Reactants	Citric acid bPEI25K	Citric acid bPEI600	Citric acid PEHA	Citric acid DMEDA	Citric acid DMEDA mPGE550	Citrate NH <sub>4</sub> <sup>+</sup> KH <sub>2</sub> PO <sub>4</sub>
Surface chemistry						
Size (nm) (saline solution, DLS)	13±3	10±2	19±4	44±10	18±4	25±5
Charge (mV) (saline solution, DLS)	+43±9	+25±3	+30±2	+21±2	+27±2	-40±1
Cytotoxicity (MTT assay)	High	High	Moderate	Moderate	None	None
Oxidative stress (Reduced GSH)	Yes	Yes	None	None	None	None
Inflammation (IL-8)	Yes	Yes	None	None	None	None
Inflammasome (IL-1 β)	Yes	Yes	None	None	None	None
Mitochondrial perturbation (JC-10)	Yes	Yes	None	Test interaction *		None
Cell uptake (FACS, Imaging)	Yes	Yes	Yes	Yes	None	None

\* Assay was not conducted due to interaction between fluorescence properties of MC131 and MC148 and the one of the probe JC-10 used to measure mitochondrial potential.

## 3.2. Evaluation of CDs as gene carriers

In this second part of my Ph.D. work, I conducted a systematic study on CDs as gene vectors. The transfection efficiency and cytotoxicity of these CDs were simultaneously investigated. During the whole research project, we investigated the effects of various synthetic factors on transfection efficiency and tentatively improved the CD-based gene carriers through a trial and error approach.

### 3.2.1. Description of the CD Library

In the synthesis of CDs for transfection purpose, two strategies were studied: a *de novo* synthesis pathway through direct pyrolysis of citric acid in the presence of a passivation reagent, and a post-functionalization method in which the polycationic passivation reagent is chemically grafted to the surface of substrate CDs. All these CDs were prepared by chemists in our group, Mickaël Claudel and Mickaël Rapp, and are referred to in table 7. For the sake of clarity, duration of activation and purification conditions (*i.e.*, MWCO of the dialysis bag, dialysis medium...) are not indicated in this table. Consequently, some samples may appear identical but are not. I systematically explored the transfection efficiency and cytotoxicity of these CDs to provide a feedback to chemists so they can identify structure-activity relationships and tentatively improve the synthetic processes and, thus, the performances of the CDs as nucleic acid carriers.

The CDs produced display sizes ranging from 4 to 290 nm (or form aggregates). Most of them exhibit positive zeta potential, up to +43 mV, but some of them are negatively charged, revealing inappropriate synthetic process or starting materials. These negatively charged CDs were not considered in transfection experiments. These transfection experiments were realized using the pCMV-Gluc plasmid encoding the *Gaussia princeps* luciferase that exhibit bioluminescence properties in the presence of its substrate, coelenterazine. Experiments were realized as two to four independent triplicates, under standardized conditions in 96-well plates, and transfection signal is expressed in relative light units per well (RLU/well). To allow comparison between CDs all along our studies, a “transfection score” is calculated for each CD sample as the ratio between the elicited transfection signal and that measured for untreated cells (control). Transfection assays were realized on the A549 cell line.

**Table 7.** CDs library and their transfection scores. Size and charge were measured by DLS in saline solution (NaCl, pH = 7.4). Values are averaged from triplicate tests.

Sample	Reagents	Ratio	Activation mode	Size (nm)	$\zeta$ (mV)	Transfection score
MC183	CA/bPEI25k	2:1	MW, 1 atm	15	+25	338
MC193	CA/bPEI25k	2:1	MW, 1 atm	100	+24	1655
MC204	CA/bPEI25k	2:1	MW, 1 atm	97	+26	776
MC210	CA/bPEI25k	2:1	MW, 1 atm	Aggregates	+2	1024
MC216	CA/bPEI25k	2:1	MW, 1 atm	Aggregates	+21	558
MC217	CA/bPEI25k	2:1	MW, 1 atm	Aggregates	+23	1563
MC218	CA/bPEI25k	2:1	MW, 1 atm	Aggregates	+5	1034
MC227-1	CA/bPEI25k	2:1	MW, 1 atm	8	+20	5896
MC227-2	CA/bPEI25k	2:1	MW, 1 atm	11	+26	4854
MC002-1	CA/bPEI25k	2:1	MW, 1 atm	6	+31	1
MC005	CA/bPEI25k	2:1	MW, 1 atm	Aggregates	-2	1
MC034	CA/bPEI25k	2:1	MW, 1 atm	7	+25	3909
MC040	CA/bPEI25k	2:1	MW, 180°C, >1 atm	Aggregates	-5	1
MC193	CA/bPEI25k	2:1	MW, 1 atm	100	+24	2225
MC227	CA/bPEI25k	2:1	MW (ST)	8	+20	5896
MC200	CA/bPEI25k	4:1	MW	86	-25	1
MC193-1	CA/bPEI25k	2:1	MW	100	+24	1693
MC224	CA/bPEI25k	1:2	MW	10	+33	3767
MC228	CA/bPEI25k	1:2	MW	10	+31	1636
MC203	CA/bPEI25k	1:4	MW	13	+36	4419
MC222	CA/bPEI25k	1:4	MW	28	+36	167
MC226	CA/bPEI25k	1:4	MW	10	+33	2639
MC223	CA/bPEI25k	1:8	MW	7	+28	2566
MC205	CA/bPEI2k	2:1	MW	40	-35	1
MC242-1	CA/bPEI600	2:1	MW	20	+18	993
MC101	CA/PEHA	2:1	MW	Aggregates	-13	1
MC078	CA/DMEDA	2:1	MW	Aggregates	-11	1
MC203	CA/bPEI25k	1:4	MW	13	+36	3563
MC225	CA/bPEI600	1:4	MW	10	+23	2404
MC229	CA/bPEI600	1:4	MW	15	+30	2965
MC242-4	CA/bPEI600	1:4	MW	19	+41	4

**Table 7. Continued.**

Sample	Reagents	Ratio	Activation mode	Size (nm)	$\zeta$ (mV)	Transfection score
MC254-1	CA/bPEI600	1:3.7	MW	19	+31	1561
MC254-2	CA/bPEI600	1:4	MW	19	+34	783
MC254-3	CA/bPEI600	1:4	MW	20	+23	377
MC254-4	CA/bPEI600	1:4	MW	21	+37	470
MC258-1	CA/bPEI600	1:4	MW	14	+34	1060
MC259	CA/bPEI600	1:4	MW	21	+33	4027
MC289	CA/bPEI600	1:4	MW	11	+35	859
MR267	CA/bPEI600	1:4	MW	17	+25	888
MC333	CA/PEHA	1:4	MW	4	+15	32
MC242-1	CA/bPEI600	2:1	MW	20	+18	993
MC242-2	CA/bPEI600	1:1	MW	7	+26	2690
MC242-3	CA/bPEI600	1:2	MW	10	+36	2117
MC289	CA/bPEI600	1:4	MW	11	+35	908
MC290	CA/bPEI600	1:4	MW	15	+33	753
MR264	CA/bPEI600	1:4	MW	31	+37	1
MC246-1	CA/bPEI600	2:1	MW, ST	Aggregates	+10	29
MC246-2	CA/bPEI600	1:2	MW, ST	Aggregates	+23	27
MC246-3	CA/bPEI600	1:4	MW, ST	36	+24	22
MC247-3	CA/bPEI600	2:1	MW, ST	290	-7	3
MC247-2	CA/bPEI600	2:1	MW, ST	130	-24	1
MC247-1	CA/bPEI600	2:1	MW, ST	70	-22	1
MR237	CA/bPEI600	2:1	MW, ST	78	-1	1
MC332-1	CA/bPEI600	1:4	MW, ST	14	+29	525
MC332-2	CA/bPEI600	1:4	MW, ST	20	+27	112
MC332-3	CA/bPEI600	1:4	MW, ST	11	+27	246
MC239-1	CA/bPEI600	1:2	ST, 100 °C	Aggregates	+24	26
MC239-2	CA/bPEI600	1:2	ST, 100 °C	Aggregates	+14	29
MC239-3	CA/bPEI600	1:2	ST, 100 °C	Aggregates	+24	7
MC240-1	CA/bPEI600	1:5	ST, 100 °C	74	+23	24

**Table 7. Continued.**

Sample	Reagents	Ratio	Activation mode	Size (nm)	$\zeta$ (mV)	Transfection score
MC240-2	CA/bPEI600	1:10	ST, 100 °C	Aggregates	+27	3
MC158	CA/bPEI600	2:1	Pyrolysis	147	+34	1
MC184	CA/bPEI600	1:1	Pyrolysis	111	+33	1
MC185	CA/bPEI600	1:2	Pyrolysis	17	+30	4
MC161	CA/bPEI600	1:3.8	Pyrolysis	36	+23	135
MC186	CA/bPEI600	1:8	Pyrolysis	22	+29	38
MC260	CA/bPEI600	1:4	ST, 200 °C	60	+29	17
MC261	CA/bPEI600	1:4	ST, 180 °C	21	+32	15
MR229-A	CA/bPEI600	1:4	ST, 240 °C, 15 min	6	+20	636
MR229-B	CA/bPEI600	1:4	ST, 240 °C, 1 h	18	+35	257
MR229-C	CA/bPEI600	1:4	ST, 240 °C, 4 h	23	+33	311
MR235-C	CA/bPEI600	2:1	ST, 240 °C	142	+0.4	1
MR235-B	CA/bPEI600	1:1	ST, 240 °C	5.1	+28	13
MR235-A	CA/bPEI600	1:2	ST, 240 °C	4	+37	2
MR241-A	CA/bPEI600	1:2	ST, 240 °C	18	+36	3
MR235-D	CA/bPEI600	1:4	ST, 240 °C	36	+33	103
MR241-D	CA/bPEI600	1:4	ST, 240 °C	23	+35	82
MR249	CA/bPEI600	1:4	ST, 240 °C	21	+19	1
MR280-A	CA/bPEI600	1:4	ST, 180 °C	11	+38	114
MR280-B	CA/bPEI600	1:4	ST, 210 °C	11	+41	112
MR280-C	CA/bPEI600	1:4	ST, 225 °C	6	+30	115
MR288-A	CA/bPEI600	1:4	ST, 225 °C	9	+20	612
MR288-B	CA/bPEI600	1:4	ST, 225 °C	11	+26	690
MR288-C	CA/bPEI600	1:4	ST, 250 °C	11	+34	314
MC328	CA/bPEI600	1:4	MW	8	+43	2454
MC329	CA/bPEI600	1:4	MW	9	+20	2423
MR276-A	CA/bPEI600	1:4	MW	12	+38	1885
MR276-B	CA/bPEI600	1:4	MW	22	+24	954

Through the transfection assays realized with the 88 CDs listed in table 7, we demonstrated that the expected CDs with outer cationic polymer layer have the ability to efficiently mediate plasmid DNA transfection in A549 cells. We initially characterized the size and surface charge of each CD sample. These two parameters were confirmed not to play a decisive role in transfection efficiency and no correlation could be established between the charge of CDs and their transfection capabilities. Indeed, not all positively charged CDs could achieve high transfection efficiency. Despite their charge, some of them appeared to be "aggregated" and, in some cases, achieved high transfection rate, probably due to accelerated sedimentation of the resulting dotplexes onto the cell membrane. One preliminary lesson we can learn from the collected data is that transfection efficiency cannot be guaranteed even if CDs have ideal nanometer size and high positive charge. Thus, it is necessary to realize some in-depth analysis and investigate the factors that may affect the transfection efficiency of CDs.

Throughout the entire transfection efficiency survey program, we have done a lot of optimization on the synthetic route to CDs, including (1) variation of activation conditions, (2) variation of activation duration, (3) variation of reagents stoichiometric ratio (citric acid vs. passivation reagent), and (4) variation of the passivation reagent (amine). In the following, I will state the factors in the synthesis process that influence the transfection performances of CDs. To provide a comprehensive overview, various CD series have been extracted from the library and classified according to the activation conditions that were used, to the stoichiometric ratio of the reagents, or to the nature of the passivation reagent.

### **3.2.2. Factors affecting the transfection efficiency of CDs**

As mentioned above, we found that transfection efficiency of CDs was affected by a variety of factors (synthetic aspects). Therefore, in the following I will select some CDs from the library to illustrate our approach and analyze these factors. Initial work was focused on CDs produced from citric acid and bPEI25k. From the data that have been collected, further optimization process led us to investigate CDs produced from citric acid and bPEI600.

### 3.2.2.1. Activation conditions (CA/bPEI25k)

In this first optimization stage, the conditions of reagent activation were investigated. As indicated in table 8, a series of CDs were produced starting from a mixture of citric acid (CA) and high molecular weight (25 kDa) branched polyethyleneimine (bPEI25k) in a 2/1 ratio (w/w). Under solvothermal conditions ( $P > 1$  atm, 180 °C), we obtained slightly negatively charged CDs, MC005 and MC040. However, as the zeta potential values were close to zero, the particles were prone to aggregation in saline environment. Under microwave irradiation at atmospheric pressure (*i.e.*, using a domestic microwave oven), MC193 was obtained. Zeta potential was determined to be +23.6 mV and these CDs still formed some aggregates, with an average size of 100 nm. Microwave irradiation under solvothermal conditions (100 °C,  $P_{\text{atm}}$ ) provided MC227. The larger zeta potential (+30.5 mV) measured for these particles improved their colloidal stability. Aggregation did not occur and the size was measured at 11.2 nm.

**Table 8:** Characteristics of CDs obtained from CA/bPEI25k 2/1, under various activation modes.

Sample	Size (nm)	$\zeta$ (mV)	Activation conditions
MC005	Aggregates	$-2.3 \pm 0.2$	Solvothermal ( $P > 1$ atm, 180 °C)
MC040	Aggregates	$-4.6 \pm 0.1$	Solvothermal ( $P > 1$ atm, 180 °C)
MC193	$100.0 \pm 1.0$	$+23.6 \pm 0.9$	MW ( $P_{\text{atm}}$ , RT to <i>ca.</i> 250 °C)
MC227	$11.2 \pm 0.5$	$+30.5 \pm 1.3$	MW ( $P_{\text{atm}}$ , 100 °C)

The transfection efficiency and cytotoxicity on A549 cells of this first series of CDs have been determined (figure 41). MC005 and MC040 exhibit no transfection efficiency, which is expected due to their negative charge. At the opposite, both positively charged MC193 and MC227 achieved significant transfection rate, though slightly below the one achieved with the gold standard *in vitro* transfection reagent bPEI25k, used as a positive control. Higher transfection efficiency was reached with MC227, probably revealing that MC193 yielded larger complexes with DNA that were less properly internalized into A549 cells. These results show that not only the size and charge of CDs are affected by the activation conditions but, as a consequence, also their



transfection efficiency may be altered. On the one hand, when no transfection was observed (MC005 and MC040), cytotoxicity of the CDs appeared non-significant. On the other hand, CDs that did efficiently mediate DNA transfection (MC193 and MC227) caused as well marked cytotoxicity that appeared to be associated with transfection efficiency. It is worth noting that cytotoxicity occurs after the transfection efficiency reaches the peak. At the ratio of 32, the transfection efficiency is significantly reduced, which is likely due to massive cytotoxicity, *i.e.*, most of cells are dead and cannot produce luciferase anymore.

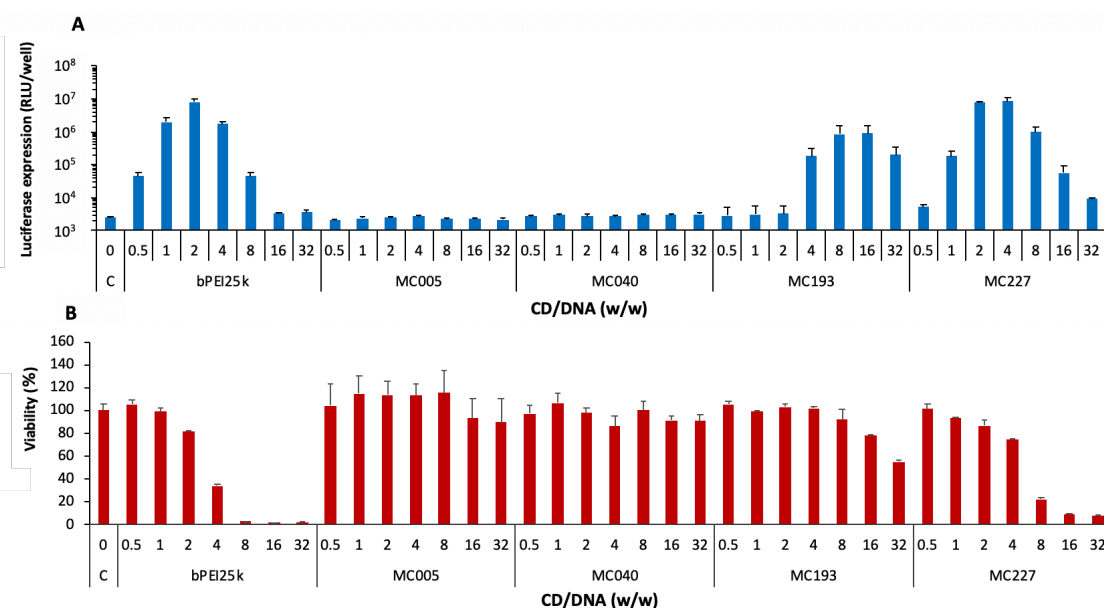


**Figure 41.** Impact of activation mode during the production of CDs (CA/bPEI25k 2/1) on transfection efficiency (A) and cytotoxicity (B) of lipoplexes made thereof. Cells not exposed to CDs served as a negative control, and bPEI25k was used as a positive control. The pDNA mass per well was fixed at 0.4  $\mu$ g. The first line of x-axis stands for the CD/pDNA ratio (w/w). Transgene expression (*Gaussia* Luciferase) is expressed as relative light units per well and viability is expressed as the percentage of the one measured in untreated cells.

### 3.2.2.2. Stoichiometry of the reagents (CA/bPEI25k)

We then explored the effect of the stoichiometric ratio of reagents on transfection efficiency. Microwave irradiation under atmospheric pressure was selected as the activation mode (*vide supra*). Varying the weight ratio between the reagents (CA/bPEI25k: 4:1, 2:1, 1:2, 1:4, 1:8), MC200, MC193-1, MC224, MC203, and MC223 were produced, respectively. As can be observed in table 9, varying the reagent ratio drastically affects the size and charge of the resulting CDs. At the higher CA/bPEI25k

ratio (MC200), negatively charged CDs are produced. Increasing the proportion of bPEI25k in the reaction mixture affords cationic CDs with gradually increasing zeta potential values. Correlatively, the size of the CDs decreases from 100 to 7 nm, which is consistent with improved colloidal stability due to the particle net charge. It is worth to note that at the higher CA/bPEI25k w/w ratio (1/8), zeta potential does not increase any more, most probably revealing that incorporation of PEI in NPs does not linearly depend on the initial concentration of the compound in the reaction mixture.

**Table 9.** Characteristics of CDs obtained from CA/bPEI25k, in various ratios, under microwave irradiation at  $P_{\text{atm}}$ .

Sample	CA/bPEI25k (w/w)	Size (nm)	$\zeta$ (mV)
MC200	4/1	86.1 $\pm$ 1.0	-25.4 $\pm$ 0.9
MC193-1	2/1	100.0 $\pm$ 1.0	+23.6 $\pm$ 1.0
MC224	1/2	10.3 $\pm$ 0.8	+33.1 $\pm$ 3.2
MC203	1/4	12.9 $\pm$ 0.7	+35.9 $\pm$ 1.6
MC223	1/8	6.9 $\pm$ 0.7	+30.8 $\pm$ 1.8

Therefore, we investigated the transfection efficiency of this series of CDs as shown in figure 42. As expected, negatively charged MC200 showed neither transfection activity nor cytotoxicity, due to their inability to bind to negatively charged pDNA. Positively charged CDs, MC193-1, MC224, MC203 and MC223, all were able to mediate transfection and transfection efficiency increased parallel to the zeta potential of the CDs. The transfection efficiency of MC193 is relatively low, probably due to the large complex it forms with DNA, which may reduce the internalization by A549 cells or hinder delay nucleic acid timely decondensation inside cells. Higher transfection rates were obtained with MC224 (CA/bPEI25k=1/2) and MC203 (CA/bPEI25k=1/4), those CDs in the series that exhibit the higher positive charges as well as relatively small size. This seems to imply that the transfection efficiency is increased as the proportion of bPEI25k increases. However, beyond the 1/4 ratio, the CD cationic charge did not increase anymore as was the case for transfection efficiency. CDs exhibit significant cytotoxicity when the transfection efficiency reaches its maximum value, and as the ratio increases, the transfection efficiency begins to decrease, most likely due to significant cell death. In addition, we found a variation of

the optimal w/w among the CD series, *i.e.*, the ratio that provides highest efficiency. The optimal ratio for MC193 is between 8-16, while it is around 4 for MC224, MC203 and MC223. In fact, a small optimal ratio may mean that CDs can bind and protect DNA more efficiently. In summary, the stoichiometric ratio of 1:4 (CA/bPEI25k) proved to provide CDs with the higher transfection efficiency, when reagents are processed under microwave irradiation at atmospheric pressure.

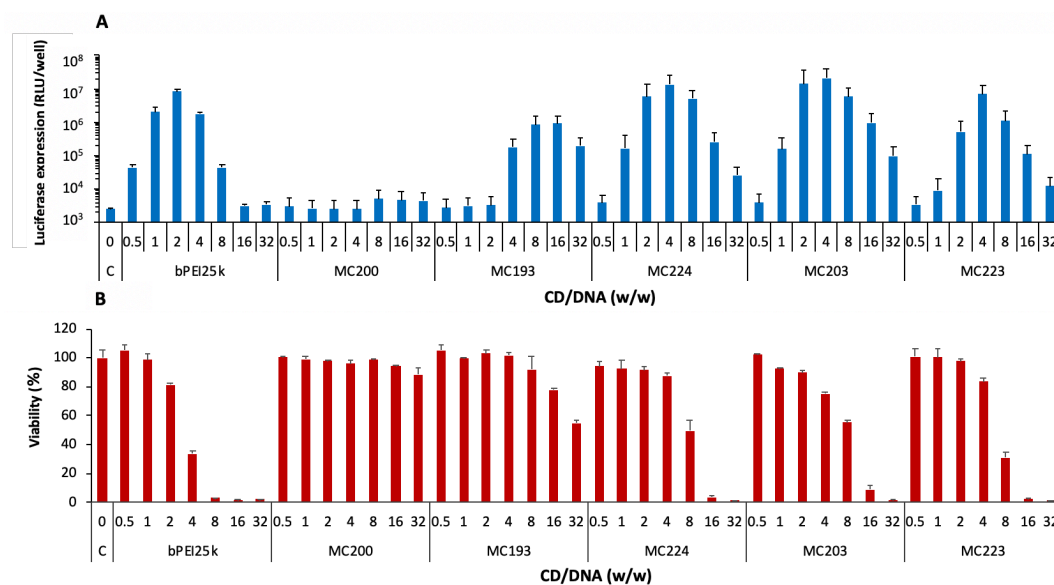


**Figure 42.** Impact of CA/bPEI25k stoichiometric ratio (w/w) on transfection efficiency (A) and cytotoxicity (B) of dotoplexes made thereof. Cells not exposed to CDs served as a negative control, and bPEI25k was used as a positive control. The pDNA mass per well was fixed at 0.4  $\mu$ g. The first line of x-axis stands for the CD/pDNA ratio (w/w). Transgene expression (*Gaussia* Luciferase) is expressed as relative light units per well and viability is expressed as the percentage of the one measured in untreated cells.

### 3.2.2.3. Nature of the passivation reagent

To investigate the effect of the passivation reagent used in the fabrication of the CDs on their transfection efficiency, we designed a series of NPs produced under microwave irradiation at atmospheric pressure, varying the passivator, at a CA/passivator w/w ratio of 1/4, as shown in table 10. One exception in the series was MC094 that was obtained by using *N,N*-dimethylethylene diamine (DMEDA) as passivator at a lower CA/DMEDA weight ratio (1/2). Due to its low negative charge (-8.2 mV), it has poor colloidal stability and forms aggregates of relatively large size (95.6 nm). Consistent with previous results, negatively charged CDs do not form

complexes with pDNA and therefore cannot mediate its transfection. Thus, DMEDA as passivating agent may not be suitable because it does not impart a positive charge to CDs. However, considering some results obtained later in our work, it would have been interesting to produce and evaluate DMEDA-based CDs involving higher CA/DMEDA w/w ratios.

MC333, MC229 and MC203 were obtained by using oligo(ethyleneimine) of increasing length as passivators, namely pentaethylenehexamine (PEHA,  $n = 5$ ), bPEI600 ( $n \approx 13$ ) and bPEI25k ( $n \approx 580$ ), respectively. The physicochemical properties of this series of CDs appear to meet the requirements for being potential gene carriers, *i. e.*, relatively small nanoscale size (4.1 to 14.8 nm) and positive charge (+15.0 to +35.9 mV). As shown in Table 10, the size and surface charge of CDs appear to be related to the length of the polyamine. The longer the polyamine, the seemingly higher size (4.1 to 14.8 nm) and surface charge (15.0 to 35.9 mV), though this correlation is not linear.

**Table 10.** Characteristics of CDs obtained from different passivation agents.

Sample	Passivator	Ratio (w/w)	Size (nm)	$\zeta$ (mV)
MC094	DMEDA	1/2	$95.6 \pm 21.6$	$-8.2 \pm 0.4$
MC333	PEHA	1/4	$4.1 \pm 0.5$	$+15.0 \pm 2.3$
MC229	bPEI600	1/4	$14.8 \pm 1.2$	$+29.5 \pm 0.9$
MC203	bPEI25k	1/4	$12.9 \pm 0.7$	$+35.9 \pm 1.6$

Next, we went ahead to study the transfection efficiency and cytotoxicity of this series of CDs (figure 43). MC333 exhibits no significant transfection efficiency. Even at the higher CDs/pDNA ratio (*i.e.* 32), transfection is still at a very low level. Accordingly, no significant cytotoxicity is caused by MC333. This may be due to the fact that the positive charge of the CDs is not high enough to cause tight binding to the pDNA, or to fully neutralize the pDNA negative charges upon binding. Longer oligo(ethyleneimine) yielded CDs with high transfection efficiency (MC229 from bPEI600, and MC203 from bPEI25k), indicating that PEI provides enough positive charge to CDs for adequate pDNA complexation and further internalization of complexes into A549 cells. In terms of cytotoxicity, we recorded consistent results, *i.e.*, increasing cytotoxicity was found

beyond the optimal ratio CD/pDNA corresponding to the highest transfection rate attained with the CDs. Interestingly, MC229 and MC203 showed identical transfection and toxicity patterns although bPEI25k is more than an order of magnitude longer than bPEI600. This is especially valuable for two reasons: 1-bPEI600 exhibits negligible transfection efficiency and cytotoxicity, and 2-it can be easily removed from crude reaction mixture when preparing CDs, which is definitely not the case for bPEI25k. Based on this, it is worthwhile to use bPEI600 as a candidate passivator instead of bPEI25k that can be only partly removed from CD samples during purification and exhibits intrinsic transfection properties that may interfere with that of CDs. In summary, we found that the type of passivation reagent has some effects on the physicochemical properties of CDs, and in turn, changes their transfection efficiency. More importantly, bPEI600 passivated CDs offer high transfection efficiency and, moreover, are easier to purify by dialysis relative to bPEI25k-passivated CDs.

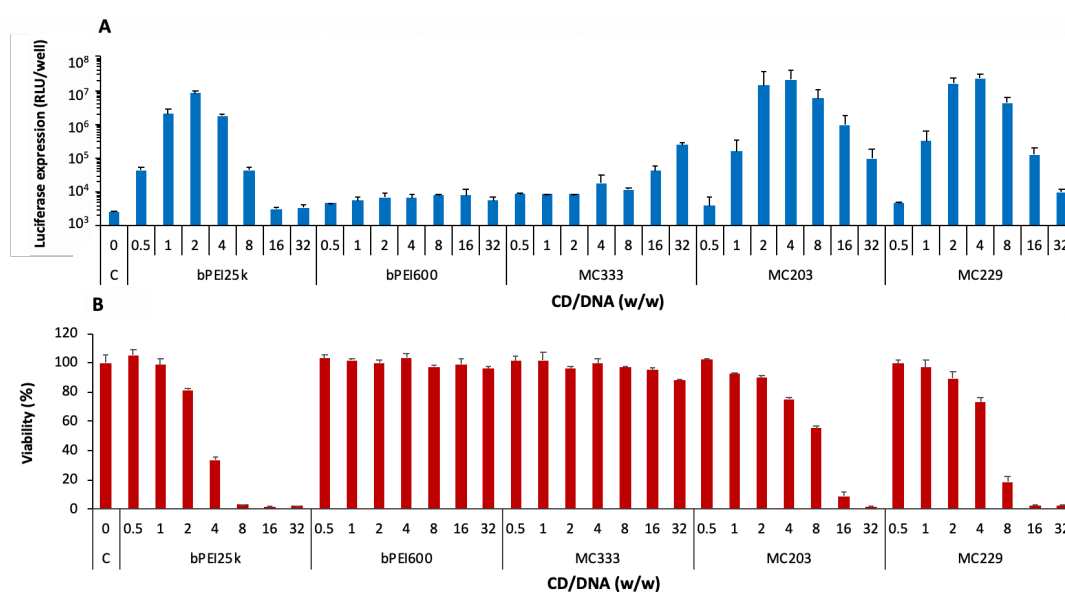


**Figure 43.** Impact of passivation reagent on transfection efficiency (A) and cytotoxicity (B) of dotoplexes made thereof. Cells not exposed to CDs served as a negative control, and bPEI25k was used as a positive control. The pDNA mass per well was fixed at 0.4  $\mu$ g. The first line of x-axis stands for the CD/pDNA ratio (w/w). Transgene expression (*Gaussia* Luciferase) is expressed as relative light units per well and viability is expressed as the percentage of the absorbance measured in untreated cells.

### 3.2.2.4. Stoichiometry of reagents (CA/bPEI600)

In the previous section, we found that bPEI600 as a passivating agent may be an interesting choice for the preparation of CDs as transfection reagents. Therefore,

we have carried out some additional work to further investigate the synthesis process of CDs involving this passivation reagent. Varying the stoichiometric ratio of citric acid and bPEI600 from 2/1 to 1/4, a new series of CDs were produced under microwave irradiation as previously established. The characteristics of the NPs obtained are shown in table 11. As can be seen, the initial content of bPEI600 in the reaction mixture does not appear to be related to the size of the CDs obtained. Indeed, all the NPs are in the range 6-20 nm, indicating high colloidal stability and very low aggregation state. The charge of the CDs increases with increasing bPEI600 content, but seems to be capped when the w/w ratio exceeds 1/2. Overall, all these bPEI600-based CDs exhibit a highly positive charge. This is an indication that bPEI600 may be a good alternative to bPEI25k as a passivating agent to impart a positive charge to CDs that is high enough for proper DNA complexation.

**Table 11.** Characteristics of CDs obtained from different stoichiometric ratios CA/bPEI600 under microwave irradiation conditions.

Sample	Ratio (w/w)	Size (nm)	$\zeta$ (mV)
MC242-1	2/1	20.0 $\pm$ 0.3	+18.4 $\pm$ 0.6
MC242-2	1/1	6.6 $\pm$ 1.6	+26.4 $\pm$ 1.3
MC242-3	1/2	10.2 $\pm$ 1.1	+36.1 $\pm$ 2.1
MC259	1/4	20.6 $\pm$ 3.6	+33.3 $\pm$ 1.8

The transfection efficiency and cytotoxicity of this series of CDs are shown in figure 44. As can be observed, all these bPEI600-based CDs efficiently mediate DNA transfection, with a score very similar to that of bPEI25k. Increasing the amount of bPEI600 in the initial reaction mixture however has a clear effect on the CD/DNA w/w ratio leading to optimum transfection efficacy, this one being decreased from 32 to 2 in the CD series. Finally, MC259 prepared from bPEI600 displays a transfection pattern that is superimposable to that of the gold standard bPEI25k. Considering cytotoxicity, the same trend as before is observed and toxicity appears only at CD doses that are sub-optimal for maximum transfection.

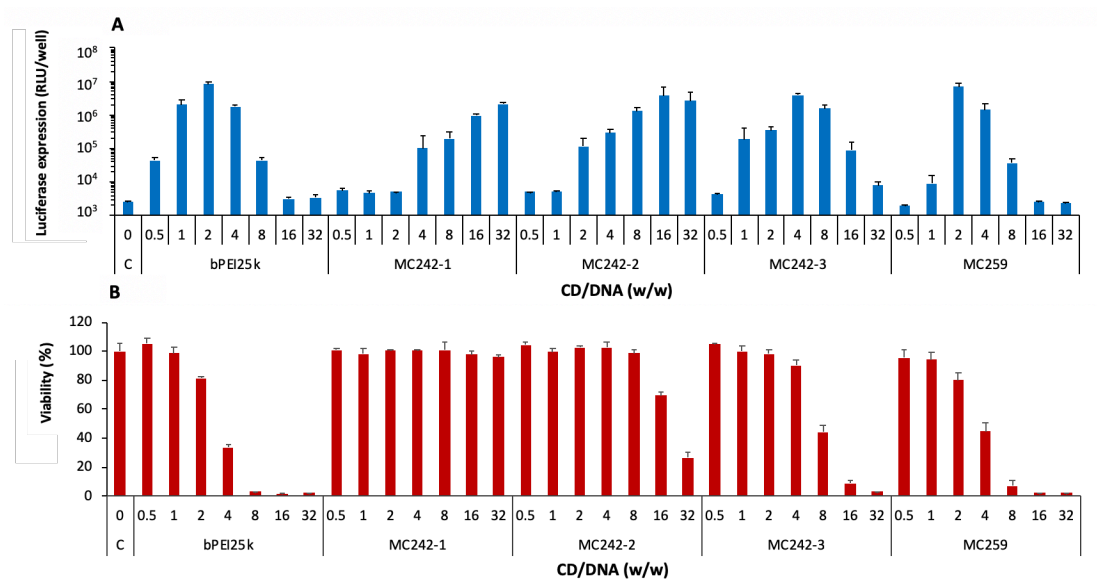


**Figure 44.** Impact of stoichiometry (CA/bPEI600) on transfection efficiency (A) and cytotoxicity (B) of dotoplexes made thereof. Cells not exposed to CDs served as a negative control, and bPEI25k was used as a positive control. The pDNA mass per well was fixed at 0.4  $\mu$ g. The first line of x-axis stands for the CD/pDNA ratio (w/w). Transgene expression (*Gaussia Luciferase*) is expressed as relative light units per well and viability is expressed as the percentage of the absorbance measured in untreated cells.

### 3.2.2.5. Activation conditions (CA/bPEI600 1/4)

According to the results discussed in the previous section, we investigated the possible effects of the activation conditions on the properties of CDs prepared from CA/bPEI600 1/4. We thus synthesized a series of CDs using different activation modes under this premise, as shown in the table 12. MC246-3 was obtained under microwave irradiation in solvothermal conditions. MC261 was obtained under solvothermal conditions ( $P > 1$  atm, 180  $^{\circ}$ C). MC161 was obtained by pyrolysis at high temperature. MC259 was obtained under microwave irradiation ( $P_{atm}$ ) in a domestic microwave oven. The size of the resulting CDs spread from 14.8 to 36.0 nm depending on the activation mode, microwave irradiation at  $P_{atm}$  providing the smallest NPs. All these CDs reveal high positive zeta potential and appear thus as potential candidates for gene delivery.

We investigated the transfection efficiency and cytotoxicity of this series of CDs, as shown in figure 45. Though all these CDs have similar size and display a marked and homogeneous positive charge, they proved variously efficient to mediate transfection. Fabrication of CDs under solvothermal conditions (MC246-3 and MC261)

**Table 12.** Characteristics of CDs obtained from a fixed stoichiometric ratio of CA/bPEI600 (1/4) using different activation modes.

Sample	Activation conditions	Size (nm)	$\zeta$ (mV)
MC246-3	Microwave under solvothermal conditions	$36.0 \pm 0.3$	$+24.3 \pm 2.6$
MC261	Solvothermal conditions ( $P > 1$ atm, $180$ °C)	$20.7 \pm 2.2$	$+32.0 \pm 3.7$
MC161	Pyrolysis at high temperature	$21.6 \pm 0.3$	$+24.9 \pm 1.8$
MC259	Microwave irradiation (Patm)	$20.6 \pm 3.6$	$+33.3 \pm 1.8$

yielded NPs that can hardly promote DNA internalization in cells. Pyrolysis of the reagents under solvent free conditions provided CDs (MC161) with intermediate transfection efficiency and requiring a large amount of CDs to properly deliver DNA to cells (optimum CD/DNA w/w ratio: 16/1). Finally, pyrolysis of the reagents at atmospheric pressure in a domestic microwave oven furnished highly potent gene carriers (MC259) that favorably compares to bPEI25k as was already mentioned in the previous section.

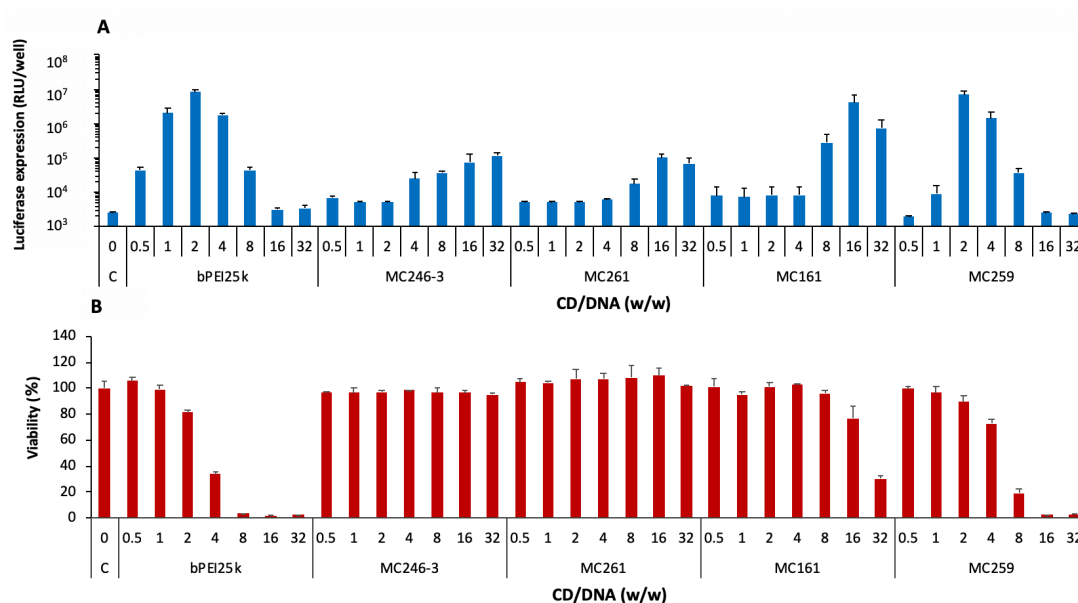


**Figure 45.** Impact of activation conditions (CA/bPEI600 1/4) on transfection efficiency (A) and cytotoxicity (B) of dotplexes made thereof. Cells not exposed to CDs served as a negative control, and bPEI25k was used as a positive control. The pDNA mass per well was fixed at  $0.4$   $\mu$ g. The first line of x-axis stands for the CD/pDNA ratio (w/w). Transgene expression (*Gaussia* Luciferase) is expressed as relative light units per well and viability is expressed as the percentage of the absorbance measured in untreated cells.



The reason why CDs prepared from the same starting material and displaying very similar physical characteristics display various transfection properties is not clear at the moment but it is likely that when using various activation modes, citric acid and bPEI600 are more or less thoroughly carbonized, yielding NPs with a distribution of nitrogen atoms that may differ in their macromolecular structure although displaying a similar cationic charge.

### **3.2.3. Conclusion**

The main results of our research are that the method used for the synthesis of CDs is a key factor determining their efficiency for delivering DNA to cells. When all other conditions are the same (the nature of the carbon source and additive, and the stoichiometric ratio of the reagents), the activation pattern used to pyrolyze the organic material to form CDs has proven to be very important for transfection efficiency. Furthermore, it is worth noting that the intrinsic positive charge of CDs does not appear to be directly related to the transfection efficiency of these vectors. It is undeniable that only positively charged particles (zeta potential higher than +15 mV) can efficiently make stable complexes with DNA and promote internalization into the cells, but the richness of positive charges does not necessarily translate into high transfection efficiency. It has also been found that CDs prepared from high molecular weight oligoamines (bPEI25k and bPEI600) are most effective in transfection. However, elimination of excess bPEI25k during the purification of CDs by dialysis is incomplete and residues of starting material (10 to 30 %) induce high toxicity and partially masks the CDs transfection potential. With this respect, the introduction of bPEI600 in the synthesis of CDs for transfection purpose conveniently addresses the problem of CD purification. Furthermore, it provides efficient carriers for gene delivery applications displaying intrinsic fluorescence properties that might be useful in theranostic applications.

### 3.3. General conclusions

From a collection of CDs available in the laboratory and continuously completed throughout the three years of my Ph.D. work, we developed a study to identify the main determinants of NP toxicity. Although the size of NP plays an important role (high specific surface area and reactivity), it is not itself a satisfactory predictor of CD toxicity. As demonstrated by our data, NP charge and, most importantly, surface chemistry largely determine the interaction between a NP and the biological medium, and therefore determines its intrinsic toxicity. The second part of my Ph.D. studies was focused to the evaluation of the activity of cationic CDs in gene transfer experiments. Through a trial-and-error approach, we were able to improve the efficacy of CDs in gene delivery and showed that NPs prepared from citric acid and bPEI600 are highly efficient gene carriers and favorably compare with the golden standard *in vitro* transfection reagent bPEI25k.

# Outlook

The study is still in infancy because the biological response to CDs is affected by many confounding factors, including size, surface charge, degree of dispersion, aggregation, passivation, and activation mode. A slight change in any of these factors can change the outcome, and these results are influenced by multiple factors rather than a single one. Our results complete a fundamental reality: the synthesis protocols applied for the preparation of CDs affects their toxicity and potential as gene carriers, and optimization of CDs is feasible. Through the close combination of biology and chemistry, we conducted CDs research according to this feedback loop model: synthesis - biological evaluation - re-optimization. Although general conclusions can be drawn about the extent to which CDs cause cell death, their toxic mechanisms such as ROS production, mitochondrial abnormalities, and immunity are preliminarily explored. Toxicological studies on CDs are insufficient compared to those that concern their potential applications. Moreover, absence of toxicity was claimed for most of the CDs reported in the literature. Nevertheless, our study did identify potential risks of CDs and thus some relationships between the physicochemical properties of CDs and

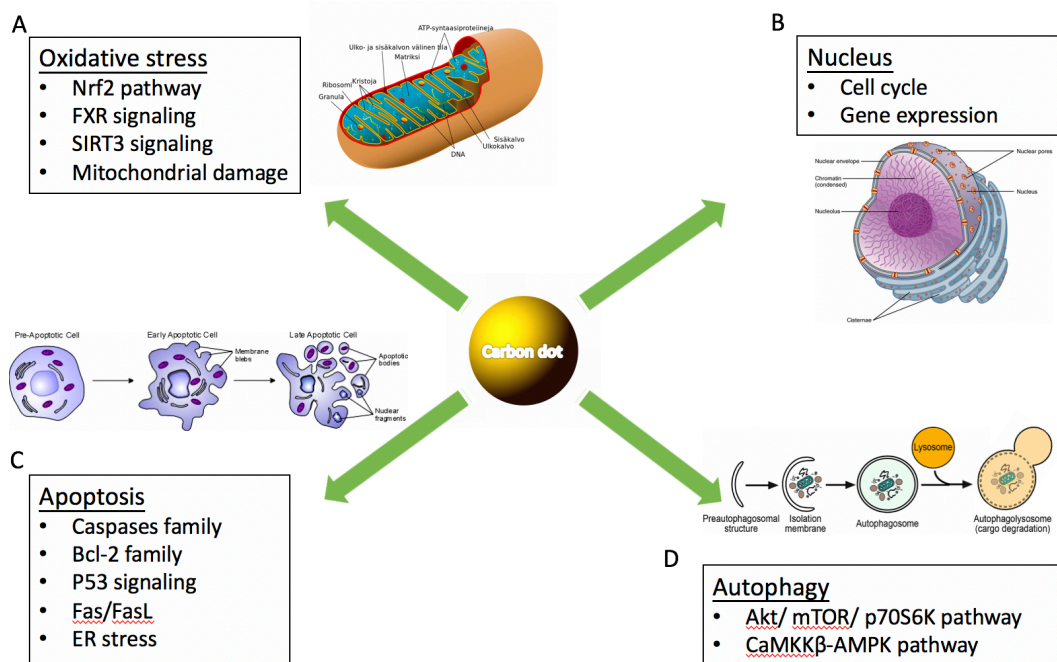


**Figure 46.** Outlook : Prospective research approaches for a better understanding of the toxicity mechanisms of CDs.

their toxicity. Our future concerns can be placed on the following aspects to provide a deeper understanding of the toxicity mechanisms of CDs as shown in figure 46: A-what is the source of oxidative stress in response to toxic CDs and the signal pathway involved, B-Do CDs exhibit effects at the nuclear level, such as effect on cell cycle or on gene expression , C-Is the cytotoxicity of CDs likely to be caused by active apoptosis, D-Can CDs affect autophagy and therefore cell homeostasis.

# Bibliography

- Abbas, Z., Labbez, C., Nordholm, S., and Ahlberg, E. (2008). Size-dependent surface charging of nanoparticles. *The Journal of Physical Chemistry C* *112*, 5715-5723.
- Abbasi, E., Aval, S.F., Akbarzadeh, A., Milani, M., Nasrabadi, H.T., Joo, S.W., Hanifehpour, Y., Nejati-Koshki, K., and Pashaei-Asl, R. (2014). Dendrimers: synthesis, applications, and properties. *Nanoscale Research Letters* *9*, 247.
- Abdal-hay, A., Hamdy Makhlof, A.S., and Khalil, K.A. (2015). Novel, Facile, Single-Step Technique of Polymer/TiO<sub>2</sub> Nanofiber Composites Membrane for Photodegradation of Methylene Blue. *ACS Applied Materials & Interfaces* *7*, 13329-13341.
- Agasti, S.S., Chompoosor, A., You, C.-C., Ghosh, P., Kim, C.K., and Rotello, V.M. (2009). Photoregulated release of caged anticancer drugs from gold nanoparticles. *Journal of the American Chemical Society* *131*, 5728-5729.
- Akbarzadeh, A., Rezaei-Sadabady, R., Davaran, S., Joo, S.W., Zarghami, N., Hanifehpour, Y., Samiei, M., Kouhi, M., and Nejati-Koshki, K. (2013). Liposome: classification, preparation, and applications. *Nanoscale Research Letters* *8*, 102.
- Al-Rawi, M., Diabaté, S., and Weiss, C. (2011). Uptake and intracellular localization of submicron and nano-sized SiO<sub>2</sub> particles in HeLa cells. *Archives of Toxicology* *85*, 813-826.
- Aleksenskii, A., Baidakova, M., Vul, A.Y., and Siklitskii, V. (1999). The structure of diamond nanoclusters. *Physics of the Solid State* *41*, 668-671.
- Allen, M.J., Tung, V.C., and Kaner, R.B. (2009). Honeycomb carbon: a review of graphene. *Chemical Reviews* *110*, 132-145.
- Antony, J.J., Sivalingam, P., and Chen, B. (2015). Toxicological effects of silver nanoparticles. *Environmental Toxicology and Pharmacology* *40*, 729-732.
- Anzai, Y., Piccoli, C.W., Outwater, E.K., Stanford, W., Bluemke, D.A., Nurenberg, P., Saini, S., Maravilla, K.R., Feldman, D.E., and Schmiedl, U.P. (2003). Evaluation of neck and body metastases to nodes with ferumoxtran 10-enhanced MR imaging: phase III safety and efficacy study. *Radiology* *228*, 777-788.
- Bae, Y., Nishiyama, N., and Kataoka, K. (2007). In vivo antitumor activity of the folate-conjugated pH-sensitive polymeric micelle selectively releasing adriamycin in the intracellular acidic compartments. *Bioconjugate Chemistry* *18*, 1131-1139.
- Baek, M., Kim, I.-S., Yu, J., Chung, H.E., Choy, J.-H., and Choi, S.-J. (2011). Effect of different forms of anionic nanoclays on cytotoxicity. *Journal of Nanoscience and Nanotechnology* *11*, 1803-1806.
- Baker, S.N., and Baker, G.A. (2010). Luminescent carbon nanodots: emergent nanolights. *Angewandte Chemie International Edition* *49*, 6726-6744.
- Bangham, A.D., and Horne, R. (1964). Negative staining of phospholipids and their structural modification by surface-active agents as observed in the electron microscope. *Journal of Molecular Biology* *8*, 660-IN610.
- Bareford, L.M., and Swaan, P.W. (2007). Endocytic mechanisms for targeted drug delivery. *Advanced Drug Delivery Reviews* *59*, 748-758.
- Behzadi, S., Serpooshan, V., Tao, W., Hamaly, M.A., Alkawareek, M.Y., Dreaden, E.C., Brown, D., Alkilany, A.M., Farokhzad, O.C., and Mahmoudi, M. (2017). Cellular

- uptake of nanoparticles: journey inside the cell. *Chemical Society Reviews* 46, 4218-4244.
- Belfiore, L., Saunders, D.N., Ranson, M., Thurecht, K.J., Storm, G., and Vine, K.L. (2018). Towards clinical translation of ligand-functionalized liposomes in targeted cancer therapy: Challenges and opportunities. *Journal of Controlled Release*.
- Benezra, M., Penate-Medina, O., Zanzonico, P.B., Schaer, D., Ow, H., Burns, A., DeStanchina, E., Longo, V., Herz, E., and Iyer, S. (2011). Multimodal silica nanoparticles are effective cancer-targeted probes in a model of human melanoma. *The Journal of Clinical Investigation* 121, 2768-2780.
- Berg, J.M., Romoser, A., Banerjee, N., Zebda, R., and Sayes, C.M. (2009). The relationship between pH and zeta potential of ~ 30 nm metal oxide nanoparticle suspensions relevant to in vitro toxicological evaluations. *Nanotoxicology* 3, 276-283.
- Berry, C.C., and Curtis, A.S. (2003). Functionalisation of magnetic nanoparticles for applications in biomedicine. *Journal of physics D: Applied Physics* 36, R198.
- Bhattacharjee, S., de Haan, L.H., Evers, N.M., Jiang, X., Marcelis, A.T., Zuilhof, H., Rietjens, I.M., and Alink, G.M. (2010). Role of surface charge and oxidative stress in cytotoxicity of organic monolayer-coated silicon nanoparticles towards macrophage NR8383 cells. *Particle and Fibre Toxicology* 7, 25.
- Bianco, A., Kostarelos, K., and Prato, M. (2005). Applications of carbon nanotubes in drug delivery. *Current Opinion in Chemical Biology* 9, 674-679.
- Bitler, B.G., Goverdhan, A., and Schroeder, J.A. (2010). MUC1 regulates nuclear localization and function of the epidermal growth factor receptor. *Journal of Cell Science*, jcs. 062661.
- Boeckle, S., von Gersdorff, K., van der Piepen, S., Culmsee, C., Wagner, E., and Ogris, M. (2004). Purification of polyethylenimine polyplexes highlights the role of free polycations in gene transfer. *The Journal of Gene Medicine* 6, 1102-1111.
- Boraschi, D., Italiani, P., Palomba, R., Decuzzi, P., Duschl, A., Fadeel, B., and Moghimi, S.M. (2017). Nanoparticles and innate immunity: new perspectives on host defence. Paper presented at: Seminars in Immunology (Elsevier).
- Borm, P.J., and Berube, D. (2008). A tale of opportunities, uncertainties, and risks. *Nano Today* 3, 56-59.
- Boussif, O., Lezoualc'h, F., Zanta, M.A., Mergny, M.D., Scherman, D., Demeneix, B., and Behr, J.-P. (1995). A versatile vector for gene and oligonucleotide transfer into cells in culture and in vivo: polyethylenimine. *Proceedings of the National Academy of Sciences* 92, 7297-7301.
- Braydich-Stolle, L.K., Schaeublin, N.M., Murdock, R.C., Jiang, J., Biswas, P., Schlager, J.J., and Hussain, S.M. (2009). Crystal structure mediates mode of cell death in TiO<sub>2</sub> nanotoxicity. *Journal of Nanoparticle Research* 11, 1361-1374.
- Brites, C.D., Lima, P.P., Silva, N.J., Millán, A., Amaral, V.S., Palacio, F., and Carlos, L.D. (2012). Thermometry at The Nanoscale. *Nanoscale* 4, 4799-4829.
- Buhleier, E., Wehner, W., and Vögtle, F. (1978). ' CASCADE'-AND' NONSKID-CHAIN-LIKE' Syntheses of Molecular Cavity Topologies. *ChemInform* 9.
- Buzea, C., Pacheco, I.I., and Robbie, K. (2007). Nanomaterials and nanoparticles: Sources and toxicity. *Biointerphases* 2, MR17-MR71.
- Caballero-Díaz, E., and Cases, M.V. (2016). Analytical methodologies for nanotoxicity

- assessment. *TrAC Trends in Analytical Chemistry* 84, 160-171.
- Cabral, H., and Kataoka, K. (2014). Progress of drug-loaded polymeric micelles into clinical studies. *Journal of Controlled Release* 190, 465-476.
- Candeloro, P., Tirinato, L., Malara, N., Fregola, A., Casals, E., Puntos, V., Perozziello, G., Gentile, F., Coluccio, M.L., and Das, G. (2011). Nanoparticle microinjection and Raman spectroscopy as tools for nanotoxicology studies. *Analyst* 136, 4402-4408.
- Cartiera, M.S., Johnson, K.M., Rajendran, V., Caplan, M.J., and Saltzman, W.M. (2009). The uptake and intracellular fate of PLGA nanoparticles in epithelial cells. *Biomaterials* 30, 2790-2798.
- Carver, L.A., and Schnitzer, J.E. (2003). Caveolae: mining little caves for new cancer targets. *Nature Reviews Cancer* 3, 571.
- Cayuela, A., Soriano, M., Carrillo-Carrión, C., and Valcarcel, M. (2016). Semiconductor and carbon-based fluorescent nanodots: the need for consistency. *Chemical Communications* 52, 1311-1326.
- Chalmers, S., Caldwell, S.T., Quin, C., Prime, T.A., James, A.M., Cairns, A.G., Murphy, M.P., McCarron, J.G., and Hartley, R.C. (2011). Selective uncoupling of individual mitochondria within a cell using a mitochondria-targeted photoactivated protonophore. *Journal of the American Chemical Society* 134, 758-761.
- Chan, J.M., Valencia, P.M., Zhang, L., Langer, R., and Farokhzad, O.C. (2010). Polymeric nanoparticles for drug delivery. In *Cancer Nanotechnology* (Springer), pp. 163-175.
- Chan, W.C., Maxwell, D.J., Gao, X., Bailey, R.E., Han, M., and Nie, S. (2002). Luminescent quantum dots for multiplexed biological detection and imaging. *Current Opinion in Biotechnology* 13, 40-46.
- Chang, C. (2010). The immune effects of naturally occurring and synthetic nanoparticles. *Journal of Autoimmunity* 34, J234-J246.
- Chao, J., Zhu, D., Zhang, Y., Wang, L., and Fan, C. (2016). DNA nanotechnology-enabled biosensors. *Biosensors and Bioelectronics* 76, 68-79.
- Chen, G., Roy, I., Yang, C., and Prasad, P.N. (2016). Nanochemistry and nanomedicine for nanoparticle-based diagnostics and therapy. *Chemical Reviews* 116, 2826-2885.
- Chen, L., Yu, H., Zhong, J., Wu, J., and Su, W. (2018). Graphene based hybrid/composite for electron field emission: A review. *Journal of Alloys and Compounds*.
- Cheng, F.-Y., Wang, S.P.-H., Su, C.-H., Tsai, T.-L., Wu, P.-C., Shieh, D.-B., Chen, J.-H., Hsieh, P.C.-H., and Yeh, C.-S. (2008). Stabilizer-free poly (lactide-co-glycolide) nanoparticles for multimodal biomedical probes. *Biomaterials* 29, 2104-2112.
- Cheng, Y., Zhao, L., Li, Y., and Xu, T. (2011). Design of biocompatible dendrimers for cancer diagnosis and therapy: current status and future perspectives. *Chemical Society Reviews* 40, 2673-2703.
- Chernenko, T., Matthäus, C., Milane, L., Quintero, L., Amiji, M., and Diem, M. (2009). Label-free Raman spectral imaging of intracellular delivery and degradation of polymeric nanoparticle systems. *ACS Nano* 3, 3552-3559.
- Cho, K., Wang, X., Nie, S., and Shin, D.M. (2008). Therapeutic nanoparticles for drug delivery in cancer. *Clinical Cancer Research* 14, 1310-1316.
- Clamme, J.P., Azoulay, J., and Mély, Y. (2003). Monitoring of the formation and dissociation of polyethylenimine/DNA complexes by two photon fluorescence

- correlation spectroscopy. *Biophysical Journal* 84, 1960-1968.
- Cole, J.T., and Holland, N.B. (2015). Multifunctional nanoparticles for use in theranostic applications. *Drug delivery and Translational Research* 5, 295-309.
- Conner, S.D., and Schmid, S.L. (2003). Regulated portals of entry into the cell. *Nature* 422, 37.
- Coulter, J.A., Jain, S., Butterworth, K.T., Taggart, L.E., Dickson, G.R., McMahon, S.J., Hyland, W.B., Muir, M.F., Trainor, C., and Hounsell, A.R.J.I.j.o.n. (2012). Cell type-dependent uptake, localization, and cytotoxicity of 1.9 nm gold nanoparticles. *International Journal of Nanomedicine*, 7, 2673.
- Cross, C.E., Halliwell, B., Borish, E.T., Pryor, W.A., Ames, B.N., Saul, R.L., McCORD, J.M., and Harman, D. (1987). Oxygen radicals and human disease. *Annals of Internal medicine* 107, 526-545.
- Dahlman, J.E., Barnes, C., Khan, O.F., Thiriot, A., Jhunjunwala, S., Shaw, T.E., Xing, Y., Sager, H.B., Sahay, G., and Speciner, L. (2014). In vivo endothelial siRNA delivery using polymeric nanoparticles with low molecular weight. *Nature Nanotechnology* 9, 648.
- Dam, D.H.M., Lee, R.C., and Odom, T.W. (2014). Improved in vitro efficacy of gold nanoconstructs by increased loading of G-quadruplex aptamer. *Nano letters* 14, 2843.
- De Duve, C. (1983). Lysosomes revisited. *European Journal of Biochemistry* 137, 391-397.
- Debbage, P., and Jaschke, W. (2008). Molecular imaging with nanoparticles: giant roles for dwarf actors. *Histochemistry and Cell Biology* 130, 845-875.
- Dellinger, A., Zhou, Z., Connor, J., Madhankumar, A., Pamujula, S., Sayes, C.M., and Kepley, C.L. (2013). Application of fullerenes in nanomedicine: an update. *Nanomedicine* 8, 1191-1208.
- Demchenko, A.P., and Dekaliuk, M.O. (2013). Novel fluorescent carbonic nanomaterials for sensing and imaging. *Methods and Applications in Fluorescence* 1, 042001.
- Derfus, A.M., Chan, W.C., and Bhatia, S.N.J.N.I. (2004). Probing the cytotoxicity of semiconductor quantum dots. *Nano Letters*, 4, 11-18.
- Deshmukh, A.S., Chauhan, P.N., Noolvi, M.N., Chaturvedi, K., Ganguly, K., Shukla, S.S., Nadagouda, M.N., and Aminabhavi, T.M. (2017). Polymeric micelles: Basic research to clinical practice. *International Journal of Pharmaceutics*.
- DiGiusto, D.L., Krishnan, A., Li, L., Li, H., Li, S., Rao, A., Mi, S., Yam, P., Stinson, S., and Kalos, M. (2010). RNA-based gene therapy for HIV with lentiviral vector-modified CD34+ cells in patients undergoing transplantation for AIDS-related lymphoma. *Science Translational Medicine* 2, 36ra43-36ra43.
- Ding, Y., Jiang, Z., Saha, K., Kim, C.S., Kim, S.T., Landis, R.F., and Rotello, V.M. (2014). Gold nanoparticles for nucleic acid delivery. *Molecular Therapy* 22, 1075-1083.
- Domaille, D.W., Zeng, L., and Chang, C.J. (2010). Visualizing ascorbate-triggered release of labile copper within living cells using a ratiometric fluorescent sensor. *Journal of the American Chemical Society* 132, 1194-1195.
- Donaldson, K., Stone, V., Tran, C., Kreyling, W., and Borm, P.J. (2004). *Nanotoxicology* (BMJ Publishing Group Ltd).
- Dong, Y., Shao, J., Chen, C., Li, H., Wang, R., Chi, Y., Lin, X., and Chen, G. (2012).



- Blue luminescent graphene quantum dots and graphene oxide prepared by tuning the carbonization degree of citric acid. *Carbon* 50, 4738-4743.
- Dos Santos, T., Varela, J., Lynch, I., Salvati, A., and Dawson, K.A. (2011). Effects of transport inhibitors on the cellular uptake of carboxylated polystyrene nanoparticles in different cell lines. *PloS One* 6, e24438.
- El Badawy, A.M., Silva, R.G., Morris, B., Scheckel, K.G., Suidan, M.T., and Tolaymat, T.M. (2010). Surface charge-dependent toxicity of silver nanoparticles. *Environmental Science & Technology* 45, 283-287.
- Elsaesser, A., and Howard, C.V. (2012). Toxicology of nanoparticles. *Advanced Drug Delivery Reviews* 64, 129-137.
- Fan, R.-J., Sun, Q., Zhang, L., Zhang, Y., and Lu, A.-H. (2014). Photoluminescent carbon dots directly derived from polyethylene glycol and their application for cellular imaging. *Carbon* 71, 87-93.
- Fichter, K.M., Ingle, N.P., McLendon, P.M., and Reineke, T.M. (2012). Polymeric nucleic acid vehicles exploit active interorganelle trafficking mechanisms. *ACS Nano* 7, 347-364.
- Firdhouse, M.J., and Lalitha, P. (2015). Biosynthesis of silver nanoparticles and its applications. *Journal of Nanotechnology* 2015.
- Fischer, D., Li, Y., Ahlemeyer, B., Krieglstein, J., and Kissel, T. (2003). In vitro cytotoxicity testing of polycations: influence of polymer structure on cell viability and hemolysis. *Biomaterials* 24, 1121-1131.
- Foley, S., Crowley, C., Smaih, M., Bonfils, C., Erlanger, B.F., Seta, P., and Larroque, C. (2002a). Cellular localisation of a water-soluble fullerene derivative. *Biochemical and Biophysical Research Communications* 294, 116-119.
- Forssen, E., and Willis, M. (1998). Ligand-targeted liposomes. *Advanced Drug Delivery Reviews* 29, 249-271.
- Fu, C., Liu, T., Li, L., Liu, H., Chen, D., and Tang, F. (2013). The absorption, distribution, excretion and toxicity of mesoporous silica nanoparticles in mice following different exposure routes. *Biomaterials* 34, 2565-2575.
- Fulda, S., Galluzzi, L., and Kroemer, G. (2010). Targeting mitochondria for cancer therapy. *Nature Reviews in Drug Discovery* 9, 447.
- Gagliardi, M., Bardi, G., and Bifone, A. (2012). Polymeric nanocarriers for controlled and enhanced delivery of therapeutic agents to the CNS. *Therapeutic Delivery* 3, 875-887.
- Gezke-Moritz, M., and Moritz, M. (2016). Solid lipid nanoparticles as attractive drug vehicles: composition, properties and therapeutic strategies. *Materials Science and Engineering: C* 68, 982-994.
- Ghosh, P., Han, G., De, M., Kim, C.K., and Rotello, V.M. (2008). Gold nanoparticles in delivery applications. *Advanced Drug Delivery Reviews* 60, 1307-1315.
- Ginzburg, V.V., and Balijepalli, S. (2007). Modeling the thermodynamics of the interaction of nanoparticles with cell membranes. *Nano Letters* 7, 3716-3722.
- Goh, E.J., Kim, K.S., Kim, Y.R., Jung, H.S., Beack, S., Kong, W.H., Scarcelli, G., Yun, S.H., and Hahn, S.K. (2012). Bioimaging of hyaluronic acid derivatives using nanosized carbon dots. *Biomacromolecules* 13, 2554-2561.
- Goodman, C.M., McCusker, C.D., Yilmaz, T., and Rotello, V.M. (2004). Toxicity of gold nanoparticles functionalized with cationic and anionic side chains.

- Bioconjugate Chemistry 15, 897-900.
- Gou, N., Onnis-Hayden, A., and Gu, A.Z. (2010). Mechanistic toxicity assessment of nanomaterials by whole-cell-array stress genes expression analysis. *Environmental Science & Technology* 44, 5964-5970.
- Greulich, C., Diendorf, J., Simon, T., Eggeler, G., Epple, M., and Köller, M. (2011). Uptake and intracellular distribution of silver nanoparticles in human mesenchymal stem cells. *Acta Biomaterialia* 7, 347-354.
- Gupta, A., Sharma, A., von Boehmer, L., Surace, L., Knuth, A., and Van den Broek, M. (2012). Radiotherapy supports protective tumor-specific immunity. *Oncoimmunology* 1, 1610-1611.
- Gupta A K, Naregalkar R R, Vaidya V D, et al. Recent advances on surface engineering of magnetic iron oxide nanoparticles and their biomedical applications. *Future Medicine*, (2007): 23-39.
- Häfeli, U.O., Riffle, J.S., Harris-Shekhawat, L., Carmichael-Baranauskas, A., Mark, F., Dailey, J.P., and Bardenstein, D. (2009). Cell uptake and in vitro toxicity of magnetic nanoparticles suitable for drug delivery. *Molecular Pharmaceutics* 6, 1417-1428.
- Hamm B, Staks T, Mühler A, et al. Phase I clinical evaluation of Gd-EOB-DTPA as a hepatobiliary MR contrast agent: safety, pharmacokinetics, and MR imaging. *Radiology*, 1995, 195(3): 785-792.
- Hanot C C, Choi Y S, Anani T B, et al. Effects of iron-oxide nanoparticle surface chemistry on uptake kinetics and cytotoxicity in CHO-K1 cells. *International Journal of Molecular Sciences*, 2015, 17(1): 54.
- Hans, M., and Lowman, A. (2002). Biodegradable nanoparticles for drug delivery and targeting. *Current Opinion in Solid State and Materials Science* 6, 319-327.
- Harush-Frenkel, O., Debotton, N., Benita, S., and Altschuler, Y. (2007). Targeting of nanoparticles to the clathrin-mediated endocytic pathway. *Biochemical and Biophysical Research Communications* 353, 26-32.
- Havrdova, M., Hola, K., Skopalik, J., Tomankova, K., Petr, M., Cepe, K., Polakova, K., Tucek, J., Bourlinos, A.B., and Zboril, R. (2016). Toxicity of carbon dots—Effect of surface functionalization on the cell viability, reactive oxygen species generation and cell cycle. *Carbon* 99, 238-248.
- He, C., Hu, Y., Yin, L., Tang, C., and Yin, C. (2010a). Effects of particle size and surface charge on cellular uptake and biodistribution of polymeric nanoparticles. *Biomaterials* 31, 3657-3666.
- He, Q., Shi, J., Zhu, M., Chen, Y., and Chen, F. (2010b). The three-stage in vitro degradation behavior of mesoporous silica in simulated body fluid. *Microporous and Mesoporous Materials* 131, 314-320.
- Hillaireau, H., and Couvreur, P. (2009). Nanocarriers' entry into the cell: relevance to drug delivery. *Cellular and Molecular Life Sciences* 66, 2873-2896.
- Himaja, A., Karthik, P., and Singh, S.P. (2015). Carbon dots: the newest member of the carbon nanomaterials family. *The Chemical Record* 15, 595-615.
- Hiura T S, Li N, Kaplan R, et al. The role of a mitochondrial pathway in the induction of apoptosis by chemicals extracted from diesel exhaust particles. *The Journal of Immunology*, 2000, 165(5): 2703-2711.
- Hoet P H M, Brüske-Hohlfeld I, Salata O V. Nanoparticles—known and unknown health risks. *Journal of Nanobiotechnology*, 2004, 2(1): 12.

- Hsiao, I.-L., and Huang, Y.-J. (2011). Effects of various physicochemical characteristics on the toxicities of ZnO and TiO<sub>2</sub> nanoparticles toward human lung epithelial cells. *Science of the Total Environment* *409*, 1219-1228.
- Hu, Y., Xie, J., Tong, Y.W., and Wang, C.-H. (2007). Effect of PEG conformation and particle size on the cellular uptake efficiency of nanoparticles with the HepG2 cells. *Journal of Controlled Release* *118*, 7-17.
- Huang, D.-M., Hung, Y., Ko, B.-S., Hsu, S.-C., Chen, W.-H., Chien, C.-L., Tsai, C.-P., Kuo, C.-T., Kang, J.-C., and Yang, C.-S. (2005). Highly efficient cellular labeling of mesoporous nanoparticles in human mesenchymal stem cells: implication for stem cell tracking. *The FASEB Journal* *19*, 2014-2016.
- Huang, P., Lin, J., Wang, X., Wang, Z., Zhang, C., He, M., Wang, K., Chen, F., Li, Z., and Shen, G. (2012). Light-triggered theranostics based on photosensitizer-conjugated carbon dots for simultaneous enhanced-fluorescence imaging and photodynamic therapy. *Advanced Materials* *24*, 5104-5110.
- Huang, X., Zhang, F., Zhu, L., Choi, K.Y., Guo, N., Guo, J., Tackett, K., Anilkumar, P., Liu, G., and Quan, Q. (2013). Effect of injection routes on the biodistribution, clearance, and tumor uptake of carbon dots. *ACS Nano* *7*, 5684-5693.
- Hussain, S., Boland, S., Baeza-Squiban, A., Hamel, R., Thomassen, L.C.J., Martens, J.A., Billon-Galland, M.A., Fleury-Feith, J., Moisan, F., Pairon, J.C., *et al.* (2009). Oxidative stress and proinflammatory effects of carbon black and titanium dioxide nanoparticles: Role of particle surface area and internalized amount. *Toxicology* *260*, 142-149.
- Hussain, S., Hess, K., Gearhart, J., Geiss, K., and Schlager, J. (2005a). In vitro toxicity of nanoparticles in BRL 3A rat liver cells. *Toxicology in Vitro* *19*, 975-983.
- Hyde, S.C., Gill, D.R., Higgins, C.F., Trezise, A.E., MacVinish, L.J., Cuthbert, A.W., Ratcliff, R., Evans, M.J., and Colledge, W.H. (1993). Correction of the ion transport defect in cystic fibrosis transgenic mice by gene therapy. *Nature* *362*, 250-255.
- Ishida, T., Kirchmeier, M., Moase, E., Zalipsky, S., and Allen, T. (2001). Targeted delivery and triggered release of liposomal doxorubicin enhances cytotoxicity against human B lymphoma cells. *Biochimica et Biophysica Acta-Biomembranes* *1515*, 144-158.
- Iversen, T.-G., Skotland, T., and Sandvig, K. (2011). Endocytosis and intracellular transport of nanoparticles: present knowledge and need for future studies. *Nano Today* *6*, 176-185.
- Janib, S.M., Moses, A.S., and MacKay, J.A. (2010). Imaging and drug delivery using theranostic nanoparticles. *Advanced Drug Delivery Reviews* *62*, 1052-1063.
- Jiang, D., Chen, Y., Li, N., Li, W., Wang, Z., Zhu, J., Zhang, H., Liu, B., and Xu, S. (2015a). Synthesis of luminescent graphene quantum dots with high quantum yield and their toxicity study. *PLoS One* *10*, e0144906.
- Jiang K, Sun S, Zhang L, et al. Red, green, and blue luminescence by carbon dots: full-color emission tuning and multicolor cellular imaging[J]. *Angewandte Chemie International Edition*, 2015, 54(18): 5360-5363.
- Jing, B., and Zhu, Y. (2011). Disruption of supported lipid bilayers by semihydrophobic nanoparticles. *Journal of the American Chemical Society* *133*, 10983-10989.
- Kanaras, A.G., Kamounah, F.S., Schaumburg, K., Kiely, C.J., and Brust, M. (2002). Thioalkylated tetraethylene glycol: a new ligand for water soluble monolayer

- protected gold clusters. *Chemical Communications*, 2294-2295.
- Kataoka, K., Harada, A., and Nagasaki, Y. (2001). Block copolymer micelles for drug delivery: design, characterization and biological significance. *Advanced Drug Delivery Reviews* 47, 113-131.
- Kedmi, R., Ben-Arie, N., and Peer, D. (2010). The systemic toxicity of positively charged lipid nanoparticles and the role of Toll-like receptor 4 in immune activation. *Biomaterials* 31, 6867-6875.
- Kerr, M.C., and Teasdale, R.D. (2009). Defining macropinocytosis. *Traffic* 10, 364-371.
- Kettler, K., Veltman, K., van de Meent, D., van Wezel, A., and Hendriks, A.J. (2014). Cellular uptake of nanoparticles as determined by particle properties, experimental conditions, and cell type. *Environmental Toxicology and Chemistry* 33, 481-492.
- Khan, S., Verma, N.C., Chethana, and Nandi, C.K. (2018). Carbon Dots for Single-Molecule Imaging of the Nucleolus. *ACS Applied Nano Materials*.
- Kim, J., Chankeshwara, S.V., Thielbeer, F., Jeong, J., Donaldson, K., Bradley, M., and Cho, W.-S. (2016). Surface charge determines the lung inflammogenicity: A study with polystyrene nanoparticles. *Nanotoxicology* 10, 94-101.
- Kim S, Samanta P, Yoo J, et al. Time-Dependent Toxicity Responses in *Daphnia magna* Exposed to CuO and ZnO Nanoparticles. *Bulletin of Environmental Contamination and Toxicology*, 2017, 98(4): 502-507.
- Kirchhausen, T. (2000). Clathrin. *Annual Review of Biochemistry* 69, 699-727.
- Kobayashi, M., Juillerat, F., Galletto, P., Bowen, P., and Borkovec, M. (2005). Aggregation and charging of colloidal silica particles: effect of particle size. *Langmuir* 21, 5761-5769.
- Kong, M., Park, H., Cheng, X., and Chen, X. (2013). Spatial-temporal event adaptive characteristics of nanocarrier drug delivery in cancer therapy. *Journal of Controlled Release* 172, 281-291.
- Konop, M., Damps, T., Misicka, A., and Rudnicka, L. (2016). Certain aspects of silver and silver nanoparticles in wound care: a minireview. *Journal of Nanomaterials* 2016, 47.
- Kraft, J.C., Freeling, J.P., Wang, Z., and Ho, R.J. (2014). Emerging research and clinical development trends of liposome and lipid nanoparticle drug delivery systems. *Journal of Pharmaceutical Sciences* 103, 29-52.
- Kresge, C., Leonowicz, M., Roth, W.J., Vartuli, J., and Beck, J. (1992). Ordered mesoporous molecular sieves synthesized by a liquid-crystal template mechanism. *Nature* 359, 710.
- Kroto, H.W., Heath, J.R., O'Brien, S.C., Curl, R.F., and Smalley, R.E. (1985). C60: Buckminsterfullerene. *Nature* 318, 162.
- Kuhn, D.A., Vanhecke, D., Michen, B., Blank, F., Gehr, P., Petri-Fink, A., and Rothen-Rutishauser, B. (2014). Different endocytotic uptake mechanisms for nanoparticles in epithelial cells and macrophages. *Beilstein Journal of Nanotechnology* 5, 1625.
- Lacerda, L., Bianco, A., Prato, M., and Kostarelos, K. (2006). Carbon nanotubes as nanomedicines: from toxicology to pharmacology. *Advanced Drug Delivery Reviews* 58, 1460-1470.
- Lai, C.-W., Hsiao, Y.-H., Peng, Y.-K., and Chou, P.-T. (2012). Facile synthesis of highly emissive carbon dots from pyrolysis of glycerol; gram scale production of carbon dots/mSiO<sub>2</sub> for cell imaging and drug release. *Journal of Materials Chemistry* 22,

- 14403-14409.
- Lam, C.-W., James, J.T., McCluskey, R., and Hunter, R.L. (2004). Pulmonary toxicity of single-wall carbon nanotubes in mice 7 and 90 days after intratracheal instillation. *Toxicological Sciences* 77, 126-134.
- Lazarides, A., Kelly, K.L., Jensen, T., and Schatz, G. (2000). Optical properties of metal nanoparticles and nanoparticle aggregates important in biosensors. *Journal of Molecular Structure: THEOCHEM* 529, 59-63.
- Lee, C.C., MacKay, J.A., Fréchet, J.M., and Szoka, F.C. (2005). Designing dendrimers for biological applications. *Nature Biotechnology* 23, 1517.
- Lewinski, N., Colvin, V., and Drezek, R. (2008). Cytotoxicity of nanoparticles. *Small* 4, 26-49.
- Li, H., He, X., Kang, Z., Huang, H., Liu, Y., Liu, J., Lian, S., Tsang, C.H.A., Yang, X., and Lee, S.T. (2010a). Water-soluble fluorescent carbon quantum dots and photocatalyst design. *Angewandte Chemie International Edition* 49, 4430-4434.
- Li, H., Luo, T., Sheng, R., Sun, J., Wang, Z., and Cao, A. (2013). Endoplasmic reticulum localization of poly ( $\omega$ -aminohexyl methacrylamide) s conjugated with (l)-arginines in plasmid DNA delivery. *Biomaterials* 34, 7923-7938.
- Li, J.J.e., Muralikrishnan, S., Ng, C.-T., Yung, L.-Y.L., and Bay, B.-H. (2010b). Nanoparticle-induced pulmonary toxicity. *Experimental Biology and Medicine* 235, 1025-1033.
- Li N, Sioutas C, Cho A, et al. Ultrafine particulate pollutants induce oxidative stress and mitochondrial damage[J]. *Environmental Health Perspectives*, 2003, 111(4): 455.
- Li, S., Guo, Z., Feng, R., Zhang, Y., Xue, W., and Liu, Z. (2017). Hyperbranched polyglycerol conjugated fluorescent carbon dots with improved in vitro toxicity and red blood cell compatibility for bioimaging. *RSC Advances* 7, 4975-4982.
- Li, S.-d., and Huang, L.-y. (2000). Nonviral gene therapy: promises and challenges. *Gene Therapy* 7, 31.
- Li, W., and Szoka, F.C. (2007). Lipid-based nanoparticles for nucleic acid delivery. *Pharmaceutical Research* 24, 438-449.
- Li, X., Zhang, S., Kulinich, S.A., Liu, Y., and Zeng, H. (2014). Engineering surface states of carbon dots to achieve controllable luminescence for solid-luminescent composites and sensitive Be 2+ detection. *Scientific Reports* 4, 4976.
- Liang, H., Tian, H., Deng, M., and Chen, X. (2015). Gold nanoparticles for cancer theranostics. *Chinese Journal of Chemistry* 33, 1001-1010.
- Liao, H.-J., and Carpenter, G. (2007). Role of the Sec61 translocon in EGF receptor trafficking to the nucleus and gene expression. *Molecular Biology of the Cell* 18, 1064-1072.
- Liberman, E., Topaly, V., Tsofina, L., Jasaitis, A., and Skulachev, V. (1969). Mechanism of coupling of oxidative phosphorylation and the membrane potential of mitochondria. *Nature* 222, 1076.
- Liechty, W.B., Kryscio, D.R., Slaughter, B.V., and Peppas, N.A. (2010). Polymers for drug delivery systems. *Annual Review of Chemical and Biomolecular Engineering* 1, 149-173.
- Lim, C.-K., Singh, A., Heo, J., Kim, D., Lee, K.E., Jeon, H., Koh, J., Kwon, I.-C., and Kim, S. (2013). Gadolinium-coordinated elastic nanogels for in vivo tumor targeting

- and imaging. *Biomaterials* *34*, 6846-6852.
- Lim, S.Y., Shen, W., and Gao, Z. (2015). Carbon quantum dots and their applications. *Chemical Society Reviews* *44*, 362-381.
- Lin, J., Zhang, H., Chen, Z., and Zheng, Y. (2010). Penetration of lipid membranes by gold nanoparticles: insights into cellular uptake, cytotoxicity, and their relationship. *ACS Nano* *4*, 5421-5429.
- Liu, H., Ye, T., and Mao, C. (2007). Fluorescent carbon nanoparticles derived from candle soot. *Angewandte Chemie International Edition* *46*, 6473-6475.
- Liu, J., Gray, W.D., Davis, M.E., and Luo, Y. (2012a). Peptide- and saccharide-conjugated dendrimers for targeted drug delivery: a concise review. *Interface Focus*, rfs20120009.
- Liu, J., Rinzler, A.G., Dai, H., Hafner, J.H., Bradley, R.K., Boul, P.J., Lu, A., Iverson, T., Shelimov, K., and Huffman, C.B. (1998). Fullerene pipes. *Science* *280*, 1253-1256.
- Liu, Q., Guo, B., Rao, Z., Zhang, B., and Gong, J.R. (2013). Strong two-photon-induced fluorescence from photostable, biocompatible nitrogen-doped graphene quantum dots for cellular and deep-tissue imaging. *Nano Letters* *13*, 2436-2441.
- Liu, W., Yao, J., Jin, J., Ma, J., and Masakorala, K. (2015). Microbial Toxicity of a Type of Carbon Dots to *Escherichia coli*. *Archives of Environmental Contamination and Toxicology* *69*, 506-514.
- Liu, Y., Liu, C.-y., and Zhang, Z.-y. (2012b). Synthesis of highly luminescent graphitized carbon dots and the application in the Hg<sup>2+</sup> detection. *Applied Surface Science* *263*, 481-485.
- Lungwitz, U., Breunig, M., Blunk, T., and Göpferich, A. (2005). Polyethylenimine-based non-viral gene delivery systems. *European Journal of Pharmaceutics and Biopharmaceutics* *60*, 247-266.
- Luo M, Shen C, Feltis B N, et al. Reducing ZnO nanoparticle cytotoxicity by surface modification. *Nanoscale*, 2014, 6(11): 5791-5798.
- Luo, X., Morrin, A., Killard, A.J., and Smyth, M.R. (2006). Application of nanoparticles in electrochemical sensors and biosensors. *Electroanalysis* *18*, 319-326.
- Ma, X., Zhao, Y., and Liang, X.-J. (2011). Theranostic nanoparticles engineered for clinic and pharmaceutics. *Accounts of Chemical Research* *44*, 1114-1122.
- Majewski, P., and Thierry, B. (2007). Functionalized magnetite nanoparticles—synthesis, properties, and bio-applications. *Critical Reviews in Solid State and Materials Sciences* *32*, 203-215.
- Manke, A., Wang, L., and Rojanasakul, Y. (2013). Mechanisms of nanoparticle-induced oxidative stress and toxicity. *BioMed Research International* *2013*.
- Marano, F., Hussain, S., Rodrigues-Lima, F., Baeza-Squiban, A., and Boland, S. (2011). Nanoparticles: molecular targets and cell signalling. *Archives of Toxicology* *85*, 733-741.
- Markovic, Z., and Trajkovic, V. (2008). Biomedical potential of the reactive oxygen species generation and quenching by fullerenes (C<sub>60</sub>). *Biomaterials* *29*, 3561-3573.
- Matea, C.T., Mocan, T., Tabaran, F., Pop, T., Mosteanu, O., Puia, C., Iancu, C., and Mocan, L. (2017). Quantum dots in imaging, drug delivery and sensor applications. *International Journal of Nanomedicine* *12*, 5421.

- Matsumura, Y., and Maeda, H. (1986). A new concept for macromolecular therapeutics in cancer chemotherapy: mechanism of tumorotropic accumulation of proteins and the antitumor agent smancs. *Cancer Research* *46*, 6387-6392.
- McCarthy, J.R., and Weissleder, R. (2008). Multifunctional magnetic nanoparticles for targeted imaging and therapy. *Advanced Drug Delivery Reviews* *60*, 1241-1251.
- McMahon, H.T., and Boucrot, E. (2011). Molecular mechanism and physiological functions of clathrin-mediated endocytosis. *Nature Reviews Molecular Cell Biology* *12*, 517.
- Mehnert, W., and Mäder, K. (2012). Solid lipid nanoparticles: production, characterization and applications. *Advanced Drug Delivery Reviews* *64*, 83-101.
- Mendonça, M.C.P., Soares, E.S., De Jesus, M.B., Ceragioli, H.J., Batista, A.n.G., Nyúl-Tóth, Á., Molnár, J., Wilhelm, I., Maróstica Jr, M.r.R., and Krizbai, I.J.M.p. (2016). PEGylation of Reduced Graphene Oxide Induces Toxicity in Cells of the Blood–Brain Barrier: An in Vitro and in Vivo Study. *13*, 3913-3924.
- Meng H, Chen Z, Xing G, et al. Ultrahigh reactivity provokes nanotoxicity: explanation of oral toxicity of nano-copper particles. *Toxicology Letters*, 2007, 175(1-3): 102-110.
- Misra, R., and Sahoo, S.K. (2010). Intracellular trafficking of nuclear localization signal conjugated nanoparticles for cancer therapy. *European Journal of Pharmaceutical Sciences* *39*, 152-163.
- Moore T L, Rodriguez-Lorenzo L, Hirsch V, et al. Nanoparticle colloidal stability in cell culture media and impact on cellular interactions. *Chemical Society Reviews*, 2015, 44(17): 6287-6305.
- Mulder, W.J., Strijkers, G.J., van Tilborg, G.A., Griffioen, A.W., and Nicolay, K. (2006). Lipid-based nanoparticles for contrast-enhanced MRI and molecular imaging. *NMR in Biomedicine* *19*, 142-164.
- Müller, R.H., MäEder, K., and Gohla, S. (2000). Solid lipid nanoparticles (SLN) for controlled drug delivery—a review of the state of the art. *European Journal of Pharmaceutics and Biopharmaceutics* *50*, 161-177.
- Mura, S., Hillaireau, H., Nicolas, J., Le Droumaguet, B., Gueutin, C., Zanna, S., Tsapis, N., and Fattal, E. (2011). Influence of surface charge on the potential toxicity of PLGA nanoparticles towards Calu-3 cells. *International Journal of Nanomedicine* *6*, 2591.
- Na, H.B., Song, I.C., and Hyeon, T. (2009). Inorganic nanoparticles for MRI contrast agents. *Advanced Materials* *21*, 2133-2148.
- Namiki, Y., Namiki, T., Yoshida, H., Ishii, Y., Tsubota, A., Koido, S., Nariai, K., Mitsunaga, M., Yanagisawa, S., and Kashiwagi, H. (2009). A novel magnetic crystal–lipid nanostructure for magnetically guided in vivo gene delivery. *Nature Nanotechnology* *4*, 598.
- Napierska, D., Thomassen, L.C., Rabolli, V., Lison, D., Gonzalez, L., Kirsch-Volders, M., Martens, J.A., and Hoet, P.H. (2009). Size-dependent cytotoxicity of monodisperse silica nanoparticles in human endothelial cells. *Small* *5*, 846-853.
- Nemmar A, Hoylaerts M F, Hoet P H M, et al. Ultrafine particles affect experimental thrombosis in an in vivo hamster model[J]. *American Journal of Respiratory and Critical Care Medicine*, 2002, 166(7): 998-1004.
- Neu, M., Fischer, D., and Kissel, T. (2005). Recent advances in rational gene transfer

- vector design based on poly (ethylene imine) and its derivatives. *The Journal of Gene Medicine* 7, 992-1009.
- Niidome, T., and Huang, L. (2002). Gene therapy progress and prospects: nonviral vectors. *Gene Therapy* 9, 1647.
- Norbury, C.C., Hewlett, L.J., Prescott, A.R., Shastri, N., and Watts, C. (1995). Class I MHC presentation of exogenous soluble antigen via macropinocytosis in bone marrow macrophages. *Immunity* 3, 783-791.
- Oberdörster, G. (2010). Safety assessment for nanotechnology and nanomedicine: concepts of nanotoxicology. *Journal of Internal Medicine* 267, 89-105.
- Oh, W.-K., Kim, S., Choi, M., Kim, C., Jeong, Y.S., Cho, B.-R., Hahn, J.-S., and Jang, J. (2010). Cellular uptake, cytotoxicity, and innate immune response of silica–titania hollow nanoparticles based on size and surface functionality. *ACS Nano* 4, 5301-5313.
- Olton, D.Y., Close, J.M., Sfeir, C.S., and Kumta, P.N. (2011). Intracellular trafficking pathways involved in the gene transfer of nano-structured calcium phosphate-DNA particles. *Biomaterials* 32, 7662-7670.
- Pan L, Sun S, Zhang A, et al. Truly Fluorescent Excitation-Dependent Carbon Dots and Their Applications in Multicolor Cellular Imaging and Multidimensional Sensing. *Advanced Materials*, 2015, 27(47): 7782-7787.
- Pan, Y., Neuss, S., Leifert, A., Fischler, M., Wen, F., Simon, U., Schmid, G., Brandau, W., and Jahnen-Dechent, W. (2007). Size-dependent cytotoxicity of gold nanoparticles. *Small* 3, 1941-1949.
- Pandey, S., Thakur, M., Mewada, A., Anjarlekar, D., Mishra, N., and Sharon, M. (2013). Carbon dots functionalized gold nanorod mediated delivery of doxorubicin: tri-functional nano-worms for drug delivery, photothermal therapy and bioimaging. *Journal of Materials Chemistry B* 1, 4972-4982.
- Pankhurst, Q., Thanh, N., Jones, S., and Dobson, J. (2009). Progress in applications of magnetic nanoparticles in biomedicine. *Journal of Physics D: Applied Physics* 42, 224001.
- Parameswaran N, Patial S. Tumor necrosis factor- $\alpha$  signaling in macrophages. *Critical Review in Eukaryotic Gene Expression*, 2010, 20(2).
- Park, M.V., Neigh, A.M., Vermeulen, J.P., de la Fonteyne, L.J., Verharen, H.W., Briedé, J.J., van Loveren, H., and de Jong, W.H. (2011a). The effect of particle size on the cytotoxicity, inflammation, developmental toxicity and genotoxicity of silver nanoparticles. *Biomaterials* 32, 9810-9817.
- Park M V D Z, Neigh A M, Vermeulen J P, et al. The effect of particle size on the cytotoxicity, inflammation, developmental toxicity and genotoxicity of silver nanoparticles. *Biomaterials*, 2011, 32(36): 9810-9817.
- Park, S., Lee, Y.K., Jung, M., Kim, K.H., Chung, N., Ahn, E.-K., Lim, Y., and Lee, K.-H. (2007). Cellular toxicity of various inhalable metal nanoparticles on human alveolar epithelial cells. *Inhalation Toxicology* 19, 59-65.
- Peer, D., Karp, J.M., Hong, S., Farokhzad, O.C., Margalit, R., and Langer, R. (2007). Nanocarriers as an emerging platform for cancer therapy. *Nature Nanotechnology* 2, 751-760.
- Pelkmans, L., and Helenius, A. (2002). Endocytosis via caveolae. *Traffic* 3, 311-320.
- Pierrat, P., Wang, R., Kereselidze, D., Lux, M., Didier, P., Kichler, A., Pons, F., and



- Lebeau, L. (2015). Efficient in vitro and in vivo pulmonary delivery of nucleic acid by carbon dot-based nanocarriers. *Biomaterials* 51, 290-302.
- Prasad P N. Introduction to nanomedicine and nanobioengineering. John Wiley & Sons, 2012.
- Probst, C.E., Zrazhevskiy, P., Bagalkot, V., and Gao, X. (2013). Quantum dots as a platform for nanoparticle drug delivery vehicle design. *Advanced Drug Delivery Reviews* 65, 703-718.
- Pujalté, I., Passagne, I., Brouillaud, B., Tréguer, M., Durand, E., Ohayon-Courtès, C., and L'Azou, B. (2011). Cytotoxicity and oxidative stress induced by different metallic nanoparticles on human kidney cells. *Particle and Fibre Toxicology* 8, 1.
- Qian, Z., Shan, X., Chai, L., Ma, J., Chen, J., and Feng, H. (2014). Si-doped carbon quantum dots: a facile and general preparation strategy, bioimaging application, and multifunctional sensor. *ACS Applied Materials & Interfaces* 6, 6797-6805.
- Ramos-Perez, V., Cifuentes, A., Coronas, N., de Pablo, A., and Borrós, S. (2013). Modification of carbon nanotubes for gene delivery vectors. In *Nanomaterial Interfaces in Biology* (Springer), pp. 261-268.
- Reilly, M.J., Larsen, J.D., and Sullivan, M.O. (2012). Polyplexes traffic through caveolae to the Golgi and endoplasmic reticulum en route to the nucleus. *Molecular Pharmaceutics* 9, 1280-1290.
- Reily, C., Mitchell, T., Chacko, B.K., Benavides, G.A., Murphy, M.P., and Darley-Usmar, V.M. (2013). Mitochondrially targeted compounds and their impact on cellular bioenergetics. *Redox Biology* 1, 86-93.
- Rejman J, Oberle V, Zuhorn I S, et al. Size-dependent internalization of particles via the pathways of clathrin-and caveolae-mediated endocytosis. *Biochemical Journal*, 2004, 377(1): 159-169.
- Ridley, M.K., Hackley, V.A., and Machesky, M.L. (2006). Characterization and surface-reactivity of nanocrystalline anatase in aqueous solutions. *Langmuir* 22, 10972-10982.
- Riggio, C., Pagni, E., Raffa, V., and Cuschieri, A. (2011). Nano-oncology: clinical application for cancer therapy and future perspectives. *Journal of Nanomaterials* 2011, 17.
- Rin Jean, S., Tulumello, D.V., Wisnovsky, S.P., Lei, E.K., Pereira, M.P., and Kelley, S.O. (2014). Molecular vehicles for mitochondrial chemical biology and drug delivery. *ACS Chemical Biology* 9, 323-333.
- Ruizendaal, L., Bhattacharjee, S., Pournazari, K., Rosso-Vasic, M., de Haan, L.H., Alink, G.M., Marcelis, A.T., and Zuilhof, H. (2009). Synthesis and cytotoxicity of silicon nanoparticles with covalently attached organic monolayers. *Nanotoxicology* 3, 339-347.
- Sahu, S., Behera, B., Maiti, T.K., and Mohapatra, S. (2012). Simple one-step synthesis of highly luminescent carbon dots from orange juice: application as excellent bio-imaging agents. *Chemical Communications* 48, 8835-8837.
- Sandvig, K., Bergan, J., Dyve, A.-B., Skotland, T., and Torgersen, M.L. (2010). Endocytosis and retrograde transport of Shiga toxin. *Toxicon* 56, 1181-1185.
- Sasidharan, A., Panchakarla, L., Chandran, P., Menon, D., Nair, S., Rao, C., and Koyakutty, M. (2011). Differential nano-bio interactions and toxicity effects of pristine versus functionalized graphene. *Nanoscale* 3, 2461-2464.

- Sayes, C.M., Wahi, R., Kurian, P.A., Liu, Y., West, J.L., Ausman, K.D., Warheit, D.B., and Colvin, V.L. (2006). Correlating nanoscale titania structure with toxicity: a cytotoxicity and inflammatory response study with human dermal fibroblasts and human lung epithelial cells. *Toxicological Sciences* 92, 174-185.
- Schaeublin, N.M., Braydich-Stolle, L.K., Schrand, A.M., Miller, J.M., Hutchison, J., Schlager, J.J., and Hussain, S.M. (2011). Surface charge of gold nanoparticles mediates mechanism of toxicity. *Nanoscale* 3, 410-420.
- Schinazi, R., Sijbesma, R., Srdanov, G., Hill, C., and Wudl, F. (1993). Synthesis and virucidal activity of a water-soluble, configurationally stable, derivatized C60 fullerene. *Antimicrobial Agents and Chemotherapy* 37, 1707-1710.
- Schmid, E.M., and McMahon, H.T. (2007). Integrating molecular and network biology to decode endocytosis. *Nature* 448, 883.
- Schmid G. *Nanoparticles*. Wiley VCH, 2005.
- Sercombe, L., Veerati, T., Mohemani, F., Wu, S.Y., Sood, A.K., and Hua, S. (2015). Advances and challenges of liposome assisted drug delivery. *Frontiers in Pharmacology* 6, 286.
- Shao, W., Ivanov, V., Zhen, L., Cui, Y., and Wang, Y. (2004). A study on graphitization of diamond in copper–diamond composite materials. *Materials letters* 58, 146-149.
- Sharma, P., Brown, S., Walter, G., Santra, S., and Moudgil, B. (2006). Nanoparticles for bioimaging. *Advances in Colloid and Interface Science* 123, 471-485.
- Sharma, S., Umar, A., Sood, S., Mehta, S.K., and Kansal, S.K. (2018). Photoluminescent C-dots: An overview on the recent development in the synthesis, physiochemical properties and potential applications. *Journal of Alloys and Compounds* 748, 818-853.
- Shen, P., and Xia, Y. (2014). Synthesis-modification integration: one-step fabrication of boronic acid functionalized carbon dots for fluorescent blood sugar sensing. *Analytical Chemistry* 86, 5323-5329.
- Shi, Y., Pan, Y., Zhong, J., Yang, J., Zheng, J., Cheng, J., Song, R., and Yi, C. (2015). Facile synthesis of gadolinium (III) chelates functionalized carbon quantum dots for fluorescence and magnetic resonance dual-modal bioimaging. *Carbon* 93, 742-750.
- Shin, S.W., Song, I.H., and Um, S.H. (2015). Role of physicochemical properties in nanoparticle toxicity. *Nanomaterials* 5, 1351-1365.
- Shukla, R.K., Sharma, V., Pandey, A.K., Singh, S., Sultana, S., and Dhawan, A. (2011). ROS-mediated genotoxicity induced by titanium dioxide nanoparticles in human epidermal cells. *Toxicology In Vitro* 25, 231-241.
- Shvedova, A.A., Kagan, V.E., and Fadeel, B. (2010). Close encounters of the small kind: adverse effects of man-made materials interfacing with the nano-cosmos of biological systems. *Annual Review of Pharmacology and Toxicology* 50, 63-88.
- Shvedova, A.A., Pietroiusti, A., Fadeel, B., and Kagan, V.E. (2012). Mechanisms of carbon nanotube-induced toxicity: focus on oxidative stress. *Toxicology and Applied Pharmacology* 261, 121-133.
- Singh, N., Manshian, B., Jenkins, G.J., Griffiths, S.M., Williams, P.M., Maffei, T.G., Wright, C.J., and Doak, S.H. (2009). NanoGenotoxicology: the DNA damaging potential of engineered nanomaterials. *Biomaterials* 30, 3891-3914.
- Singh, S., Mishra, A., Kumari, R., Sinha, K.K., Singh, M.K., and Das, P. (2017). Carbon dots assisted formation of DNA hydrogel for sustained release of drug. *Carbon* 114,

- 169-176.
- Slowing, I., Trewyn, B.G., and Lin, V.S.-Y. (2006). Effect of surface functionalization of MCM-41-type mesoporous silica nanoparticles on the endocytosis by human cancer cells. *Journal of the American Chemical Society* *128*, 14792-14793.
- Slowing, I.I., Vivero-Escoto, J.L., Wu, C.-W., and Lin, V.S.-Y. (2008). Mesoporous silica nanoparticles as controlled release drug delivery and gene transfection carriers. *Advanced Drug Delivery Reviews* *60*, 1278-1288.
- Society, A.C. (2013). *Cancer facts and figures 2013* (American Cancer Society Atlanta).
- Sohaebuddin, S.K., Thevenot, P.T., Baker, D., Eaton, J.W., and Tang, L. (2010). Nanomaterial cytotoxicity is composition, size, and cell type dependent. *Particle and Fibre Toxicology* *7*, 22.
- Sonnefeld, J. (1995). Surface charge density on spherical silica particles in aqueous alkali chloride solutions. *Colloid and Polymer Science* *273*, 932-938.
- Soppimath, K.S., Aminabhavi, T.M., Kulkarni, A.R., and Rudzinski, W.E. (2001). Biodegradable polymeric nanoparticles as drug delivery devices. *Journal of Controlled Release* *70*, 1-20.
- Srivastava, V., Gusain, D., and Sharma, Y.C. (2015). Critical review on the toxicity of some widely used engineered nanoparticles. *Industrial & Engineering Chemistry Research* *54*, 6209-6233.
- Stone V, Shaw J, Brown D M, et al. The role of oxidative stress in the prolonged inhibitory effect of ultrafine carbon black on epithelial cell function[J]. *Toxicology In Vitro*, 1998, 12(6): 649-659.
- Strayer D S. Viral Gene Delivery[J]. *Expert opinion on investigational drugs*, 1999, 8(12): 2159-2172.
- Subbiah R, Veerapandian M, S Yun K. Nanoparticles: functionalization and multifunctional applications in biomedical sciences[J]. *Current Medicinal Chemistry*, 2010, 17(36): 4559-4577.
- Sun, T., Zhang, Y.S., Pang, B., Hyun, D.C., Yang, M., and Xia, Y. (2014). Engineered nanoparticles for drug delivery in cancer therapy. *Angewandte Chemie International Edition* *53*, 12320-12364.
- Sun, X., Jin, X., Pan, W., Guo, E., Liu, W., Li, D., Lu, K., Si, S., Zhang, N., and Jia, Z. (2016). Highly Luminescent Carbon Dots Synthesized by Microwave-Assisted Pyrolysis and Evaluation of Their Toxicity to *Physa acuta*. *Journal of Nanoscience and Nanotechnology* *16*, 648-653.
- Sun, Y.-P., Zhou, B., Lin, Y., Wang, W., Fernando, K.S., Pathak, P., Meziani, M.J., Harruff, B.A., Wang, X., and Wang, H. (2006a). Quantum-sized carbon dots for bright and colorful photoluminescence. *J Am Chem Soc* *128*, 7756-7757.
- Sun, Y.-P., Zhou, B., Lin, Y., Wang, W., Fernando, K.S., Pathak, P., Meziani, M.J., Harruff, B.A., Wang, X., and Wang, H. (2006b). Quantum-sized carbon dots for bright and colorful photoluminescence. *Journal of the American Chemical Society* *128*, 7756-7757.
- Taggart, M.J. (2001). Smooth muscle excitation-contraction coupling: a role for caveolae and caveolins? *Physiology* *16*, 61-65.
- Tang, J., Kong, B., Wu, H., Xu, M., Wang, Y., Wang, Y., Zhao, D., and Zheng, G. (2013). Carbon nanodots featuring efficient FRET for real-time monitoring of drug delivery and two-photon imaging. *Advanced Materials* *25*, 6569-6574.

- Tarragó-Trani, M.T., and Storrie, B. (2007). Alternate routes for drug delivery to the cell interior: pathways to the Golgi apparatus and endoplasmic reticulum. *Advanced Drug Delivery Reviews* 59, 782-797.
- Tebar, F., Bohlander, S.K., and Sorkin, A. (1999). Clathrin assembly lymphoid myeloid leukemia (CALM) protein: localization in endocytic-coated pits, interactions with clathrin, and the impact of overexpression on clathrin-mediated traffic. *Molecular Biology of the Cell* 10, 2687-2702.
- Terry, L.J., Shows, E.B., and Wentz, S.R. (2007). Crossing the nuclear envelope: hierarchical regulation of nucleocytoplasmic transport. *Science* 318, 1412-1416.
- Tomalia, D.A., Baker, H., Dewald, J., Hall, M., Kallos, G., Martin, S., Roeck, J., Ryder, J., and Smith, P. (1985). A new class of polymers: starburst-dendritic macromolecules. *Polymer Journal* 17, 117.
- Tomić S, Đokić J, Vasilijić S, et al. Size-dependent effects of gold nanoparticles uptake on maturation and antitumor functions of human dendritic cells in vitro[J]. *PloS One*, 2014, 9(5): e96584.
- Tuzar, Z., and Kratochvil, P. (1976). Block and graft copolymer micelles in solution. *Advances in Colloid and Interface Science* 6, 201-232.
- Ulbrich, K., Hola, K., Subr, V., Bakandritsos, A., Tucek, J., and Zboril, R. (2016). Targeted drug delivery with polymers and magnetic nanoparticles: covalent and noncovalent approaches, release control, and clinical studies. *Chemical Reviews* 116, 5338-5431.
- Underhill, D.M., and Ozinsky, A. (2002). Phagocytosis of microbes: complexity in action. *Annual Review of Immunology* 20, 825-852.
- Vasir, J.K., and Labhasetwar, V. (2008). Quantification of the force of nanoparticle-cell membrane interactions and its influence on intracellular trafficking of nanoparticles. *Biomaterials* 29, 4244-4252.
- Verma, A., and Stellacci, F. (2010). Effect of surface properties on nanoparticle-cell interactions. *Small* 6, 12-21.
- Wang, F., Wang, Y.-C., Dou, S., Xiong, M.-H., Sun, T.-M., and Wang, J. (2011a). Doxorubicin-tethered responsive gold nanoparticles facilitate intracellular drug delivery for overcoming multidrug resistance in cancer cells. *ACS Nano* 5, 3679-3692.
- Wang, K., Gao, Z., Gao, G., Wo, Y., Wang, Y., Shen, G., and Cui, D. (2013a). Systematic safety evaluation on photoluminescent carbon dots. *Nanoscale Research Letters* 8, 122.
- Wang K, Gao Z, Gao G, et al. Systematic safety evaluation on photoluminescent carbon dots[J]. *Nanoscale Research Letters*, 2013, 8(1): 122.
- Wang, K., Kievit, F.M., Sham, J.G., Jeon, M., Stephen, Z.R., Bakthavatsalam, A., Park, J.O., and Zhang, M. (2016). Iron-Oxide-Based Nanovector for Tumor Targeted siRNA Delivery in an Orthotopic Hepatocellular Carcinoma Xenograft Mouse Model. *Small* 12, 477-487.
- Wang, L., Mercer, R.R., Rojanasakul, Y., Qiu, A., Lu, Y., Scabilloni, J.F., Wu, N., and Castranova, V. (2010). Direct fibrogenic effects of dispersed single-walled carbon nanotubes on human lung fibroblasts. *Journal of Toxicology and Environmental Health, Part A* 73, 410-422.
- Wang, R., Lu, K.-Q., Tang, Z.-R., and Xu, Y.-J. (2017). Recent progress in carbon

- quantum dots: synthesis, properties and applications in photocatalysis. *Journal of Materials Chemistry A* 5, 3717-3734.
- Wang, T., Bai, J., Jiang, X., and Nienhaus, G.U. (2012). Cellular uptake of nanoparticles by membrane penetration: a study combining confocal microscopy with FTIR spectroelectrochemistry. *ACS Nano* 6, 1251-1259.
- Wang W J, Hai X, Mao Q X, et al. Polyhedral oligomeric silsesquioxane functionalized carbon dots for cell imaging[J]. *ACS Applied Materials & Interfaces*, 2015, 7(30): 16609-16616.
- Wang, X., Cao, L., Lu, F., Meziani, M.J., Li, H., Qi, G., Zhou, B., Harruff, B.A., Kermarrec, F., and Sun, Y.-P. (2009a). Photoinduced electron transfers with carbon dots. *Chemical Communications*, 3774-3776.
- Wang, X., Li, Q., Xie, J., Jin, Z., Wang, J., Li, Y., Jiang, K., and Fan, S. (2009b). Fabrication of ultralong and electrically uniform single-walled carbon nanotubes on clean substrates. *Nano Letters* 9, 3137-3141.
- Wang, X., Qu, K., Xu, B., Ren, J., and Qu, X. (2011b). Microwave assisted one-step green synthesis of cell-permeable multicolor photoluminescent carbon dots without surface passivation reagents. *Journal of Materials Chemistry* 21, 2445-2450.
- Wang, Y., Anilkumar, P., Cao, L., Liu, J.-H., Luo, P.G., Tackett, K.N., Sahu, S., Wang, P., Wang, X., and Sun, Y.-P. (2011c). Carbon dots of different composition and surface functionalization: cytotoxicity issues relevant to fluorescence cell imaging. *Experimental Biology and Medicine* 236, 1231-1238.
- Wang, Y., Zhao, Q., Han, N., Bai, L., Li, J., Liu, J., Che, E., Hu, L., Zhang, Q., and Jiang, T. (2015b). Mesoporous silica nanoparticles in drug delivery and biomedical applications. *Nanomedicine: Nanotechnology, Biology and Medicine* 11, 313-327.
- Whitesides, G.M. (2003). The 'right' size in nanobiotechnology. *Nature Biotechnology* 21, 1161-1165.
- Williams J M, Ferraro J R, Thorn R J, et al. Organic superconductors (including fullerenes): synthesis, structure, properties, and theory[M]. Englewood Cliffs, NJ: Prentice Hall, 1992.
- Wilson M R, Lightbody J H, Donaldson K, et al. Interactions between ultrafine particles and transition metals in vivo and in vitro[J]. *Toxicology and Applied Pharmacology*, 2002, 184(3): 172-179.
- Wissing, S., Kayser, O., and Müller, R. (2004). Solid lipid nanoparticles for parenteral drug delivery. *Advanced Drug Delivery Reviews* 56, 1257-1272.
- Wolfbeis, O.S. (2015). An overview of nanoparticles commonly used in fluorescent bioimaging. *Chemical Society Reviews* 44, 4743-4768.
- Wolfert, M., and Seymour, L. (1996). Atomic force microscopic analysis of the influence of the molecular weight of poly (L) lysine on the size of polyelectrolyte complexes formed with DNA. *Gene Therapy* 3, 269-273.
- Wood, Z.A., Poole, L.B., and Karplus, P.A. (2003). Peroxiredoxin evolution and the regulation of hydrogen peroxide signaling. *Science* 300, 650-653.
- Wu, Z.L., Liu, Z.X., and Yuan, Y.H. (2017). Carbon dots: materials, synthesis, properties and approaches to long-wavelength and multicolor emission. *Journal of Materials Chemistry B* 5, 3794-3809.
- Wu, Z.L., Zhang, P., Gao, M.X., Liu, C.F., Wang, W., Leng, F., and Huang, C.Z. (2013). One-pot hydrothermal synthesis of highly luminescent nitrogen-doped amphoteric

- carbon dots for bioimaging from *Bombyx mori* silk–natural proteins. *Journal of Materials Chemistry B* *1*, 2868-2873.
- Xia, T., Kovochich, M., Brant, J., Hotze, M., Sempf, J., Oberley, T., Sioutas, C., Yeh, J.I., Wiesner, M.R., and Nel, A.E. (2006a). Comparison of the abilities of ambient and manufactured nanoparticles to induce cellular toxicity according to an oxidative stress paradigm. *Nano Letters* *6*, 1794-1807.
- Xia T, Kovochich M, Brant J, et al. Comparison of the abilities of ambient and manufactured nanoparticles to induce cellular toxicity according to an oxidative stress paradigm[J]. *Nano Letters*, 2006, 6(8): 1794-1807.
- Xiao, Y.-Y., Liu, L., Chen, Y., Zeng, Y.-L., Liu, M.-Z., and Jin, L. (2016). Developmental Toxicity of Carbon Quantum Dots to the Embryos/Larvae of Rare Minnow (*Gobiocypris rarus*). *BioMed Research International* *2016*.
- Xie, J., Lee, S., and Chen, X. (2010). Nanoparticle-based theranostic agents. *Advanced Drug Delivery Reviews* *62*, 1064-1079.
- Xu, X., Ray, R., Gu, Y., Ploehn, H.J., Gearheart, L., Raker, K., and Scrivens, W.A. (2004). Electrophoretic analysis and purification of fluorescent single-walled carbon nanotube fragments. *Journal of the American Chemical Society* *126*, 12736-12737.
- Yamamoto, A., Honma, R., Sumita, M., and Hanawa, T. (2004). Cytotoxicity evaluation of ceramic particles of different sizes and shapes. *Journal of Biomedical Materials Research Part A: An Official Journal of The Society for Biomaterials, The Japanese Society for Biomaterials, and The Australian Society for Biomaterials and the Korean Society for Biomaterials* *68*, 244-256.
- Yamanaka, J., Hibi, S., Ikeda, S., and Yonese, M. (2004). Particle size dependence for effective charge density of ionic colloids. *Molecular Simulation* *30*, 149-152.
- Yameen, B., Choi, W.I., Vilos, C., Swami, A., Shi, J., and Farokhzad, O.C. (2014). Insight into nanoparticle cellular uptake and intracellular targeting. *Journal of Controlled Release* *190*, 485-499.
- Yan, Q.-L., Gozin, M., Zhao, F.-Q., Cohen, A., and Pang, S.-P. (2016). Highly energetic compositions based on functionalized carbon nanomaterials. *Nanoscale* *8*, 4799-4851.
- Yang, L., Wang, Z., Wang, J., Jiang, W., Jiang, X., Bai, Z., He, Y., Jiang, J., Wang, D., and Yang, L. (2016). Doxorubicin conjugated functionalizable carbon dots for nucleus targeted delivery and enhanced therapeutic efficacy. *Nanoscale* *8*, 6801-6809.
- Yang, S.-T., Cao, L., Luo, P.G., Lu, F., Wang, X., Wang, H., Mezziani, M.J., Liu, Y., Qi, G., and Sun, Y.-P. (2009a). Carbon dots for optical imaging in vivo. *Journal of the American Chemical Society* *131*, 11308-11309.
- Yang S T, Cao L, Luo P G, et al. Carbon dots for optical imaging in vivo[J]. *Journal of the American Chemical Society*, 2009, 131(32): 11308-11309.
- Yang, S.-T., Wang, X., Wang, H., Lu, F., Luo, P.G., Cao, L., Mezziani, M.J., Liu, J.-H., Liu, Y., and Chen, M. (2009c). Carbon dots as nontoxic and high-performance fluorescence imaging agents. *The Journal of Physical Chemistry C, Nanomaterials and interfaces* *113*, 18110.
- Yang, S.-T., Wang, X., Wang, H., Lu, F., Luo, P.G., Cao, L., Mezziani, M.J., Liu, J.-H., Liu, Y., and Chen, M. (2009d). Carbon dots as nontoxic and high-performance fluorescence imaging agents. *The Journal of Physical Chemistry C* *113*, 18110-

18114.

- Yang S T, Wang X, Wang H, et al. Carbon dots as nontoxic and high-performance fluorescence imaging agents[J]. *The Journal of Physical Chemistry C*, 2009, 113(42): 18110-18114.
- Yang, W., Zhang, H., Lai, J., Peng, X., Hu, Y., Gu, W., and Ye, L. (2018a). Carbon dots with red-shifted photoluminescence by fluorine doping for optical bio-imaging. *Carbon* 128, 78-85.
- Yang, Y., Ren, X., Sun, Z., Fu, C., Liu, T., Meng, X., and Wang, Z. (2018b). Toxicity and bio-distribution of carbon dots after single inhalation exposure in vivo. *Chinese Chemical Letters*.
- Yin, H., Kanasty, R.L., Eltoukhy, A.A., Vegas, A.J., Dorkin, J.R., and Anderson, D.G. (2014). Non-viral vectors for gene-based therapy. *Nature Reviews Genetics* 15, 541.
- Yingchoncharoen, P., Kalinowski, D.S., and Richardson, D.R. (2016). Lipid-based drug delivery systems in cancer therapy: what is available and what is yet to come. *Pharmacological Reviews* 68, 701-787.
- Yu, T., Malugin, A., and Ghandehari, H. (2011). Impact of silica nanoparticle design on cellular toxicity and hemolytic activity. *ACS Nano* 5, 5717-5728.
- Zhai, X., Zhang, P., Liu, C., Bai, T., Li, W., Dai, L., and Liu, W. (2012). Highly luminescent carbon nanodots by microwave-assisted pyrolysis. *Chemical Communications* 48, 7955-7957.
- Zhang, J., and Yu, S.-H. (2016). Carbon dots: large-scale synthesis, sensing and bioimaging. *Materials Today* 19, 382-393.
- Zhang, L., Wang, D., Huang, H., Liu, L., Zhou, Y., Xia, X., Deng, K., and Liu, X. (2016). Preparation of Gold–Carbon Dots and Ratiometric Fluorescence Cellular Imaging. *ACS Applied Materials & Interfaces* 8, 6646-6655.
- Zhang, X.-D., Wu, D., Shen, X., Liu, P.-X., Yang, N., Zhao, B., Zhang, H., Sun, Y.-M., Zhang, L.-A., and Fan, F.-Y. (2011). Size-dependent in vivo toxicity of PEG-coated gold nanoparticles. *International Journal of Nanomedicine* 6, 2071.
- Zhang, Y., Ali, S.F., Dervishi, E., Xu, Y., Li, Z., Casciano, D., and Biris, A.S. (2010). Cytotoxicity effects of graphene and single-wall carbon nanotubes in neural pheochromocytoma-derived PC12 cells. *ACS Nano* 4, 3181-3186.
- Zhang, Y., Rhee, K.Y., Hui, D., and Park, S.-J. (2018). A critical review of nanodiamond based nanocomposites: Synthesis, properties and applications. *Composites Part B: Engineering*.
- Zhao, A., Chen, Z., Zhao, C., Gao, N., Ren, J., and Qu, X. (2015). Recent advances in bioapplications of C-dots. *Carbon* 85, 309-327.
- Zhao, F., Zhao, Y., Liu, Y., Chang, X., Chen, C., and Zhao, Y. (2011). Cellular uptake, intracellular trafficking, and cytotoxicity of nanomaterials. *Small* 7, 1322-1337.
- Zhao, Q.-L., Zhang, Z.-L., Huang, B.-H., Peng, J., Zhang, M., and Pang, D.-W. (2008). Facile preparation of low cytotoxicity fluorescent carbon nanocrystals by electrooxidation of graphite. *Chemical Communications*, 5116-5118.
- Zhao X, Ng S X, Heng B C, et al. Cytotoxicity of hydroxyapatite nanoparticles is shape and cell dependent[J]. *Archives of Toxicology*, 2013, 87(6): 1037-1052.
- Zheng, M., Liu, S., Li, J., Qu, D., Zhao, H., Guan, X., Hu, X., Xie, Z., Jing, X., and Sun, Z. (2014). Integrating oxaliplatin with highly luminescent carbon dots: an unprecedented theranostic agent for personalized medicine. *Advanced Materials* 26,

3554-3560.

- Zheng X T, Ananthanarayanan A, Luo K Q, et al. Glowing graphene quantum dots and carbon dots: properties, syntheses, and biological applications[J]. *Small*, 2015, 11(14): 1620-1636.
- Zhou, J., Booker, C., Li, R., Zhou, X., Sham, T.-K., Sun, X., and Ding, Z. (2007). An electrochemical avenue to blue luminescent nanocrystals from multiwalled carbon nanotubes (MWCNTs). *Journal of the American Chemical Society* 129, 744-745.
- Zhou, J., Sheng, Z., Han, H., Zou, M., and Li, C. (2012). Facile synthesis of fluorescent carbon dots using watermelon peel as a carbon source. *Materials Letters* 66, 222-224.
- Zhu, S., Meng, Q., Wang, L., Zhang, J., Song, Y., Jin, H., Zhang, K., Sun, H., Wang, H., and Yang, B. (2013). Highly photoluminescent carbon dots for multicolor patterning, sensors, and bioimaging. *Angewandte Chemie* 125, 4045-4049.
- Zhu, Y., Zhao, Q., Li, Y., Cai, X., and Li, W. (2006). The interaction and toxicity of multi-walled carbon nanotubes with *Stylynychia mytilus*. *Journal of Nanoscience and Nanotechnology* 6, 1357-1364.
- Zolnik, B.S., Gonzalez-Fernandez, A., Sadrieh, N., and Dobrovolskaia, M.A. (2010). Minireview: nanoparticles and the immune system. *endocrinology* 151, 458-465.
- Zuo, P., Lu, X., Sun, Z., Guo, Y., and He, H. (2016). A review on syntheses, properties, characterization and bioanalytical applications of fluorescent carbon dots. *Microchimica Acta* 183, 519-542.





## Résumé

Les carbon dots (CDs), dernier membre de la famille des nanoparticules (NPs) carbonées à avoir été découverts, sont des particules hydrophiles quasi-sphériques qui sont généralement présentées comme biocompatibles et seulement faiblement toxiques. Ils sont facilement accessibles par voie de synthèse et peuvent être tout aussi aisément modifiés par modification chimique des groupes fonctionnels présents à leur surface. Leurs propriétés de fluorescence intrinsèques les rendent intéressants pour de nombreuses applications, notamment dans le domaine biomédical où les CDs trouvent des applications en tant que vecteurs de principes actifs, comme d'autres NPs développées dans ce domaine. Les travaux développés au cours de cette thèse visaient premièrement à identifier les propriétés physicochimiques intrinsèques des CDs qui conditionnent leur toxicité. Pour cela, le profil toxicologique d'une large collection de CDs présentant des propriétés de taille, charge et chimie de surface a été établi en utilisant des modèles *in vitro* et *in vivo*. Nous avons pu montrer ainsi que, bien que la taille des NPs joue un rôle important dans leur toxicité, elle ne constitue pas à elle seule un facteur prédictif de cette dernière. En effet, la charge et la chimie de surface régissent de façon importante les interactions entre les NPs et l'environnement biologique dans lequel elles sont introduites et, donc, leur toxicité. Le deuxième objectif de cette thèse était d'étudier le potentiel qu'offrent les CDs dans le domaine de la délivrance de gènes. Nous avons pu montrer la supériorité de CDs préparés à partir d'acide citrique et de bPEI600 sur tous les autres CDs cationiques préparés et évalués dans notre étude. Une approche systématique nous a permis d'améliorer, pas à pas, l'efficacité des CDs jusqu'à surpasser celle du bPEI25k, un agent de référence dans le domaine.

Dans l'ensemble, nos études ont ouvert de nouvelles perspectives dans le domaine des NPs en apportant des éléments de compréhension des mécanismes de leur toxicité et en identifiant des conditions de production qui permettent d'optimiser leur propriétés en tant qu'agent de transfection.

**Mots clés:** carbon dots, toxicologie, délivrance de gènes.

## Abstract

Carbon dots (CDs) are the latest member of the family of carbon nanoparticles (NPs) to be discovered. They were isolated for the first time in 2004, during electrophoresis purification of carbon nanotubes. In addition to their nanometric size, these objects are almost spherical and hydrophilic, and are generally presented as biocompatible and very weakly toxic NPs. They are fairly easily accessible by synthesis and can be conveniently modified by reaction of the functional groups present on their surface (amines, carboxylic acids, alcohols, *etc.*). Finally, they exhibit intrinsic fluorescence properties, are relatively resistant to photobleaching, and can be excited by multi-photon irradiation. Thus, like the other members of the family of carbon NPs (graphene, nanodiamonds, fullerenes, nanotubes), CDs have remarkable properties which are the subject of intense research for applications in fields as different as those of electronics, catalysis, energy storage, imaging, and medicine. In the latter area, CDs can find applications as drug delivery systems, like other NPs successfully developed in this field. The work developed during this thesis had two distinct objectives. The first one was to identify the intrinsic physicochemical properties responsible for the toxicity of NPs. For this, the toxicological profile of a large collection of CDs produced in the laboratory and exhibiting various size, charge, and surface chemistry was characterized using *in vitro* lung models and mice. We found that although the size of the NPs plays an important role it is not, by itself, a predictive element of the toxicity of the NPs. The charge and the surface chemistry largely effect the interactions between the NPs and the biological medium systems and, therefore, their intrinsic toxicity. The second objective of this thesis was to assess the potential of CDs in the field of drug delivery as synthetic gene carriers. We were able to show the superiority of NPs prepared from citric acid and bPEI600 over all other cationic CDs produced in the laboratory. A systematic evaluation has allowed us, step by step, to improve the efficiency of these transfection agents, to exceed that of bPEI25k, a gold standard for *in vitro* transfection, without significant toxicity.

Overall, this work opens up new horizons in NPs research that may provide 1-a better understanding of the toxicological mechanisms of NPs, especially their determinants, and 2-identification of the relationship between the CDs synthesis methods and the efficiency of these NPs as DNA transfection reagents.

**Key words:** carbon dots, toxicology, gene delivery.